A Piezoelectric Ink Jet Printing Platform to Engineer Microparticles for Drug Delivery Applications

By

Michael Anthony Marin

Dissertation

Submitted to the Faculty of the

Graduate School of Vanderbilt University

In partial fulfillment of the requirements

for the degree of

DOCTOR OF PHILOSOPHY

in

Chemical and Biomolecular Engineering

August 10, 2018

Nashville, Tennessee

Approved:

Eva M. Harth, Ph.D.

Kane Jennings, Ph.D.

John T. Wilson, Ph.D.

Leon M. Bellan, Ph.D.

To my family, for being supportive throughout my PhD

and

To my friends, for supporting me and enriching my PhD experience

ACKNOWLEDGEMENTS

This work would not have been possible without the financial support from the Materials Science and Engineering Department, VINSE, and the Chemical and Biomolecular Engineering Department of Vanderbilt University.

I am very thankful for my lab members who have helped me become stronger with subjects I am weak in, and for support throughout my PhD.

I would like to thank my committee members for providing me with guidance on the direction for my research.

I would like to thank my research advisor, Dr. Harth for providing me with mentorship and support throughout my PhD, and for helping develop me into the scientist I am today.

I would like to thank the members of my family that have been there to support me throughout my journey in graduate school. They are responsible for my resilient and hardworking personality.

I also want to thank my friends for all the good times and fun weekends.

I also would like to thank my FitFams at CrossFit Nashville and CrossFit Derive for helping me keep manageable stress levels, and a special thanks to CrossFit Derive for helping make my transition to Houston easier.

TABLE OF CONTENTS

Page

LIST OF TABLES

Table **Page**

LIST OF FIGURES

Figure **Page**

CHAPTER 1

1. INTRODUCTION

1.1 Importance and overview of microparticles for drug delivery

Particles for drug delivery are widely researched for use as drug delivery devices due to several advantages over conventional drug tablets. Figure 1 shows an example graph that illustrates two key advantages of drug loaded particles for the consumer. Each curve shown in Figure 1 illustrates an example blood drug concentration profile for one administered dose for either a conventional drug tablet or the optimal drug loaded particles. As shown in the Figure the conventional drug tablet requires three times more doses to get approximately the same effect as a single dose of the optimal drug loaded particles. Additionally, it is important to notice that the profile for the conventional tablet spikes to the side effects region and immediately decreases. Whereas the drug loaded particles result in a sustained blood drug concentration within the therapeutic region for an extended period of time. In summary, for the consumer, conventional drug tablets require more doses and can have side effects, whereas the optimal drug loaded particles allow you to reduce the number of doses and eliminate potential side effects, increasing patient comfort and compliance.

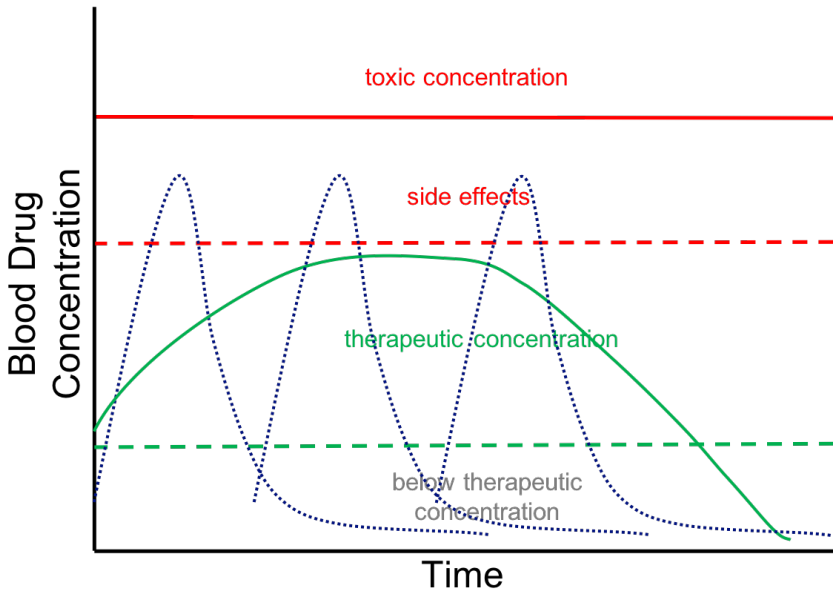

Figure 1. Example graph illustrating two key advantages for the optimal drug loaded particles over conventional drug tablets; conventional drug tablet (blue dotted line) and optimal particles for drug delivery (green line).

In additional to these consumer advantages, for the manufacturer, the development of drug delivery devices is 100 times cheaper and take half the time to develop than a new drug.[1]

Particle sizes typically fabricated for drug delivery applications are either in the nano or micron size range. However, the micron size range has several advantages over the nano size range. In particular, local and inhalation delivery are not easily targetable for nanoparticle drug delivery. For local delivery nanoparticles do not stay at the site of injection due to their small size, whereas microparticles of a large enough size do, such as 55 to 60 micron size particles for sciatic nerve block.[2] For inhalation delivery nanoparticles are inhaled then exhaled[3], whereas microparticles that are 1 to 2 microns in aerodynamic diameter achieve efficient distribution in the deep lungs.[4] Lastly, there is one crucial, but simple advantage of microparticles over nanoparticles. This is the fact that microparticles will always have a longer extended release than their corresponding nanoparticles, due to an increased diffusion path length and degradation time.

Several researchers have capitalized on the advantages previously stated. Figures 2 and 3 show the variety of publications on microparticles used for different applications and routes of administration respectively. As shown in Figure 2 the most common diseases targeted for microparticles in drug delivery are cancer and diabetes. Furthermore, Figure 3 shows that the routes of administration that are most frequently published on are oral and inhalation.

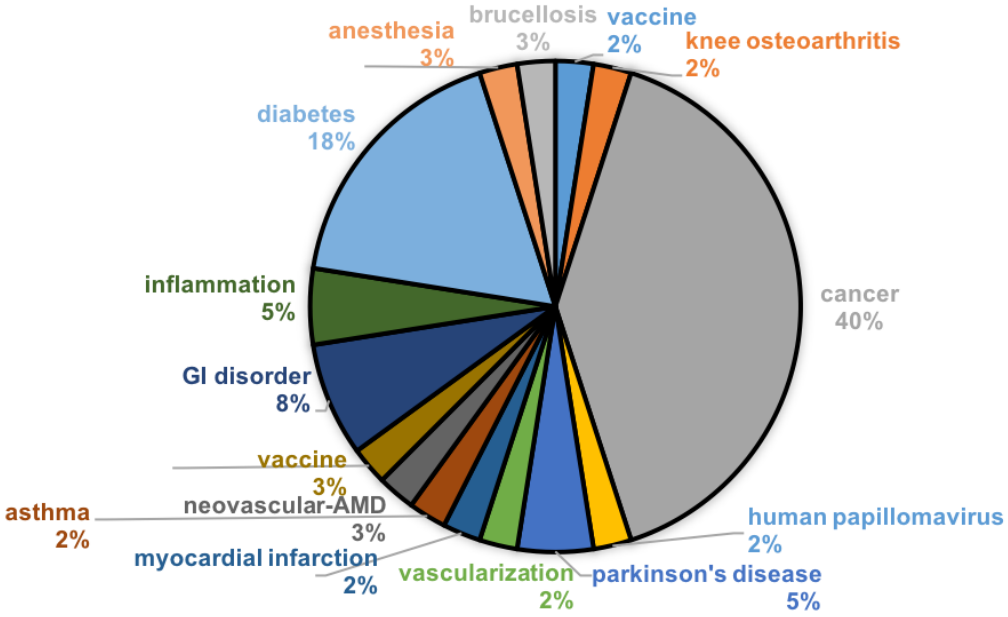

Figure 2. Percentage of publications on different diseases treated using drug loaded microparticles. The figure summarizes data that was extracted by Michael Anthony Marin from 100+ publications mostly from 2010 to 2018. See the Appendix for tables containing detailed data from the summarized articles.

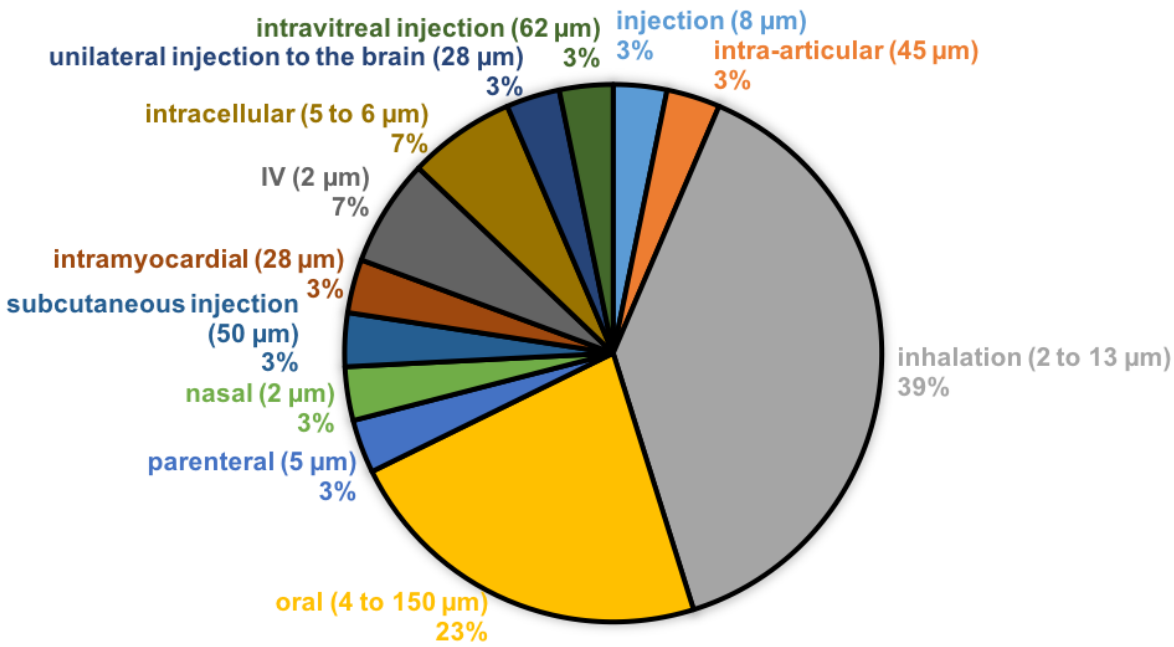

Figure 3. Percentage of publications on different routes of administration for drug loaded microparticles. The figure summarizes data that was extracted by Michael Anthony Marin from 100+ publications mostly from 2010 to 2018. See the Appendix for tables containing detailed data from the summarized articles.

1.2 Microparticle networks for drug encapsulation and delivery

A key part in designing microparticles for a specific drug delivery application is microparticle network selection. In general, microparticle networks are formed by precipitation/physical entanglement, polymerization/covalent crosslinking, or ionic crosslinking. Figure 4 shows the percentage of publications on the different type of microparticle networks. As shown in Figure 4 the highest frequency of publications are on the preparation of microparticles composed of precipitation/physical entanglement networks.

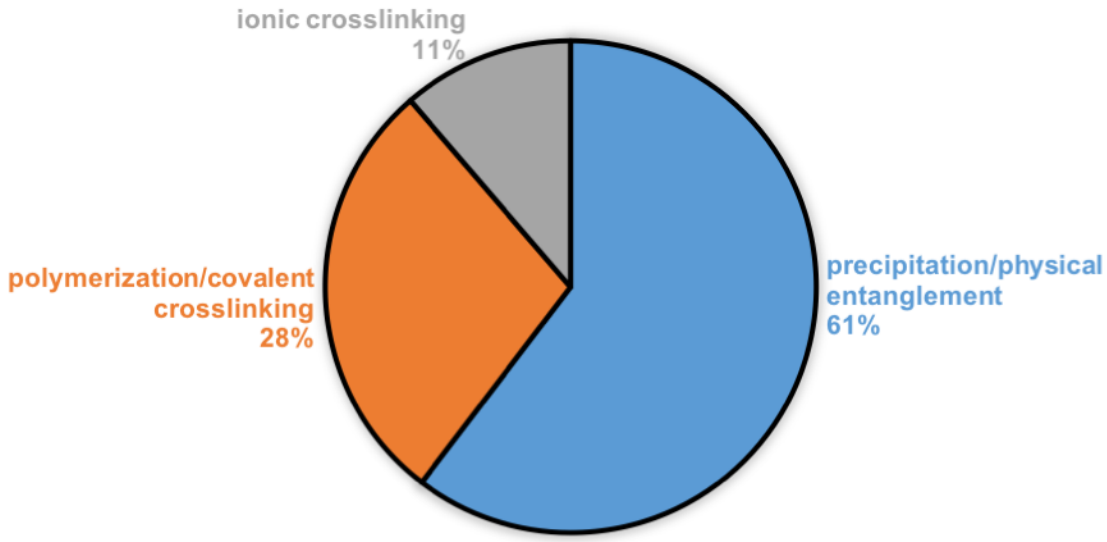

Figure 4. Percentage of publications on different microparticle networks for drug delivery. The figure summarizes data that was extracted by Michael Anthony Marin from 100+ publications mostly from 2010 to 2018. See the Appendix for tables containing detailed data from the summarized articles.

One significant difference between these three categories of networks is that polymerization/covalent crosslinked networks have a high degree of tunability and allow for a controlled and extended release of drug.[5] These features are highly desirable and the work presented here is focused on the development of covalently crosslinked microparticles.

1.3 Precision of microparticle fabrication methods

Methods commonly used to fabricate microparticles include emulsion, spray drying, supercritical fluid, and microfluidics. Figure 5 shows the percentage of publications on each of the different methods used to prepare microparticles for drug delivery. This figure shows that emulsion and spray drying methods are the most common.

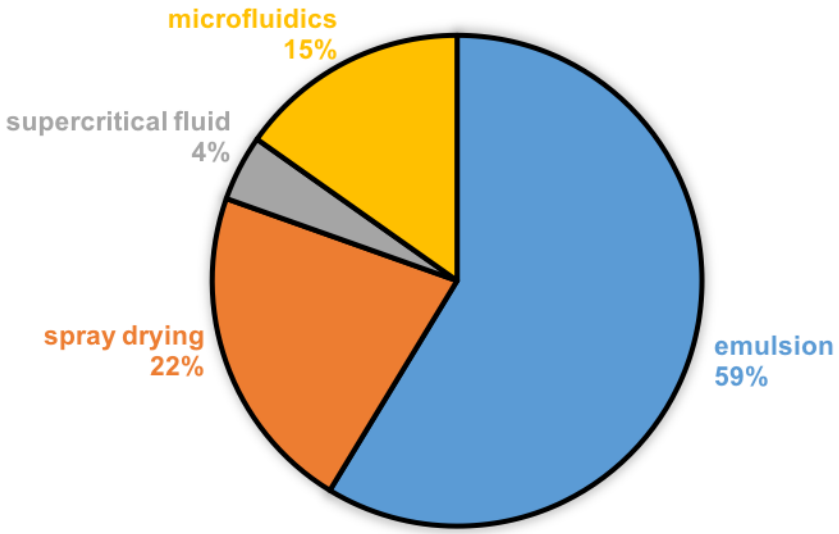

Figure 5. Percentage of publications on microparticle fabrication methods. The figure summarizes data that was extracted by Michael Anthony Marin from 100+ publications mostly from 2010 to 2018. See the Appendix for tables containing detailed data from the summarized articles.

In general, each microparticle fabrication method shown in Figure 4 fabricates microparticles with a characteristic coefficient of variation (CV) defined as;

$$\text{coefficient of variation (CV)} = \frac{\sigma_d}{a_d} \quad (1)$$

where σ_d is the standard deviation for the microparticle diameter and a_d is the average microparticle diameter. The CV value measures how well the method can prepare precisely sized microparticles. The higher the CV value, the less precise in size the fabricated microparticles are. A low CV value is very important to ensure consistent and predictable release kinetics. Low CV is also important for certain routes of administration such as inhalation, which require distinct particle sizes from 1 to 15 microns to reach different locations within the lung.[4] Table 1 shows a size range summary of microparticles fabricated utilizing each technique shown in Figure 5 and the typical coefficient of variation obtained.

Table 1. Size range and coefficient of variation of microparticles prepared utilizing different fabrication methods. The size range and coefficient of variation data was extracted by Michael Anthony Marin from 100+ publications mostly from 2010 to 2018. See the Appendix for tables containing detailed data from the summarized articles.

Fabrication Method	Size Range (μm)	CV (%)
Emulsion	1.0 to 95.0	42 ± 32
Spray drying	1.7 to 10.0	59 ± 28
Supercritical fluid	1.6 to 2.3	88 ± 13
Microfluidics	2.0 to 142.1	10 ± 6

As shown in Table 1 emulsion, spray drying, and supercritical fluid fabrication methods typically result in microparticles with high coefficient of variations averaging 42, 59, and 88% respectively. Whereas microfluidics fabricates microparticles with an average CV value of 10%, a much higher size precision.

1.4 Drug loading and encapsulation efficiency obtained for microparticle fabrication methods

Drug loading in microparticles is achieved by post soaking, covalent bonding of drug, or physical entrapment during network formation. In general, post soaking methods and covalent bonding of drug result in optimal encapsulation efficiency and high drug loading. However, post soaking methods are typically only used for biologicals and hydrophilic drugs. Post soaking methods are also limited to the use of polymers that swell in cold water and shrink above 37 °C. The swelling behavior of these polymers can result in unpredictable release profiles. Covalent bonding of drug is a specialized technique that requires complex chemistry and testing to ensure that the covalent bonds do not alter the activity of the therapeutic, and only release drug through degradation. The reasons mentioned here limit the drug loading tunability and the practicality of post soaking and covalent bonding drug loading. This work only focuses on methods that involve the physical entrapment of drugs, which is practical and results in a high level of tunability.

The highest drug loading percentage and encapsulation efficiency for each method is shown in Tables 2, 3, and 4 for biologicals, synthetic hydrophilic drugs, and synthetic hydrophobic

drugs respectively. Table 2 shows that for biologicals the method that resulted in the highest loading was emulsion precipitation/physical entanglement, whereas a microfluidics method resulted in the highest encapsulation efficiency. Table 3 shows that for hydrophilic drug loading and encapsulation efficiency a spray drying precipitation method resulted in the highest values. Lastly, Table 4 shows that for hydrophobic drug loading a microfluidics precipitation method resulted in the highest encapsulation efficiency whereas a spray drying precipitation method resulted in the highest drug loading. In summary, there is not one method that is optimal for high drug loading and optimal encapsulation efficiency for synthetic hydrophilic, synthetic hydrophobic, and biological therapeutics. Additionally, there are only a few articles on dual loading as shown in Table A3 in the Appendix, and no articles on triple loading of drugs.

Table 2. Drug loading and encapsulation efficiency for biologicals loaded by physical entrapment. The drug loading and encapsulation efficiency data was extracted by Michael Anthony Marin from 100+ publications mostly from 2010 to 2018. See the Appendix for tables containing detailed data from the summarized articles.

Fabrication Method	Highest drug loading (%)	R	Highest encapsulation efficiency (%)	R
Emulsion Precipitation	22.1	[6]	90	[6]
Emulsion Polymerization	1.9	[7]	36	[8]
Spray Drying Precipitation	9.7	[9]	97	[9]
Supercritical Precipitation	48	[10]	97	[10]
Microfluidics Precipitation	5.9	[11]	99	[11]

Table 3. Drug loading and encapsulation efficiency for hydrophilic loaded drugs by physical entrapment. The drug loading and encapsulation efficiency data was extracted by Michael Anthony Marin from 100+ publications mostly from 2010 to 2018. See the Appendix for tables containing detailed data from the summarized articles.

Fabrication Method	Highest drug loading (%)	R	Highest encapsulation efficiency (%)	R
Emulsion Ionic Crosslinking	13	[12]	66	[12]
Emulsion Polymerization	0.4	[8]	7.6	[8]
Spray Drying Precipitation	14	[13]	95	[13]
Microfluidics Precipitation	1	[14]	30	[14]

Table 4. Drug loading and encapsulation efficiency for hydrophobic loaded drugs by physical entrapment. The drug loading and encapsulation efficiency data was extracted by Michael Anthony Marin from 100+ publications mostly from 2010 to 2018. See the Appendix for tables containing detailed data from the summarized articles.

Fabrication Method	Highest drug loading (%)	R	Highest encapsulation efficiency (%)	R
Emulsion Precipitation	20	[15]	93	[16]
Spray Drying Precipitation	49	[17]	96	[18]
Supercritical Precipitation	14	[19]	63	[19]
Microfluidics Precipitation	30	[20]	97	[21]

1.5 Development of a comprehensive technology to engineer tunable drug loaded microparticles

As summarized previously, a comprehensive method has not been invented that can easily fabricate tunable microparticles at a high rate with low CV, and have the ability to encapsulate synthetic hydrophilic, synthetic hydrophobic, and/or biologicals with a high drug loading and encapsulation efficiency. The goal of this work was to develop a comprehensive technology that can accomplish this. The approach to accomplish this goal was to first identify properties important in drug delivery such as release kinetics, route of administration, dose, type of drug loading (hydrophilic, hydrophobic, and/or biological), and microparticle circulation time. Microparticle properties were then identified that could tune these drug delivery properties. For example, the release kinetics can be tuned by the microparticle network density, the route of administration through the microparticle size, the type of drug loading (hydrophilic, hydrophobic, and/or biological) through the microparticle hydrophilic character, and the microparticle circulation time through the microparticle softness[22]. A goal was then set to tune the identified microparticle properties over a wide range thereby allowing us to engineer microparticles for a wide range of drug delivery applications. The strategy to accomplish this goal was to utilize piezoelectric ink jet printing, a method known to produce precisely sized droplets in the micron size range with tunable ejection volume, and development of a fundamental set of photoreactive monomer and copolymer

inks that allow us to tune the microparticle softness, hydrophilicity, and network density over a wide range. By innovatively selecting piezoelectric ink jet printing to fabricate microparticles we should be able to easily tune the microparticle size through the ejected droplet volume while maintaining high size precision, and also tune the drug loading while maintaining high encapsulation efficiency. The droplet volume can be tuned through the jetting waveform, nozzle temperature, and/or nozzle size while maintaining high size precision through properly tuned jetting. The drug loading can be tuned simply by changing the ink, and high encapsulation efficiency should be achieved because the droplets are rapidly crosslinked after printing encapsulating the drug within. Surprisingly, no one has published on the use piezoelectric ink jet printing to fabricate drug loaded microparticles. By printing photoreactive inks we can covalently crosslink the printed droplets after printing using UV or visible light, physically encapsulating the drug within the covalently crosslinked microparticle networks. The microparticles could then be collected by washing or by dissolving the substrate depending on the microparticle-substrate interaction. With the fabrication method now selected we just had to develop a small set of photoreactive inks that allow us to obtain microparticles with a wide range of softness, hydrophilicity, and network density. We hypothesized that by strategically incorporating ink network precursors composed of reactive copolymer and crosslinker combinations (different structure and molecular weight) or photoreactive crosslinking monomers, we could tune the softness, hydrophilicity, and network density over a wide range. To ensure that a minimum amount of inks were needed we exploited the structure-property relationship boundaries of these copolymer and monomer network precursors. This was done by synthesizing a functionalized hydrophilic semibranched copolymer and hydrophobic linear copolymer with varying amounts of functionality, and the utilization of a crosslinking monomer. The functionalized copolymers were

synthesized to contain allyl groups that can react with dithiol crosslinkers to form the microparticle network. By preparing mixtures of these two copolymers we sought to obtain a wide range of microparticle hydrophilicity. Tunable softness and network density was obtained by changing the dithiol crosslinker length or by changing the % of allyl group incorporation. The developed photoreactive copolymer inks allow for fabrication of microparticles with a wide range of properties. However, in case fully crosslinked microparticle networks are needed for extreme extended release applications, we developed an ink composed of 100% reactive precursor network components through the incorporation of a tri-functionalized crosslinking monomer. Through this fundamental set of copolymer and monomer network precursors and strategic selection of other ink components, we developed four photoreactive inks that can fabricate a wide range of microparticles for a wide range of drug delivery applications.

1.6 Testing of the developed comprehensive technology

Microparticles were fabricated using each of the four developed inks. To facilitate microparticle characterization, a dye was incorporated into each ink formulation to allow for microparticle visualization using fluorescent microscopy. Microparticle-laden substrates were characterized using wide field microscopy to investigate the droplet placement on the substrate. Whereas confocal microscopy was utilized to investigate the microparticle shape, dye distribution throughout the microparticle, and microparticle size precision. We then sought to verify our predicted structure-property relationships. This was accomplished by designing and implementing efficient experiments to test the softness through unconfined compression testing, hydrophilicity through swelling studies, and size tuning using confocal microscopy. After verification of tunable properties we utilized the developed technology to fabricate optimal microparticles for a high impact drug delivery application, malaria elimination.

Malaria is a disease most prominent in sub-Saharan Africa where 80% of the global burden is present. Without proper treatment severe complications and death is inevitable.[23] In 2016, 216 million cases of the disease were reported in 91 countries, an increase of 5 million cases since 2015. As mentioned in the World Health Organization (WHO) 2017 World Malaria Report, if new interventions are not developed for malaria treatment, then cases and death will almost certainly increase.[24]

Malaria elimination is a very challenging disease to eliminate since it is easily and rapidly transferred through mosquitos. Currently the primary malaria prevention is an insecticide-treated mosquito net which is implemented for over 54% of people at risk. Other strategies include employing rapid diagnostic tests (RDT) to determine if a patient is positive for the infection, then giving antimalarial drugs via oral administration for treatment. However, as indicated by the WHO report these therapeutic strategies are insignificant, and will likely not result in malaria elimination. A promising alternative strategy is mass drug administration (MDA). MDA eliminates the need for rapid diagnostic testing and mosquito nets and would ensure that the entire population is under treatment, proactively preventing infection from developing, eliminating malaria.

Mass drug administration is commonly executed using oral administration of therapeutics. However, the bioavailability of orally administered drugs is very low, due to the brief transit time in the gastric intestinal (GI) tract typically from 8 to 12 hours.[25] A promising strategy to significantly improve the bioavailability of common orally administered therapeutics is to develop an extended release drug delivery device. One therapeutic that would be very effective when delivered using an extended release device is ivermectin. This drug can function

as a systematic insecticide which kills the mosquito after the mosquito sucks blood containing an ivermectin concentration of at least 8 ng/mL.[26]

The development of a drug delivery device for extended ivermectin delivery would make a significant step toward the elimination of malaria. In terms of feasible routes of administration for MDA therapeutics; oral, nasal, and inhalation are most attractive due to their non-invasive nature. Oral therapeutics however are exposed to a very acidic environment that can result in aggressive degradation of polymer drug delivery devices. Nasal administration has mucociliary clearance mechanisms that are hard to overcome. On the other hand, inhalation administration, with the properly engineered devices, can result in a successful extended release of drug via pulmonary drug delivery. Properties that would be essential to the success of these devices include 1) an aerodynamic diameter of 1 to 2 microns for efficient distribution in the deep lungs[4], 2) high drug loading of hydrophobic drug (ivermectin), and 3) a dense crosslinked network that results in an extended drug release.

Our fabrication strategy to engineer these microparticles for malaria elimination was to use our invented piezoelectric ink jet printing technology and the photoreactive monomer ink. Advantages of our technology include precise microparticle fabrication in the low micron size range which should result in microparticles with efficient lung distribution and consistent release kinetics. Furthermore, the photoreactive monomer ink was chosen since it is fundamentally composed of 100% of photoreactive hydrophobic monomers which should result in the highest density crosslinked network with the longest extended release of drug, and high drug loading due to the hydrophobic environment being very favorable for the hydrophobic drug ivermectin.

After fabrication the microparticles were evaluated solely using microparticle characterization and *in vitro* experiments that investigate the ivermectin loaded microparticle

transport steps from the time of inhalation, to the time of elimination. The transport steps encountered include; 1) the ivermectin loaded microparticle transport from the mouth to the deep lungs, 2) ivermectin transport from the microparticle to the lung epithelial layer, 3) ivermectin transport through the lung epithelial layer into the systematic circulation, 4a) ivermectin transport throughout the body and elimination from the body, and 4b) microparticle degradation/elimination from the body. Step 1 was not investigated via *in vitro* studies since it is well known to be governed by the aerodynamic particle size of 1 to 2 microns.[4] Step 2 was first evaluated using *in vitro* release studies. Steps 2 and 3 were then simultaneously investigated utilizing an *in vitro* lung model and an *in vitro-in vivo* lung absorption correlation. Step 4a was not investigated since ivermectin is well known to have an elimination half-life of 18 hours once in the plasma.[27] Lastly, step 4b was investigated using *in vitro* degradation studies at conditions relevant to those found in the deep lungs.

Microparticles were fabricated with 13 wt% of ivermectin with an aerodynamic diameter of 1.6 ± 0.7 microns, resulting in a high hydrophobic drug loading and the optimal size for efficient drug distribution in the deep lungs. *In vitro* release experiments show that the ivermectin release can be tuned through the monomer concentration. Through the *in vitro* lung permeability studies and an *in vitro-in vivo* drug absorption correlation we determined that ivermectin lung absorption should occur *in vivo* over approximately 21 days. Lastly, *in vitro* degradation studies showed that the degradation rate can be tuned by the monomer concentration. The results show promise that the fabricated microparticles will make a significant step towards malaria elimination via pulmonary drug delivery, but also demonstrate the potential of the developed comprehensive technology.

CHAPTER 2

2. MATERIALS AND METHODS

2.1 Materials

All reaction solvents used were HPLC quality and purchased from Sigma Aldrich. All NMR solvents were purchased from Cambridge Isotope Laboratories, Inc. 2,2-bis(hydroxymethyl) propionic acid (Bis-HPA), Amberlyst® 15 Hydrogen Form (A-15), allyl glycidyl ether (AGE), ≥ 99%, sodium hydroxide, ≥97%, anhydrous isoamyl alcohol (IAOH), 3,6-Dioxa-1,8-octanedithiol, nile red, coumarin 30, and 2,2-dimethoxy-2-phenylacetophenone (DMPA) were purchased from Sigma Aldrich. A sulfo-cyanine3 carboxylic acid dye was purchased from Lumiprobe Corporation. Glycidol (GLY), 96% was purchased from Sigma Aldrich and vacuum distilled prior to use with a Kugelrohr short-path distillation device. Dulbecco's Phosphate Buffered Saline (PBS), no calcium, no magnesium, was purchased from Life Technologies and the pH was optimized using either sodium hydroxide or hydrochloric acid prior to use. Poly(methyl methacrylate) and poly(ethylene glycol) calibration kits were purchased from Agilent Technologies. Thiol PEG dithiol (HS-PEG-SH) (1,500 g/mol) was purchased from Nanocs. 2,2'-Azobis[2-(2-imidazolin-2-yl)propane]dihydrochloride (VA-044) was purchased from Wako chemicals. Tin(II) trifuoromethane sulfonate, $Sn(OTf)_2$ was purchased from Strem Chemicals Inc. Teflon sheets were obtained from ePlastics. Dialysis membranes (Spectra/Por® 7, molecular weight cut-off (MSCO) : 1,000 Da) were obtained from Spectrum Laboratories, Inc. 5-methyl-5-allyloxycarbonyl-1,3-dioxane-2-one (MAC), and 5-methyl-5-ethyloxycarbonyl-1,3-dioxane-2-one (MEC) were synthesized according to the literature and recrystallized prior to use.[28-29] All reaction solvents were HPLC quality and purchased from Sigma Aldrich. Triethylamine, eosin Y, ivermectin, dimethyl sulfoxide, ascorbic acid, and trimethylolpropane

triacrylate (technical grade, contains 600 ppm monomethyl ether hydroquinone as inhibitor), inhibitor remover (replacement packing for removing hydroquinone and monomethyl ether hydroquinone), cobalt chloride, hydrogen peroxide (50%), penicillin-streptomycin solution stabilized with 10,000 units penicillin and 10 mg streptomycin/mL (sterile-filtered, BioReagent, suitable for cell culture), hydrocortisone solution (50 μM, sterile-filtered, BioXtra, suitable for cell culture), sodium selenite (BioReagent, suitable for cell culture ≥98%), transferrin human (powder, BioReagent, suitable for cell culture), retinoic acid (≥98%, HPLC, powder), insulin human (recombinant, expressed in yeast (proprietary host)), dimethyl sulfoxide (for molecular biology), ethanolamine (liquid, BioReagent, suitable for cell culture, ≥ 98%), TWEEN® 80 (viscous liquid), and ivermectin were purchased from Sigma Aldrich. Polyvinyl alcohol film was purchased from Tianjin Teda Ganghua Trade Co., LTD (China). Invitrogen™ Molecular Probes™ Vybrant™ MTT cell proliferation assay kits, Corning™ Transwell™ multiple well plate with permeable polycarbonate membrane inserts, Gibco™ trypsin-EDTA (0.25%) phenol red, Gibco™ trypan blue solution (0.4%), Gibco™ Ham's F-12K (Kaighn's) medium, Gibco™ fetal bovine serum, Certified One Shot™, US origin, Gibco™ DMEM/F-12, o-phosphoethanolamine (MP Biomedicals™), Forskolin from Coleus forskohlii (MP Biomedicals™), bovine pituitary extract BT-215 Alfa Aesar™, and Gibco™ phosphate buffered saline solution pH 7.4 were purchased from Fischer Scientific.

2.2 Synthesis of novel functionalized copolymers for microparticle fabrication

2.2.1 Synthesis and characterization of hydrophobic linear poly(carbonate) copolymers

Gel permeation chromatography (GPC) was carried out with a Waters chromatograph system equipped with a Waters 2414 refractive index detector, a Waters 2481 dual λ absorbance detector, a Waters 1525 binary HPLC pump, and four 5 mm Waters columns (300 mm x 7.7

mm) connected in series with increasing pore size (100, 1000, 100,000 and 1,000,000 Å respectively). All runs were performed using dimethylformamide (DMF) with lithium bromide (LiBr) (1 mg/mL) and poly(styrene) standards.

To prepare methyl ethyl carbonate/methyl allyl carbonate (MEC/MAC) copolymers a 25 mL round bottom flask equipped with a stir bar was capped with a rubber septum then flame dried under nitrogen. $Sn(OTf)_2$ (14mg; 33.6 μmol; 4 eq) was then added to the round bottom flask and the reaction vessel was immediately purged with nitrogen prior to the addition of isoamyl alcohol (IAOH) (37 mg; 2.42 mmol; 50 eq) via microsyringe. The initiator-catalyst mixture was then allowed to stir at room temperature for 30 minutes before the addition of the MEC and MAC monomers. The reaction flask was then submerged in an 80 °C oil bath and the reaction was allowed to proceed until stirring was impeded. The resulting polymer product was dialyzed against dichloromethane (DCM) in tubing with a molecular weight cut-off (MWCO) of 1 kDa for 3 days with 5 solvent changes. The pure MEC/MAC copolymer product was collected and dried using a rotovap then a high-pressure pump (80% yield). The PDI was determined as 1.1.

2.2.2 Synthesis and characterization of hydrophilic semibranched poly(glycidol) copolymers

Gel permeation chromatography (GPC) was carried out with a Waters chromatograph system equipped with a Waters 2414 refractive index detector, a Waters 2481 dual λ absorbance detector, a Waters 1525 binary HPLC pump, and four 5 mm Waters columns (300 mm x 7.7 mm), connected in series with increasing pore size (100, 1000, 100,000 and 1,000,000 Å respectively). All runs were performed using dimethylformamide (DMF) with LiBr (1 mg/mL) and polyethylene glycol standards.

To prepare the metal catalyzed semibranched glycidol/allyl glycidyl ether (GLY/AGE) copolymers a 25 mL round bottom flask (RBF) equipped with stir bar was capped with a rubber

septum then flame dried under nitrogen. $Sn(OTf)_2$ (5.2 mg; 12.48 μmol; 0.4 eq) was then added to the round bottom flask and the reaction vessel was then immediately purged with nitrogen prior to the addition of isoamyl alcohol (43.7 mg 495.6 μmol; 17.4 eq) via microsyringe. The initiator-catalyst mixture was then allowed to stir at room temperature for 30 minutes before lowering the reaction vessel into an ice water bath. After the reaction vessel had been cooled for 5 minutes the AGE monomer (834 mg; 7.31 mmol; 250 eq) was added drop wise to the stirring reaction. The GLY monomer (2.17 g; 29.24 mmol; 1000 eq) was then added drop wise in 4 separate aliquots, allowing 5 minute breaks between each aliquot. This ensured the exothermic reaction did not overheat and decompose the components. After stirring was impeded (~14 hours) the crude reaction mixture was solubilized in a minimal amount of methanol and precipitated into vigorously stirring ethyl acetate. The precipitation solvent was then allowed to settle before carefully decanting the ethyl acetate. The resulting GLY/AGE copolymer was solubilized in methanol, removed to a weighed 6-dram vial, dried using a rotavap then a high vacuum pump to afford the translucent viscous product with a 75% yield. The PDI was determined as 1.6 with a Mw and Mn values of 7,480 g/mol and 4,622 g/mol respectively. The $Sn(OTf)_2$ GLY homopolymers were synthesized by first flame drying and nitrogen purging a 25 mL round bottom flask (RBF) equipped with a stir bar and septum. The catalyst $Sn(OTf)_2$ (5.4 mg, 0.013 mmol) was then added and the RBF was purged with nitrogen again. The initiator 3-methyl-1-butanol (54.48 μL, 0.5 mmol) was added and the RBF was stirred for 30 minutes at room temperature then cooled to 0 ºC. Glycidol (2.7 mL, 40.5 mmol) was added to the round bottom flask drop wise ¼ at a time in 5 minute intervals. The reaction was then left to stir overnight at room temperature. For purification, the crude product was precipitated in room temperature ethyl acetate, then collected using

methanol and dried using a rotovap then a high-pressure pump to afford the purified product with 94% yield.

2.2.3 Green synthesis and characterization of hydrophilic semibranched poly(glycidol) copolymers

^{1}H and ^{13}C NMR spectrum were obtained using a Bruker 600 spectrometer operating at 600 and 150 MHz, respectively. The instrument was equipped with a 14.1 Tesla Bruker magnet, which was controlled by a Bruker AV-II console, and a 5mm Z-gradient TCI Cryo-probe. A 10 second recycle delay was used to insure full relaxation between pulses, allowing for quantitative measurements. This data was then used to assign individual monomer peaks specific to the ring opening structure, thus allowing for the calculation of the polymer degree of branching and relative abundance of repeat units.

Gel permeation chromatography (GPC, Agilent 1260 GPC/SEC system) was used to determine molecular weight and polydispersity (Mw/Mn, PDI) of the poly(glycidol) polymers. Dimethylformamide (DMF) containing 0.1% LiBr at 60 °C was used as the mobile phase through three serial Tosoh Biosciences TSKGel Alpha columns (Tokyo, Japan). A Shimadzu RID-10A refractive index detector and a Wyatt miniDAWN Treos multi-angle light scattering detector were used to calculate absolute molecular weight based on dη/dC values. The dη/dC values were experimentally determined by measuring the refractive index of serial dilutions of each polymer in the GPC mobile phase with an Abbemat 300 digital refractometer (Anton Paar). All GPC data was analyzed using ASTRA V software (Wyatt Technology). GPC derived polymer Mn values were calculated by comparison to poly(methyl methacrylate) (PMMA) standards (PMMA Calibration Kit, Agilent Technologies) and poly(ethylene glycol) standards (PEG Calibration Kit, Agilent Technologies). Briefly, a series of PMMA standards of known Mn were analyzed by GPC and quadratic regression analysis was performed to determine Mn as a

function of peak elution time. Mw and corresponding polydispersity (PDI) values were determined with Astra V software (Wyatt Technologies).

Matrix assisted laser desorption/ionization-time of flight-mass spectroscopy (MALDI-Tof-MS) measurements were performed using a Voyager DE-STR MS in reflector mode equipped with a nitrogen gas laser of wavelength 337 nm utilizing external calibration. The instrument parameters were set to 25,000 V, 90% grid, 600ns delay, and 1000 shots per spectrum. The poly(glycidol) based samples were formed using solutions of 10 mg polymer/mL water and saturated dithranol matrix solution in 2:1 water/acetonitrile.

The green glycidol/allyl glycidyl ether (GLY/AGE) 70/30 copolymers were prepared by first adding glycidol monomer (17.5mmol, 2.3 eq) to a flame dried 25mL RBF equipped with a stir bar. The allyl glycidyl ether monomer (7.5mmol, 1.0 eq) was then added via syringe and the reaction vessel was lowered into an oil bath at 80 °C before the addition of Dulbecco's Phosphate Buffer Saline (DPBS) (0.25mL; pH= 6.0). The reaction was then allowed to run for 72 hours before the crude product was removed from the oil bath, dissolved in a minimal amount of methanol, and precipitated into vigorously stirring ethyl acetate. After allowing the solution to settle, the supernatant was decanted and the resulting copolymer product was collected in methanol, transferred to a 6-dram vial, and dried using a rotovap then a high-pressure pump resulting in a yield of 40%.

The green GLY homopolymers were prepared by first adding glycidol monomer (33mmol, 1.0eq) to a flame dried 25 mL round bottom flask (RBF). The reaction vessels were then lowered into oil baths of varying temperature (60°C, 80°C, or 100°C) to ensure consistent reaction temperatures, followed by the addition of DPBS (0.25mL; pH= 6.0) to reach a concentration of 13.5 mM. After 72 hours, the crude viscous polymer product was dissolved in a minimal amount

of methanol and precipitated into vigorously stirring acetone. The resulting solution was decanted to afford the pure GLY product as a translucent viscous material. The product was collected in methanol, transferred to a massed 6-dram vial, and dried using a rotovap and a high-pressure pump resulting in a yield of 31.8% and a PDI of 1.1. Table 5 shows the Mn and Mw values as determined using poly(methyl methacrylate), poly(ethylene glycol), and poly(styrene) standards.

Table 5. Mean and weight average molecular weights for semibranched poly(glycidol) homopolymers determined using gel permeation chromatography with poly(methyl methacrylate), poly(ethylene glycol), and poly(styrene) standards.

Standards	Mn (g/mol)	Mw (g/mol)
poly(methyl methacrylate)	1101	1156
poly(ethylene glycol)	1253	1316
poly(styrene)	10380	10800

2.3 Microparticle fabrication using photoreactive copolymer inks and piezoelectric ink jet printing

Three photoreactive copolymer inks were prepared to fabricate microparticles with a wide range of softness, hydrophilicity, and network density. In a general procedure for the poly(carbonate) ink (PC Ink) and the poly(carbonate)-poly(glycidol) ink (PC:PG - 70:30 Ink), the allyl functionalized copolymers, poly(MEC MAC) and poly(GLY AGE) were solubilized in dimethyl sulfoxide (DMSO) before the addition of the 2,2-Dimethyoxy-2-phenylacetophenone (DMPA) photoinitiator calculated for 0.2 eq per alkene. After manual mechanical mixing, the dithiol 3,6-Dioxa-1,8-octanedithiol (0.5 eq per alkene) was added via syringe to the solution and mixed to form a homogenous solution. The addition order for the various ink components was varied for the PG Ink. For this ink we first dissolved the poly(GLY AGE) and solid dithiol-PEG (1.5 kDa), 0.5 eq per alkene, in half of the desired amount of water until completely dissolved, followed by the second half of water containing the water soluble photoinitiator (VA-44). The exact percentile of allyl functionality incorporation was determined using ^{1}H-NMR spectroscopy. If the molecular weight is unknown or cannot be exactly determined, the molecular weight of the

repetition unit containing the allyl functionality (AGE) or (MAC) can be used to determine the quantity of the allyl groups of the sample. This quantity can then be utilized to calculate the exact amount of the initiator and crosslinker needed in the stated equivalents.

The PC Ink was used to fabricate poly(carbonate) microparticles. In a more exact procedure the PC Ink was prepared as follows. Considering poly(MEC MAC) copolymers with a R.U. = 952.2 g/mol and a 20% MAC unit incorporation. First, 9.57 mg (8.55 μL) which equals 52.5 μmol of 3,6-Dioxa-1,8-octanedithiol (182.3 g/mol, 0.5 eq. per alkene) was added via micro syringe to a solution of 100 mg poly(MEC MAC), 2,2,-dimethoxy-2-phenylacetophenone (DMPA, 0.2 eq. per alkene, stock solution), and 1 mg of nile red in 200 μL DMSO.

The PG Ink was used to fabricate poly(glycidol) microparticles which was prepared as follows. Considering poly(GLY AGE) copolymers with a R.U. 410.5 g/mol and 20% of AGE unit incorporation. First, 182.7 mg = 121.8 μmol of HS-PEG-SH (1,500 g/mol, 0.5 eq. per alkene) was dissolved in 0.5 mL distilled water together with 100 mg poly(GLY AGE). A second solution of 0.5 mL distilled water and 15.74 mg = 48.72 μmol 2,2'-Azobis[2-(2-imidazolin-2-yl)propane] dihydrochloride (VA-044, 0.2 eq. per alkene) and <1 mg water-soluble sulfo-cyanine carboxylic acid Cy3 dye was then added to the first solution and mixed.

The PC:PG Ink was used to fabricate poly(carbonate)-poly(glycidol) microparticles. Since this ink was prepared with PC and PG at a weight ratio of 30:70 this ink will be abbreviated as PC:PG (70:30) Ink. The procedure is as follows when considering poly(MEC MAC) copolymers with a R.U. = 952.2 g/mol that have a 20% MAC unit incorporation and poly(AGE GLY) copolymers with a R.U. 410.5 g/mol with 20% AGE unit incorporation. First, 11.94 μL (13.36 mg, 73.3 μmol) 3,6-Dioxa-1,8-octanedithiol (182.3 g/mol, 0.5 eq. per alkene) was added via micro syringe to a solution of 70 mg poly(MEC MAC), 2,2-dimethoxy-2-phenylacetophenone (DMPA,

0.2 eq. per alkene, stock solution), 30 mg poly(GLY AGE) copolymer. and 1 mg of coumarin 30 in 400 μL DMSO.

After the ink was prepared, it was injected into a printer cartridge (Dimatix Materials Cartridge Model # DMC-11601/PN 700-10701-01) using a glass pipet. Both ink compositions that used DMSO as the solvent and contained hydrophobic network precursors (PC Ink and PC:PG (70:30)) were printed on glass slides coated with a sacrificial water-soluble poly(glycidol) coating. The poly(glycidol) was prepared as previously reported.[30] The glass slides were prepared by spin-coating with a sacrificial poly(glycidol) solution utilizing a Laurell Technologies Corporation, Model WS-400A-6NPP/LITE spin-coater. Before spin coating, each glass slide was cleaned using compressed nitrogen. The glass slide was then placed onto the spin-coater platform and the spin-coater was set to 3500 rpm with a spin time of 25 seconds. Immediately after the spinning was started 10 to 15 drops of a 1 g of poly(glycidol) in 1 g of methanol solution were added using a glass pipet. The coated slides were then allowed to air dry overnight. For the ink using water as a solvent and the hydrophilic network precursors (PG Ink) Teflon sheets were used as printing substrates.

Once the printer cartridge and appropriate substrates were prepared, the cartridge was inserted into the printer and the substrates were loaded onto the printer platform. The printer cartridge was then set to 37 °C and the recommended manufacturer's waveform was chosen and set to have a maximum voltage of 40 V as shown in Figure 6.

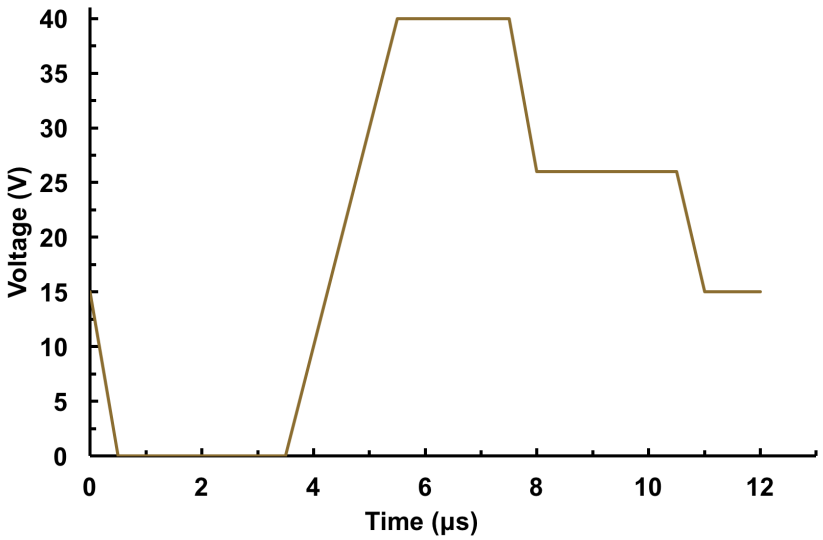

Figure 6. Multistep pulse waveform with a maximum voltage of 40 V used to eject one set of droplets from the printer cartridge nozzles.

The spacing between the printed droplets was then set for placement 100 microns apart from center to center in rows and columns on the 12" x 8" platform. After printing, the microparticles were illuminated with long wave UV light to initiate the crosslinking.

2.3.1 Characterization

Gelation kinetic studies were performed to determine the effect of molecular weight and concentration on copolymer gelation at constant concentration and molecular weight respectively. The model copolymers investigated were poly(carbonate) copolymers with 20% of allyl incorporation. For the constant molecular weight experiments the concentration was kept at 17.9 wt%. Whereas for the constant concentration experiments the molecular weight was kept at 6802 ± 35 g/mol. The solution was prepared in a glass vial using the same procedure as the PC Ink. Once prepared, the solutions were illuminated with long wave UV until gelation occurred. The gelation time was recorded as the time when the solution did not move upon vial inversion.

Fluorescent microscopy was used to investigate the size of fabricated microparticles and the microparticle-laden substrate. A Nikon AZ 100M wide field microscope equipped with a 5x

Plan Fluor was used to image the microparticles printed on the substrates. Excitation wavelengths were varied based upon the dye encapsulated within each particle. Microparticles containing nile red were irradiated with 543 nm light, while 488 nm was utilized for the coumarin 30 encapsulated microparticles, and 633 nm for the Sulfo-Cy7 encapsulated microparticles. The substrates were then washed with water in order to transfer the microparticles into confocal dishes for imaging on a Zeiss LSM 510 inverted confocal microscope to investigate the microparticle size precision, dye distribution throughout the microparticle, and the microparticle shape. The same wavelengths were utilized for the confocal microscope but with a 10x Plan Neofluar lens for wide field imaging to determine microparticle uniformity and a 63x Plan-APOCHROMAT OIL lens was used for investigation of single microparticles.

Mechanical testing was used on the hydrogel samples to investigate softness. The hydrogel samples were prepared using ink preparation procedures previously described. The resulting hydrogel products were tested in triplicate. For the mechanical testing a rate of 1 mm/min was utilized on an Instron 5944. The compressive modulus was determined using the initial linear region for each sample on the stress versus strain curves.

The hydrophilicity of bulk hydrogels was investigated using swelling studies. Bulk hydrogels were prepared using the ink preparation procedures as stated previously. Once the respective hydrogel was formed, the gels were then rinsed sequentially with 3 mL aliquots of water, methanol, methylene chloride, methanol and water again to remove any unreacted starting materials. The hydrogels were then freeze dried and weighed before commencing the swelling studies. The gel swelling was investigated by first soaking the gels in deionized water for 24 hours. Swelling measurements were then taken by gently blotting the gels dry before recording the

swelled mass. The percent water content post-swelling was quantified using the following equation:

$$\frac{(M_{sw}-M_{dry})}{M_{dry}} \times 100\% \quad (2)$$

where M_{sw} is the mass of the swelled hydrogel and M_{dry} is the weight of the dried gel.

2.4 Microparticle fabrication using photoreactive monomer inks and piezoelectric ink jet printing

Photoreactive monomer inks were developed to yield microparticles with low softness, high network density, and low hydrophilicity. The reactive monomer used for the ink was trimethylolpropane triacrylate, which polymerized via free radical polymerization to form crosslinked poly(acrylate) (PA) microparticles. Prior to ink preparation eosin Y (EY) stock solution was prepared in dimethyl sulfoxide (DMSO) (7.3 mg EY/mL DMSO). The trimethylolpropane triacrylate (TMPTA) monomer was purified by pipetting the pure monomer into the top of a 5 3/4" glass pipet filled with 80% inhibitor remover. Initially the liquid is allowed to flow from gravity, then it was slowly pressurized by hand utilizing a pipet bulb. The ink formulation was investigated by preparing three PA Inks, which will be denoted as PA Ink 1, 2, and 3. PA Ink 1 was prepared by first dissolving 51.1 µL of EY stock, 307.5 µL DMSO, 13.1 µL triethylamine (EtO_3), and <0.01 mg nile red (NR) in a 1-dram vial. Next, 782 µL of purified TMPTA was added to the 1-dram vial and vortexed vigorously for a few minutes to obtain a homogenous solution. PA Ink 2 was prepared in a similar way as PA Ink 1; however, 1803 µL of DMSO was added instead of 307.5 µL of DMSO. PA Ink 1-AA was also prepared in a similar way as PA Ink 1; however, 14.3 mg of ascorbic acid (AA) was added instead of EtO_3. After ink preparation, a small aliquot was syringed into a 1-dram vial and illuminated with blue light to ensure the solution gelled. After the gelation check test, the remaining solution was syringed into

a Dimatix Materials Cartridge Model # DMC-11610/PN 2100201146, and the printer head was snapped into place. The cartridge was then placed into the Dimatix 2831 inkjet printer and the polyvinyl alcohol film (PVA) was placed on the 12" x 8" platform. Utilizing the printer software the droplets were programed for placement 254 microns apart from center to center. The printer cartridge temperature was set to 37 °C. The printing height from the substrate was set to 2000 microns with a substrate height of 1000 microns. The waveform used to eject droplets is shown in Figure 7.

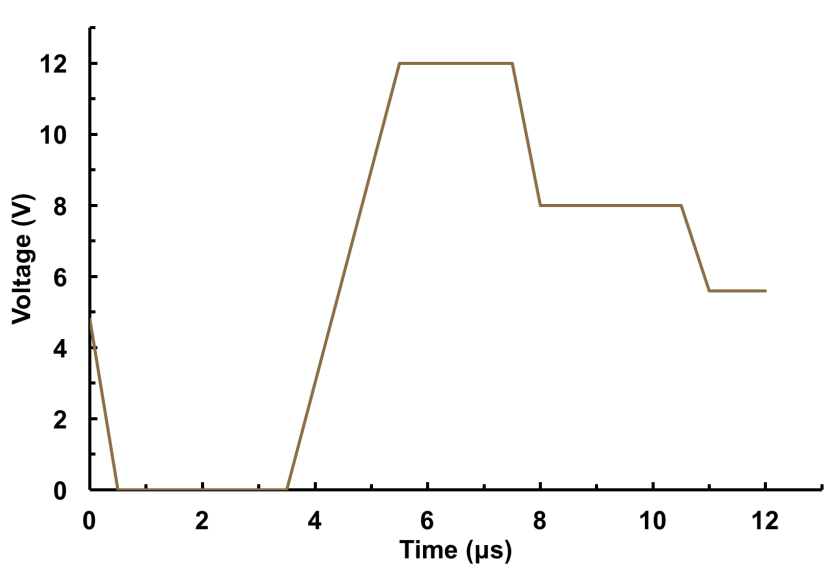

Figure 7. Multistep pulse waveform with a maximum voltage of 12 V used to eject one set of droplets from the printer cartridge nozzles.

Next, the printing was started and a desk lamp containing a sunlite® (80145/3W/B 3WE261506 120V 60Hz 46mA) blue light bulb was held approximately one cm above the substrate and moved behind the printer head. Figure 8 shows the strength of the light source with distance as determined utilizing a radiometer.

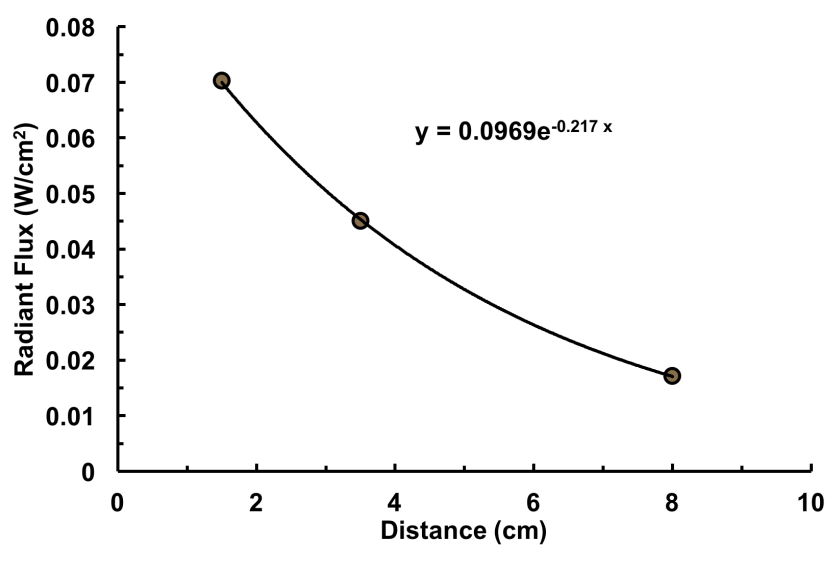

Figure 8. Radiant flux for the visible light source (desk lamp containing a sunlite® (80145/3W/B 3WE261506 120V 60Hz 46mA) blue light bulb) as a function of the distance from the radiometer.

Once the printing was completed the PVA film was placed in a container lined with aluminum foil where illumination with visible light was continued for at least five minutes. The printed film was kept covered until use.

2.4.1 Ink optimization via gel yield studies

Gelation kinetics of potential photoreactive ink components were investigated utilizing gel yield studies. These experiments were started by first pipetting 10 μL of the ink solution onto a Teflon substrate. The droplet was then illuminated with blue light for different periods of time depending on the rate of reaction. After each time point the droplet was moved into a 1-dram vial containing water. If the droplet dispersed in the water then it was noted that no gel was formed. However, if part of the droplet stayed intact in the water, then it was rinsed with three mL aliquots of methanol, dichloromethane, methanol, water, and then soaked in water for 24 hours. This ensured that any unreacted starting material was removed.

The gel was then freeze dried and the yield was determined utilizing the following equation;

$$\text{Gel yield (\%)} = \frac{W_{dry}}{W_{solid}} \times 100 \quad (3)$$

where W_{dry} is the weight of the freeze-dried gel and W_{solid} is the theoretical weight of solid in the initial droplet.

2.4.2 Drug loading and encapsulation efficiency of a model hydrophobic drug

Quantitation of a model hydrophobic drug ivermectin (875.1 g/mol) was determined utilizing high performance liquid chromatography (HPLC). The HPLC instrument was equipped with a Waters 2487 Dual λ Absorbance Detector, Waters binary HPLC pump, Waters In-line Degasser AF, Waters 600 Controller, Waters 717 plus Autosampler, and a reverse phase column (100 x 4.6 mm i.d., pore size 5 µm, Thermo Scientific). The mobile phase was composed of acetonitrile:water (75:25) and was degassed and filtered before use. An isocratic flow rate of 1 mm/min was used at 35 °C to elute the drug and the absorbance was taken at 243 nm. Serial dilutions of ivermectin in acetonitrile:water (ACN:H_2O 75:25) were prepared from 0.3 to 400 µg/mL for the calibration curve. The prepared calibration curve had an R-squared value of 0.99993. The encapsulation efficiency was determined for ivermectin loaded bulk hydrogels. This was done by first submerging the freshly gelled material in 100 mL of ACN:H_2O (75:25) for a few seconds to wash the gel of non-encapsulated ivermectin. Next, the ivermectin was quantitated in an aliquot from the 100 mL solution to determine the amount of ivermectin that was not encapsulated within the hydrogel.

The encapsulation efficiency was determined utilizing the following equation;

$$\frac{(M_{i,\ (i)} - M_{i\,(w)})}{M_{i,\ (i)}} \text{x } 100\% \quad (4)$$

where $M_{i,\,(i)}$ is the initial mass of ivermectin added to the ink solution and $M_{i,\,(w)}$ is the mass of the washed ivermectin as determined by HPLC.

2.4.3 Characterization

Fluorescent microscopy was used to investigate the microparticles on the poly(vinyl alcohol) PVA film and while suspended in water. The microparticles were irradiated with 543 nm light to induce fluorescence of the encapsulated nile red. Wide field fluorescent microscopy (Nikon AZ 100M) was used to investigate the droplet placement on the PVA film. Confocal imaging (Zeiss LSM 510) was used to investigate the microparticle size, microparticle shape, and distribution of the hydrophobic dye. For confocal analysis a piece of microparticle-laden PVA film was cut out and dissolved in a confocal dish containing water. The microparticles prepared from PA Ink 1 were sized using the 40x Plan-APOCHROMAT OIL lens and the Zeiss LSM Image Browser. The microparticles prepared from PA Ink 2 were sized using the 100x Plan-APOCHROMAT OIL lens. The z-stack for PA Ink 1 microparticles was taken using a 63x Plan-APOCHROMAT OIL lens. The z-stack for PA Ink 2 was taken using a 100x Plan-APOCHROMAT OIL lens.

Unconfined compression testing (Instron 5944) was used to evaluate the softness of hydrogels prepared from PA Ink 1 and 2. The bulk hydrogels were synthesized utilizing a syringe mold. Briefly, the top of a 6 mL syringe was cut off. Next, 1 mL of the solution was pipetted into the top of the syringe containing a syringe plunger. The top of the liquid was then illuminated for 20 minutes. The formed hydrogel was then popped out of the syringe with the syringe plunger and rinsed with 5 mL aliquots of water, methanol, dichloromethane, methanol,

and water. The hydrogel was then soaked in 225 mL of water for 24 hours and freeze-dried**.** Prior to compression testing the freeze-dried gels were soaked in deionized water for 24 hours. The compression head rate was set to 1 mm/min during testing. From the compression testing the stress versus strain curves were determined, and the compressive modulus was determined using the initial linear region from 0 to 2% for each sample.

Swelling studies were used to evaluate the hydrophilicity of the hydrogels. The studies were performed by measuring the weight change of freeze-dried gels after soaking in deionized water at 37 °C. The bulk gels for PA Ink 1 and 2 were fabricated in a syringe mold. Briefly, the top of a 1 mL syringe was cut off. Next, 150 µL of liquid was pipetted into the top of the syringe containing the syringe plunger. The top of the liquid was then illuminated for 10 minutes. The formed hydrogel was then popped out of the syringe with the syringe plunger and rinsed with 3 mL aliquots of water, methanol, dichloromethane, methanol, and water. Lastly, the hydrogel was soaked in 100 mL of water for 24 hours and freeze-dried. During testing the weight change was determined utilizing the following equation;

$$\frac{(M_s - M_d)}{M_d} \text{ x } 100 \quad (5)$$

where M_s is the mass of the swollen gel and M_d is the mass of the dry gel.

2.5 One-pot microparticles for controlled pulmonary drug delivery to eliminate malaria

Two PA inks were formulated that would result in microparticles with extremely different network properties. This was done to efficiently determine the range of tunable degradation and release kinetics, and thereby allow us to efficiently determine the optimal ink formulation. Prior to ink preparation, eosin Y (EY) stock solution was prepared in dimethyl sulfoxide (DMSO) at 7.3 mg EY/mL DMSO and trimethylolpropane triacrylate (TMPTA) was purified by flowing monomer through a 5 ¾" glass pipet filled with 80% inhibitor remover.

Initially the TMPTA is allowed to flow from gravitational forces, then is slowly pressurized by hand utilizing a pipet bulb. Ivermectin was then weighed in an aluminum foil wrapped 1-dram vial after which the EY stock, triethylamine, TMPTA, and DMSO were added. The solution was then vortexed to ensure all components were completely dissolved. Next, the TMPTA was added and the solution was vortexed again to obtain a homogenous solution. Table 6 shows the composition of the formulated inks.

Table 6. Formulated ink compositions for the fabrication of ivermectin loaded microparticles.

Ink	Eosin Y (mM)	Triethylamine (mM)	Trimethylpropyl triacrylate (mM)	Ivermectin (mM)	Ivermectin (wt%)*
PA Ink 1-IV13wt%	0.49	79.0	2445	126.7	13
PA Ink 2-IV13wt%	0.22	35.4	1096	57.2	13

*wt% is based on final dry weight of microparticles. Abbreviation IV = ivermectin.

2.5.1 *In vitro* release of ivermectin from bulk gels

Ivermectin loaded bulk gels were prepared from PA Ink 1-IV13wt% and PA Ink 2-IV13wt% ink compositions shown in Table 6. Gels were formed by pipetting 50 μL of ink solution into a cut-off 1 mL syringe. The blue light source, desk lamp containing a sunlite® (80145/3W/B 3WE261506 120V 60Hz 46mA), is rested on the syringe until complete gelation. The gels were then plunged from the syringe into a beaker containing 100 mL of ACN:H_2O (75:25) for several seconds before being removed into an empty glass vial.

The concentration of ivermectin was determined using high performance liquid chromatography (HPLC). The HPLC instrument utilized was an Agilent 1290 Infinity II LC System. The mobile phase was acetonitrile:water (75:25), and the method settings were set to 1 mm/min eluent flow rate, 35 °C column temperature, and 243 nm absorbance measurements. The calibration curve was prepared using serial dilutions of ivermectin in acetonitrile:water (75:25) from 0.3 to 400 μg/mL.

The *in vitro* ivermectin release from the bulk gels was performed in phosphate buffer saline (7.4 pH) containing 2 wt% tween 80 at 37 °C. Ivermectin solubility was determined as 3000 mg/mL in the release media using HPLC. The ivermectin solubility results in a perfect sink concentration less than 300 μg/mL which is 10% of the maximum ivermectin solubility in the media. The release study was performed in a 50 mL centrifuge tube containing perfect sink media at 37 °C under gentle stirring at 100 rpm. Once the media was ready the gel was dropped into the release media and 550 μL aliquots of media were taken over time for HPLC analysis. The removed volume for each time point was then replaced with fresh media to maintain perfect sink conditions.

2.5.2 *In vitro* degradation of bulk gels by reactive oxygen species

In vitro degradation of bulk gels was investigated at conditions relevant to the deep lungs. The most likely mechanism of degradation for hydrophobic poly(acrylate) in the lungs is through oxidation by reactive oxygen species. Here the H_2O_2 concentration is expected to be in the micromolar to tens of micromolar range.[31] The degradation study was performed at the higher end of this concentration range, 100 micromolar H_2O_2. Additionally, cobalt chloride was added in excess to generate free radical oxygen species that oxidize the esters in the poly(acrylate) backbone. The bulk gels for this experiment were prepared using PA Ink 1 and 2 in a similar way as the bulk gels for the release study. The degradation study was run in 45 mL of aqueous 100 μM H_2O_2 1.53 μM $CoCl_2$ that was gently stirring at 100 rpm. The degradation media was replaced twice weekly. For each measurement, the samples were removed from degradation media and soaked in 100 mL deionized water for three 30 minute periods, refreshing the deionized water each time. The gels were then freeze dried and weighed.

The gel weight loss over time was determined using the following equation;

$$\text{weight loss } (\%) = \frac{W_t}{W_i} \text{ x } 100 \quad (8)$$

where W_t is the dry weight after some period of time and W_i is the initial dry weight.

2.5.3 Characterization

Scanning electron microscopy (JEOL JSM 6400) was utilized to determine the microparticle size. The samples were first mounted on a metal stub containing double sided tape. They were then carbon coated with 400 nm layers using a Ladd Research Industries Vacuum Evaporator (Burlington, VT) before SEM imaging. The microparticle size was determined from the SEM images after which the aerodynamic diameter was calculated using the following equation;

$$\left(d_a = d_g\sqrt{\rho}\right) \quad (9)$$

where d_a is the aerodynamic diameter, d_g is the geometric diameter, and ρ is the bulk density.

Ink gelation kinetics were investigated using gel yield studies. First, 10 μL of ink solution was pipetted onto a Teflon substrate. Next, the droplet was illuminated with a blue light source (desk lamp containing a sunlite® 80145/3W/B 3WE261506 120V 60Hz 46mA) for different periods of time depending on the rate of reaction. After the specified time period the droplet was physically moved using a spatula into a 1-dram vial containing approximately 1 mL of water. If the droplet remained intact then it was considered that the gel was formed. If the gel fell apart and dispersed in the water then the gel was considered to not have formed. The water was then removed and the gels were washed with aliquots of methanol, dichloromethane, methanol, and water. The gels were then soaked in water for 24 hours and freeze-dried.

The gel yield was calculated using the following equation;

$$\text{Gel yield} = \frac{W_{dry}}{W_{solid}} \text{x } 100 \quad (11)$$

where W_{dry} is the weight of the freeze-dried gel and W_{solid} is the theoretical weight of solid in the initial droplet.

Rheometry (TA Instruments) was used to determine the viscosity of inks. A 40 mm plate geometry was used with a gap of 500 nm. The test type was a steady state flow with a 5% tolerance and a 1 minute max point time at 30 ºC. The shear rate was ramped from 400 1/s to 600 1/s linearly with 10 sample points each with a 5 second sample period.

2.5.4 Microparticle fabrication using piezoelectric inkjet printing

The microparticles were fabricated using a Dimatix materials printer (DMP-2850) with a Dimatix Materials Cartridge Model #DMC-11610/PN 2100201146. In a general procedure, the prepared ink was first injected into the cartridge using a glass pipet. The 16 nozzle printer head was then snapped to the cartridge and the assembled cartridge was inserted into the printer. The printer settings were then selected in the Dimatix software. The waveform selected was a multipulse waveform set to a maximum voltage of 12 V (see Figure 7). The nozzle temperature was set to 30 °C, the print speed to 1 kHz, the printed droplet spacing to 125 microns, the substrate height was set to 1000 microns, and the printing height above the substrate was set to 2000 microns. A 220 mm x 160 mm polyvinyl alcohol film was then placed onto the printing area and the printing was commenced. During printing the printer head was followed with a desk lamp containing a sunlite (80145/3W/B 3WE261506 120V 60 Hz 46 mA) blue light bulb that was held approximately one cm above the substrate. See Figure 8 for the strength of the light source with distance. After printing was complete, the light was illuminated on the printed substrate for another five minutes. The microparticles were then removed from the PVA film by

dissolving the film at a PVA concentration of approximately 6.7 mg PVA/mL D.I water in a 50 mL conical then spinning down at 7830 rpm for 5 minutes. The supernatant was then removed and the microparticles were spun down again, re-suspended with 1.5 mL of deionized water, and pipetted into a "stock conical". Once all microparticles were removed from the PVA film, the stock conical was spun down at 7830 rpm for 20 minutes and freeze-dried.

2.5.5 *In vitro* drug efficacy of ivermectin and ivermectin loaded microparticles

Chinese hamster ovary cells (CHO-K1, ATCC® CCL-61™) were purchased from American Type Culture Collection (ATCC®) and growth media was prepared by adding 10% FBS (Gibco, USA) and 5% penicillin/streptomycin to Kaighn's modification of Ham's F-12. Cells were grown in tissue culture flasks (75 cm^2) and maintained under 5% CO_2 atmosphere at 37 °C in complete growth media. After the cells reached approximately 80% confluency they were split and seeded at a 1:5 to 1:10 ratio.

Standard MTT (Invitrogen™ Molecular Probes™ Vybrant™) assays were used to determine the cell cytotoxicity of poly(acrylate) microparticles, pure ivermectin, and ivermectin loaded poly(acrylate) microparticles. CHO cells were used as model mammalian cells as done previously for ivermectin.[32] The MTT experiments were done as follows. The CHO cells were first harvested from confluent cultures by trypsinization. The concentration of cells in the suspension was then determined by counting the live cells in a 1:1 mixture of cell suspension:tryphan blue using a hemocytometer. The stock cell suspension was then adjusted to 50,000 cells/mL with complete media. The suspension (200 μL) was then pipetted to wells in a 96 well plate and incubated for 3 to 4 hours. After the cells were attached, the media was replaced with sample solutions suspended in complete media and incubated for 72 hours. The poly(acrylate) microparticles were prepared by fabricating bulk gels from PA Ink 1. The bulk

gels were then frozen using liquid nitrogen and crushed with a mortar and pestle. Suspensions of crushed microparticles were then prepared at 100, 10, 1, 0.1, and 0.01 μg/mL, and complete media was used as blanks for these samples. The pure ivermectin samples were prepared by preparing a stock solution of pure ivermectin in DMSO, then adding aliquots of this solution to complete media with 1 v/v% DMSO to obtain samples that had concentrations of 100, 10, 1, 0.1, and 0.01 μg/mL. Blanks composed of 1 v/v% DMSO were used for these samples. The ivermectin loaded poly(acrylate) microparticles were fabricated using the PA Ink 1-IV13wt% microparticle formulation. These samples were prepared by adding appropriate amounts of microparticles to complete media with 1 v/v% DMSO to obtain ivermectin concentrations of 100, 10, 1, 0.1, and 0.01 μg/mL after complete drug release. After the 200 μL sample solutions were incubated with the cells for 72 hours the sample solution was removed and 200 μL of PBS was used to wash the wells. Next, 150 μL of MTT solution (500 μg/mL in complete media) was added, and the wells were incubated for 3 to 4 hours. A 125 μL portion of the MTT solution was then removed and 50 μL of DMSO was added to dissolve the formed formazan crystals. The 96 well plate was then incubated at 37 °C for 10 minutes. After incubation, the sample absorbance at 540 nm was determined using a Tecan Infinite M200 PRO plate reader, and the cell viability was calculated using the following equation;

$$\text{Cell viability (\%)} = \frac{A_t}{A_c} \text{ x } 100 \qquad (12)$$

where A_t is the absorbance in A.U. for the test solution and A_c is the absorbance for the control solution.

2.5.6 *In vitro* transport of ivermectin from ivermectin loaded microparticles through a lung epithelial cell monolayer

Rat epithelial lung cells (RL-65, ATCC® CRL-10354) were purchased from American Type Culture Collection (ATCC®). The cells were grown in tissue culture flasks (75 cm^2) and maintained under 5% CO_2 atmosphere at 37 °C in a serum free media, Gibco™ DMEM/F-12 supplemented with 0.005 mg/mL insulin, 0.01 mg/mL human transferrin, 0.1 mM ethanolamine, 0.1 mM phosphoethanolamine, 25 nM selenium, 500 nM hydrocortisone, 0.005 mM forskolin, and 0.15 mg/mL bovine pituitary extract. The medium was exchanged three times weekly, and the cells were split 1:20 at 90% confluency.

The apparent permeability of ivermectin through rat lung cell monolayers from ivermectin loaded microparticles was investigated using an *in vitro* lung model. The ivermectin loaded microparticles were fabricated using the PA Ink 1-IV13wt% formulation. Transwell® cell culture supports (1.13 cm^2 polyester, 0.4 μm pore size) were seeded at a density of 1 x 10^5 cells/cm^2. The cells were allowed to attach for 24 hours before removing the media to develop cells at air-liquid (AL) interface conditions. The AL conditions were established by adding 0.5 mL of media to the basolateral chamber only, which was replaced every other day. The media utilized for these studies was Gibco™ DMEM/F-12 supplemented with 10% v/v Gibco™ fetal bovine serum and 100 IU/mL penicillin and 100 ug/mL streptomycin antibiotic solution. Over time trans-epithelial electrical resistance (TEER) measurements were recorded using a Millicell® ERS-2 Volt-Ohm Meter with MERSSTX01 electrodes. Before taking resistance measurements 0.5 and 1 mL of media were added to the apical and basolateral chambers respectively and allowed to equilibrate in the incubator for 20 minutes. The measured value was corrected for the resistance and surface area of the Transwell® filters. Additionally, before starting the transport

experiments the TEER value for the cell monolayers were taken and only cells with a monolayer resistance greater than 250 Ω cm^2 were used as suggested by Hutter et al.[33]

The transport experiment was performed by first equilibrating the cell monolayers with 1.5 mL of PBS 2 wt% tween in the basolateral compartment and 0.51 mL of PBS 2 wt% tween in the apical chamber for one hour. The buffer solution in the basolateral chamber was then refreshed with 0.51 mL of sample solution. The same initial concentration was used for each sample solution which was chosen to ensure perfect sink conditions were maintained. After certain periods of time 550 μL samples were taken from the basolateral chamber for HPLC analysis. The removed media was replaced with fresh buffer to ensure perfect sink conditions were maintained. Using the transport profile the apparent permeability coefficients were determined as done by Lang et al.[34] using the following equation

$$P_{app} = \left(\frac{d[I]}{dt}\right)_{ss} \frac{V}{AC_0} \quad (13)$$

where P_{app} is the apparent permeability coefficient, $(d[I]/dt)_{ss}$ is the change of concentration with time across the transwell filter, A is the surface area of the transwell filter, C_0 is the initial amount of drug in the apical compartment, and V is the volume of the receiver compartment.

CHAPTER 3

3. RESULTS AND DISCUSSION

3.1 Novel functionalized copolymers for microparticle fabrication

3.1.1 Hydrophobic linear poly(carbonate) copolymers

Hydrophobic functionalized linear poly(carbonate) copolymers were fabricated as one of the network precursor copolymer building blocks for microparticle fabrication. Poly(carbonate)s are advantageous over other copolymers due to their degradation products being less acidic than other copolymers used for drug delivery such as poly(ester)s. As done previously by our group the poly(carbonate) copolymers were synthesized through the copolymerization of methyl ethyl carbonate and methyl allyl carbonate using ring opening metathesis polymerization with $Sn(OTf)_2$ as the catalyst.[35] In this work, the copolymers were synthesized to contain 20% of allyl incorporation which can react with dithiol crosslinkers through a thiolene "click" reaction. To ensure extended release of drug was achieved the copolymers were synthesized with a mean average molecular weight of 4,000 g/mol which should result in small mesh sizes. After synthesis, the mean average molecular weight was determined using ^{1}H-NMR. Figure 9 shows a representative ^{1}H-NMR spectrum for the poly(carbonate) copolymer.

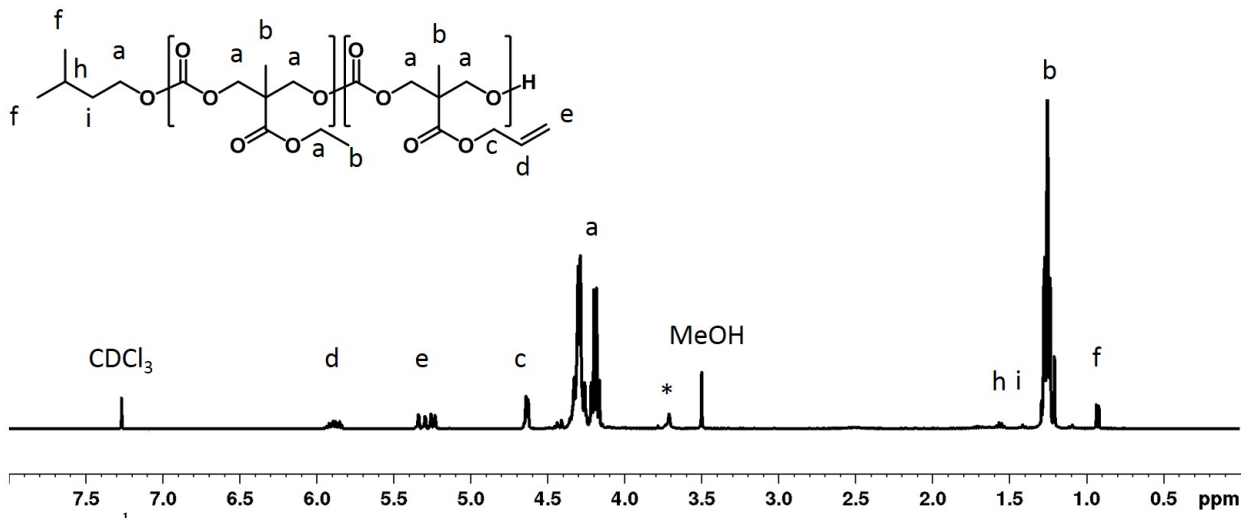

Figure 9. ^{1}H-NMR for the methyl ethyl carbonate:methyl allyl carbonate (MEC:MAC) copolymer in $CDCl_3$ (* = protons from terminal unit on polymer). δ: 5.91-5.85 (m, -OCH_2CHCH_2), 5.34-5.23 (m, -OCH_2CHCH_2), 4.64-4.62 (m, -OCH_2CHCH_2), 4.0-4.15 (m, MAC and MEC, -$OC(O)OCH_2$), 1.30-1.22 (m, MAC and MEC, CH_3; MEC, -OCH_2CH_3), 0.93-0.91 (d, 3-methyl-1-butanol, $OCH_2CH_2CH(CH_3)_2$).

The mean average molecular weight was determined by first setting the doublet f at 0.9 ppm shown in Figure 9 to 2.0. Peaks i at 1.24 ppm and d at 6 ppm were then integrated. The mean average molecular weight was then calculated using the following equation;

$$\mathrm{M_n} = \frac{(([\mathrm{i}]-(4*[\mathrm{d}]))}{6} * [\mathrm{MEC\ M_W}] + [\mathrm{d}] * [\mathrm{MAC\ M_W}] \qquad (14)$$

where MEC M_W is the molecular weight of methyl ethyl carbonate (188.18 g/mol), MAC M_W is the molecular weight of methyl allyl carbonate (200.19 g/mol), [i] is the integrated area for the i peak, and [f] is the integrated area for the f peak. The methyl ethyl carbonate percentage of incorporation was calculated using the following equation;

$$\mathrm{MEC\ (\%)} = \frac{\frac{(([\mathrm{i}]-(4*[\mathrm{d}]))}{6} * [\mathrm{MEC\ M_W}]}{\mathrm{M_n}} \mathrm{\ x\ 100} \qquad (15)$$

where Mn is the mean average molecular weight calculated from equation (14).

The methyl allyl carbonate % of incorporation was calculated using the following equation;

$$\text{MAC (\%)} = \frac{[d]*[\text{MAC } M_W]}{M_n} \text{x } 100 \quad (16)$$

where Mn is the mean average molecular weight calculated from equation (14). Mn values ranged from 4,000 to 4,300 g/mol with 20% MAC incorporation.

3.1.2 Hydrophilic semibranched poly(glycidol) copolymers

The second copolymer synthesized was opposite of character to the hydrophobic linear poly(carbonate) copolymer. This copolymer was a hydrophilic semibranched poly(glycidol) that was also synthesized to contain 20% of pendant allyls that can react with dithiol crosslinkers. These copolymers were synthesized through the copolymerization of glycidol (GLY) and allyl glycidol ether (AGE) using cationic polymerization with $Sn(OTf)_2$ as the catalyst. This synthesis strategy was done previously in our lab for a homopolymerization of poly(glycidol).[30] This polymerization was invented in our lab and is more advantageous over traditional methods to fabricate branched poly(glycidol) since it doesn't use protection of hydroxyl groups and it is much more controlled. Traditionally without the protection of glycidol monomers hyperbranched structures occur with no degree of control over the branching through anionic polymerization under stringent water free conditions.[36] In general, hyperbranched poly(glycidol)s have a degree of branching of 0.56 to 0.63 where a 0.0 degree of branching would be a linear poly(glycidol).

Additionally, these copolymers overcome the limitations of conventional PEG equivalents due to their increased tunability. For example, PEG copolymers are typically only commercially available in high molecular weights which result in large mesh sizes and fast release rates. Whereas our poly(glycidol) copolymers were synthesized at small molecular weight to target smaller mesh sizes and slow release rates. The low copolymer molecular weight is also advantageous for its faster elimination after the microparticle structure degrades. Additionally, commercially available

PEG copolymers are not branched like the synthesized poly(glycidol) in this work. The branched nature of the poly(glycidol) copolymers results in a large amount of hydrophilic end groups which results in the copolymer having a high hydrophilicity. These properties make the copolymer water soluble and give it an ability to protectively solubilize biologicals which improves their biological half-life and circulation time.[37] Additionally, the hydroxyl groups open the doors to graft molecules for specialized applications in drug delivery.[38]

Inverse gated ^{13}C-NMR was utilized to determine the degree of branching. Figure 10 shows a comparison of the GLY/AGE (80:20) copolymer and GLY homopolymer catalyzed with $Sn(OTf)_2$.

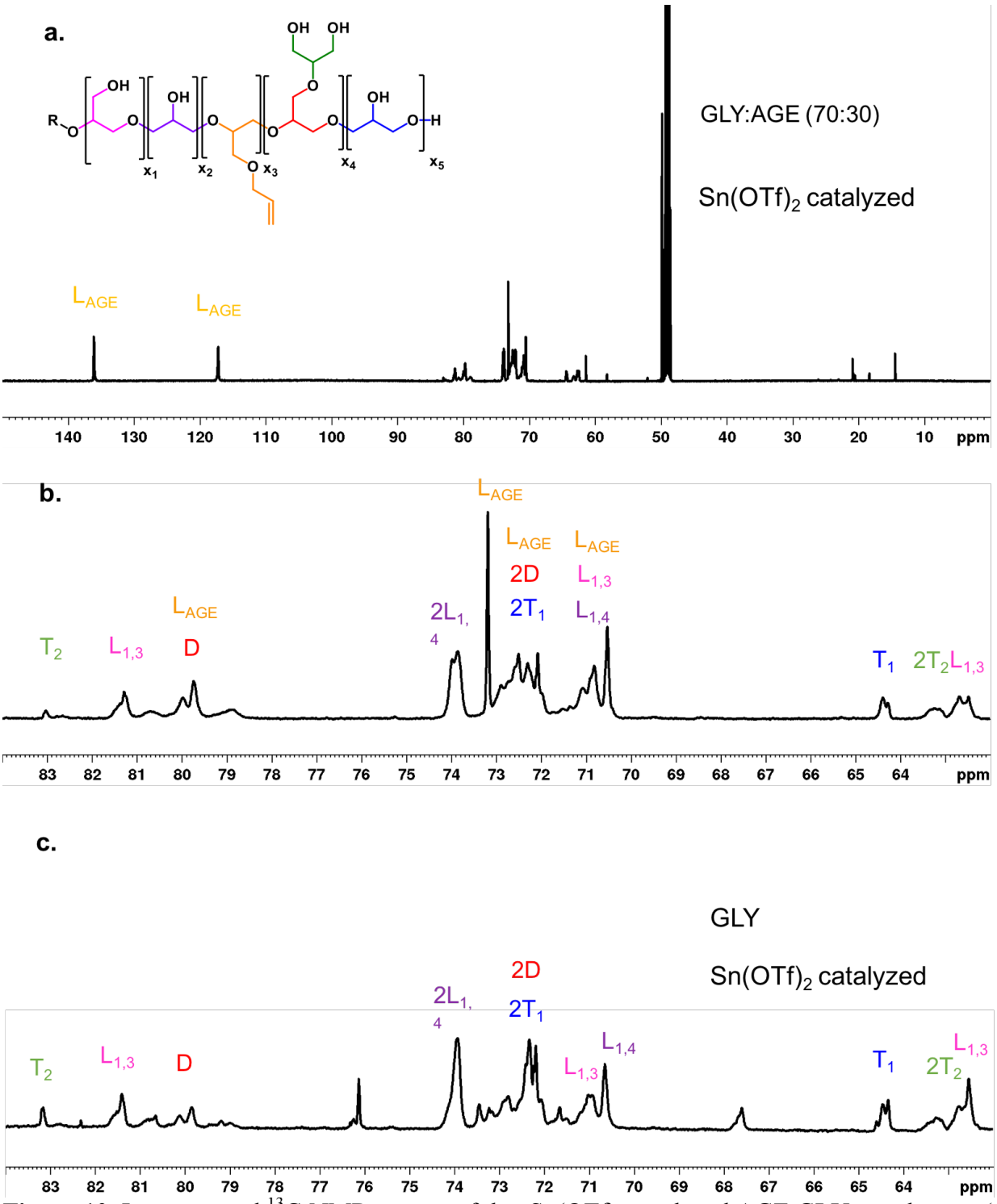

Figure 10. Inverse gated ^{13}C-NMR spectra of the; $Sn(OTf)_2$ catalyzed AGE:GLY copolymers (a. full spectra and b. zoomed in spectra), ^{13}C-NMR (150MHz, MeOD) δ: 136.31, 117.39, 81.37, 79.81, 75.12, 73.88, 72.01-72.94, 70.42-71.17, 64.41, 62.53, 62.06, 27.99, 27.60 and the $Sn(OTf)_2$ catalyzed GLY homopolymers (c. zoomed out spectra), ^{13}C-NMR (150MHz, $MeOD_4$) δ: 81.33, 79.75 73.84, 72.36, 70.90, 70.62, 64.32, 62.71.

The degree of branching was calculated for the AGE:GLY copolymer using the following equation

$$\text{Degree of branching} = \frac{(2*\text{D})}{(2*\text{D}+\text{L}_{1,3}+\text{L}_{1,4}+\text{L}_{\text{AGE}})} \quad (17)$$

where D, $L_{1,3}$, $L_{1,4}$ and L_{AGE} are the integrated peaks corresponding to each repeat unit. Whereas the degree for the GLY homopolymer was calculated using the following equation

$$\text{Degree of branching} = \frac{(2*\text{D})}{(2*\text{D}+\text{L}_{1,3}+\text{L}_{1,4})} \quad (18)$$

The degree of branching for the AGE/GLY copolymer and GLY homopolymer were 0.21 and 0.39 respectively which indicate semibranched structures and that the GLY homopolymer had a higher degree of branching than the AGE/GLY copolymer. The allyl group incorporation for the green AGE/GLY copolymers was determined using ^{1}H-NMR. Figure 11 shows a representative ^{1}H-NMR spectrum for the copolymer in $MeOD_4$.

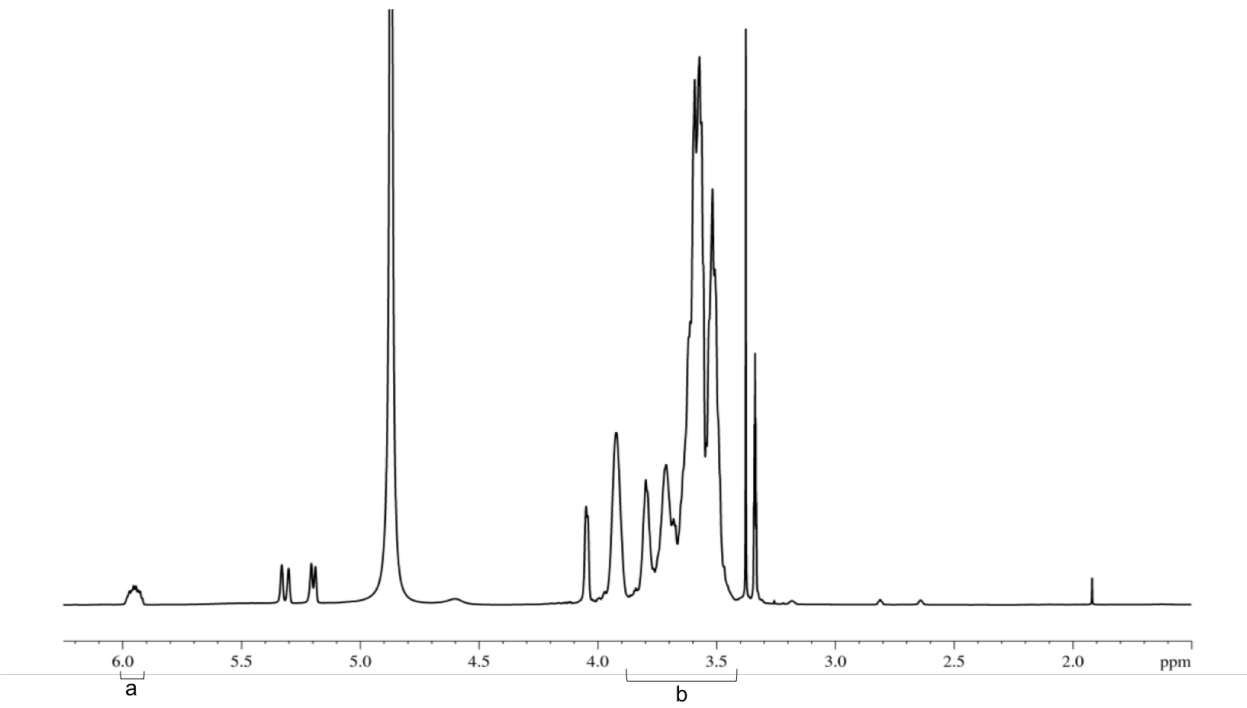

Figure 11. ^{1}H-NMR for the AGE/GLY copolymer in $MeOD_4$, δ:6.0-5.90 (m, –OCH_2CHCH_2), 5.37–5.17 (m, –OCH_2CHCH_2) 3.97-3.42 (6H).

The allyl group incorporation was determined as follows. First, the number of GLY monomers per repeat unit were calculated using the following equation

$$\text{GLY R. U. (\#)} = \frac{[b] - 4}{4} \tag{19}$$

where [b] is the area of the peak integrated in Figure 11. The allyl group incorporation was then calculated using the following equation

$$\text{AGE (\%)} = \frac{[a]}{[a]+\text{GLY R.U.(\#)}} \text{ x } 100 \tag{20}$$

where [a] is the area of the peak integrated in Figure 11. The molecular weight of the repeat unit (R.U.) was then calculated using the following equation

$$\text{R. U. (g/mol)} = \text{AGE } M_W + \frac{\text{GLY (\%)}}{\text{AGE (\%)}} * \text{GLY } M_W \tag{21}$$

where AGE Mw and GLY Mw are the molecular weights of the monomers which are 114 g/mol and 74 g/mol respectively. Incorporation of AGE was 20% as determined using ^{1}H-NMR.

The poly(glycidol) was also synthesized using a "green synthesis". The advantage of this synthesis is that it is run in water without the $Sn(OTf)_2$ catalyst, and a higher degree of control is afforded. For example, the PDI for the $Sn(OTf)_2$ poly(glycidol) was 1.6 whereas the green synthesis results in a PDI of 1.1. The temperature for the homo GLY polymerization was optimized to ensure the best yield and purity. We found that the polymerization at 60 °C resulted in a very low yield, 100 °C resulted in impurities present, and 80 °C to be the optimal reaction temperature in terms of yield and purity. In a similar way as reported for the $Sn(OTf)_2$ synthesized GLY/AGE and GLY copolymers, the degree of branching was also determined for the green synthesized GLY/AGE and GLY copolymers using inverse gated ^{13}C NMR. Figure 12 shows representative ^{13}C-NMR spectra for the green synthesized GLY/AGE (70:30) copolymer and GLY homopolymer.

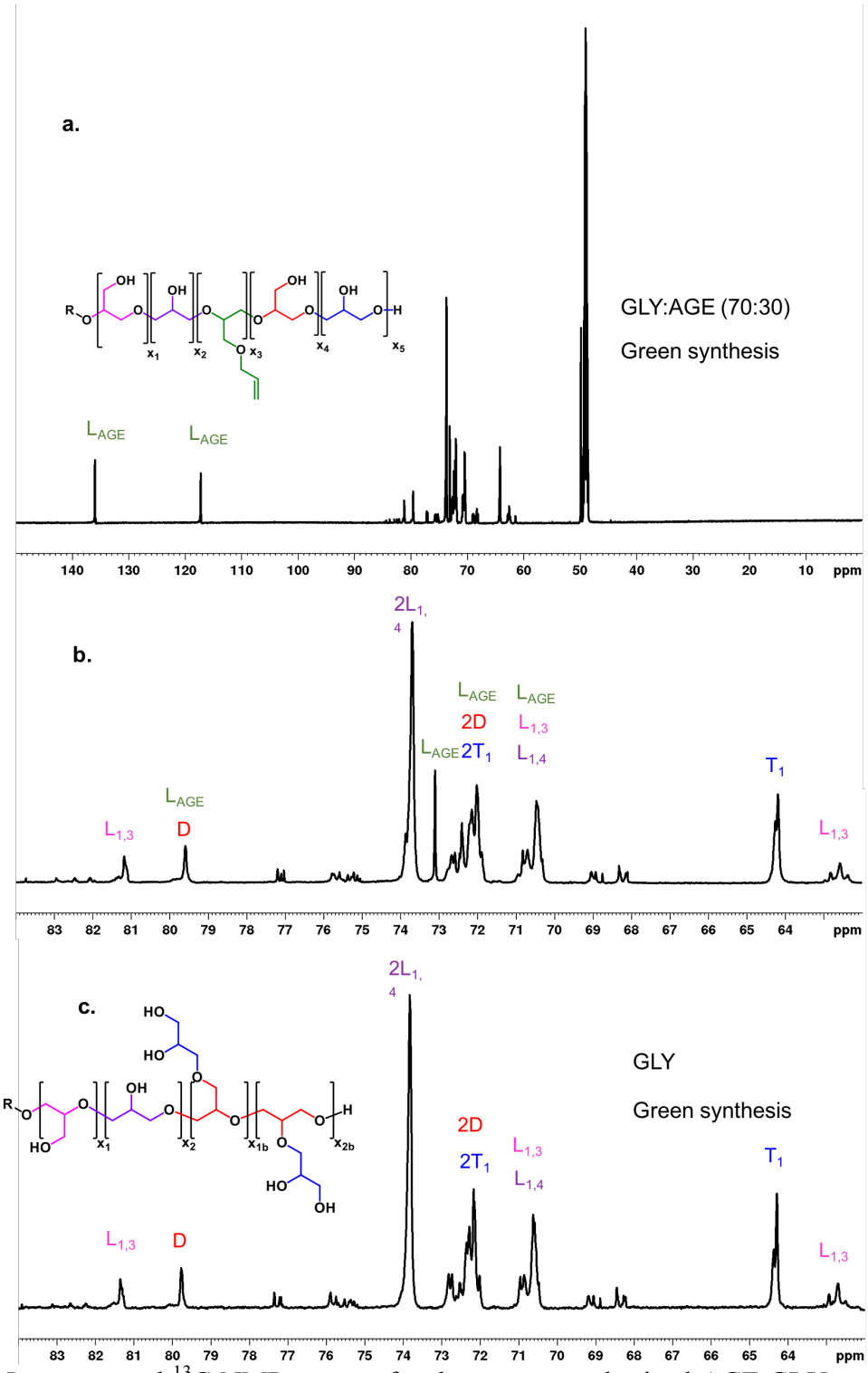

Figure 12. Inverse gated ^{13}C-NMR spectra for the; green synthesized AGE:GLY copolymer (a. full spectra and b. zoomed in spectra), ^{13}C-NMR (150MHz, $MeOD_4$) δ: 136.31, 117.39, 81.37, 79.81, 75.12, 73.88, 72.01-72.94, 70.42-71.17, 64.41, 62.53, 62.06, 27.99, 27.60; green synthesized GLY homopolymer (c. zoomed out spectra), ^{13}C-NMR (150MHz, $MeOD_4$) δ: 81.33, 79.75 73.84, 72.36, 70.90, 70.62, 64.32, 62.71.

The degrees of branching were calculated using equations (17) and (18) for the green synthesized AGE/GLY copolymer and GLY homopolymer which were determined as 0.21 and 0.25 respectively. These values indicate semibranched structures, with the GLY homopolymer having a higher degree of branching than the AGEGLY copolymer. MALDI was utilized to determine the Mn and Mw of the green synthesized homopolymer. In order to determine the molecular weight of the polymer species, direct integration of the obtained peaks was performed. This allowed for the calculation of Mn and Mw values, which also allowed for the determination of PDI. Shown in Figure 13 representative peaks are identified and assigned to a structural unit of the poly(glycidol). M_x* + M = 1 polymer chains were initiated by water and correspond to monomer units illustrated.

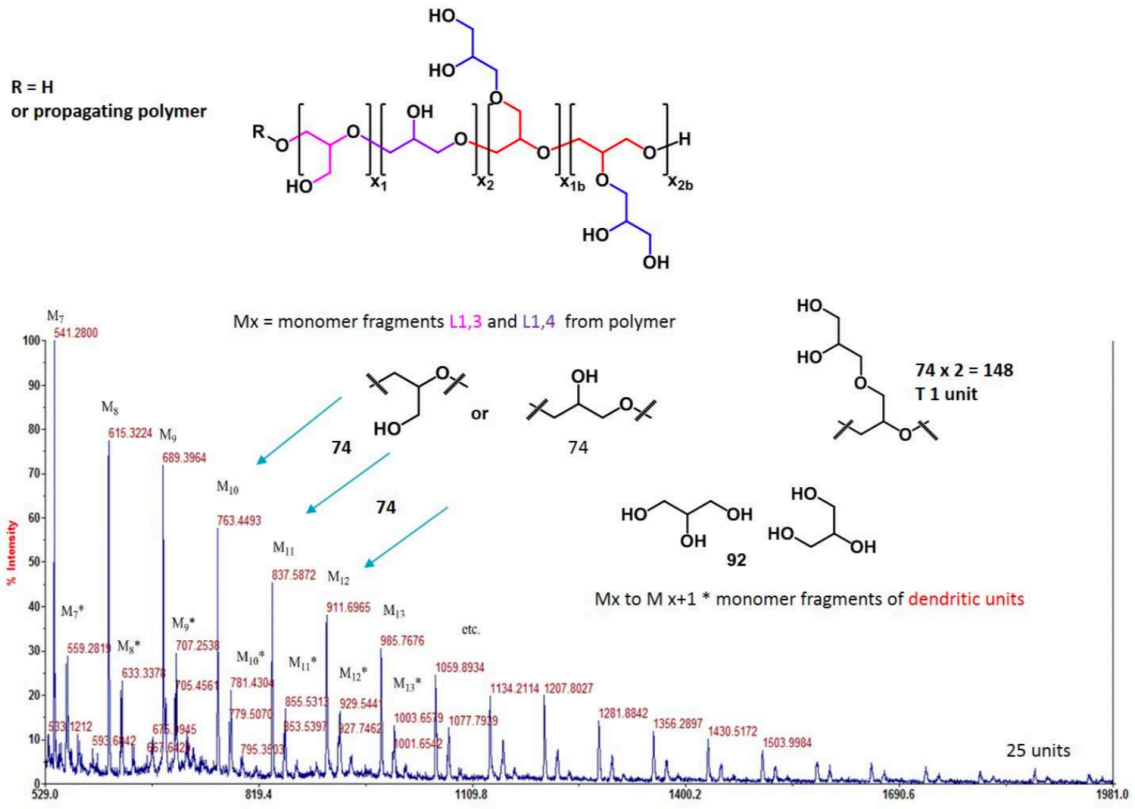

Figure 13. MALDI spectra of the green synthesized poly(glycidol) homopolymer.

The Mn was determined from the MALDI spectra as 925 g/mol and the Mw was determined as 1041 g/mol which results in a PDI of 1.1. The allyl incorporation for the green synthesized

AGE/GLY copolymer was determined as 11% using the integrated ^{1}H-NMR spectrum and equation (20). When we targeted for a higher incorporation of AGE into the copolymer using a 50/50 feed ratio of the monomers, the polymerization achieved very low yield.

3.2 Microparticle fabrication using photoreactive copolymer inks and piezoelectric ink jet printing

The goal for the photoreactive inks was to develop a minimal amount of inks that can be utilized to fabricate microparticles with a wide range of properties important in drug delivery. This results in one comprehensive technology to fabricate microparticles for a wide range of drug delivery applications. This goal was partly accomplished by developing a small set of diverse tunable copolymers and strategic selection of other ink components. The developed inks allow for tunability of properties important in drug delivery such as the release kinetics, type of drug loading (synthetic hydrophobic, synthetic hydrophilic, and/or biologicals), and microparticle circulation time. In general, the inks allowed for the preparation of microparticles with tunable release kinetics through tuning microparticle network density, the type of drug loading through the final microparticle hydrophilic character, and the circulation time through the microparticle softness.

3.2.1 Poly(carbonate) microparticles

PC Ink 1 was utilized to fabricate poly(carbonate) microparticles. The target properties for these microparticles were high to medium network density, low hydrophilicity, and high to medium softness. Figure 14 shows a scheme that contains the chemical structures for the ink components and the proposed chemical structure for the crosslinked microparticles.

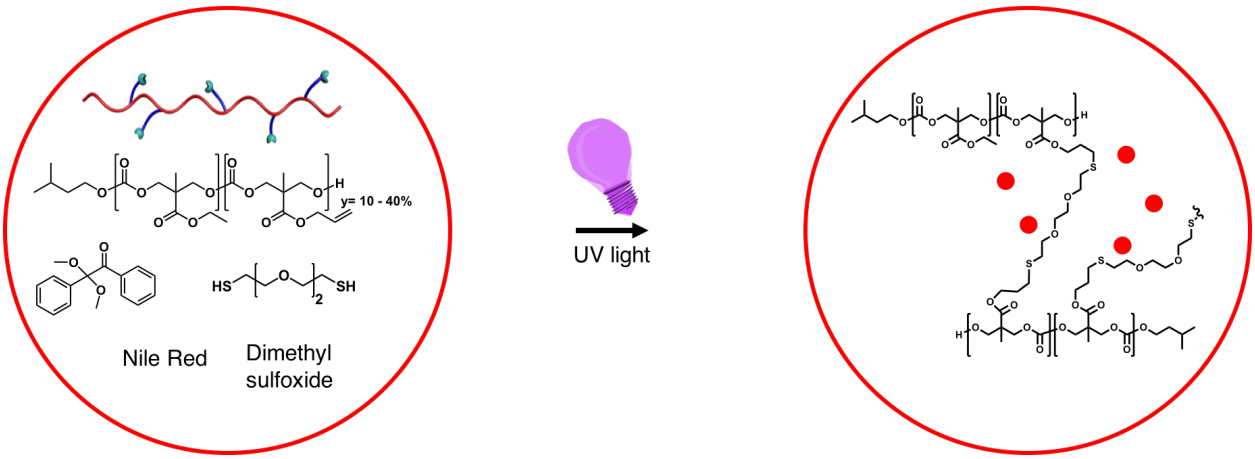

Figure 14. Chemical structures for the PC ink components and the crosslinked microparticle network.

The high to medium network density comes from the incorporation of 10 to 40% of reactive monomers in the copolymer and the incorporation of a crosslinker that only has 2 repeat units. The low hydrophilicity comes from the fact that there are no hydrophilic functional groups in the copolymer. The high to medium softness comes from the 10 to 40% of reactive monomer incorporation and the crosslinker that only has 2 repeat units. The crosslinking for this ink occurs through a thiolene "click" reaction. The reason for this name is that it occurs rapidly, and is also very efficient.[39] These fast gelation kinetics are important in printing applications for high-throughput microparticle production. Furthermore, 2,2-Dimethoxy-2-phenylacetophenone (DMPA) is the initiator incorporated which is activated via UV light, and nile red is incorporated to enable visualization of the microparticles after printing. Dimethyl sulfoxide is used because it is able to dissolve chemically diverse species. Although this ink is optimal for fabrication of hydrophobic microparticles that are optimal for an extended release of hydrophobic drug, a hydrophilic drug could also be incorporated allowing for dual drug loading.

Confocal microscopy was utilized to image the distribution of the fluorescent molecule throughout the microparticle, as well as to investigate the shape and size precision of the fabricated microparticles. Figure 15a and 15b shows a still image and a z-stack of the microparticles floating

in water respectively. The z-stack is a collection of several images that start at the bottom of the microparticles and move to the top of the microparticles along the z axis at a constant x and y location. Utilizing the software for the microscope, the microparticle size was determined as 10.6 ± 0.5 μm, resulting in a low CV of 5%. Furthermore, as shown in Figures 15a and 15b the nile red has good uniformity throughout the microparticles and the microparticles are spherical.

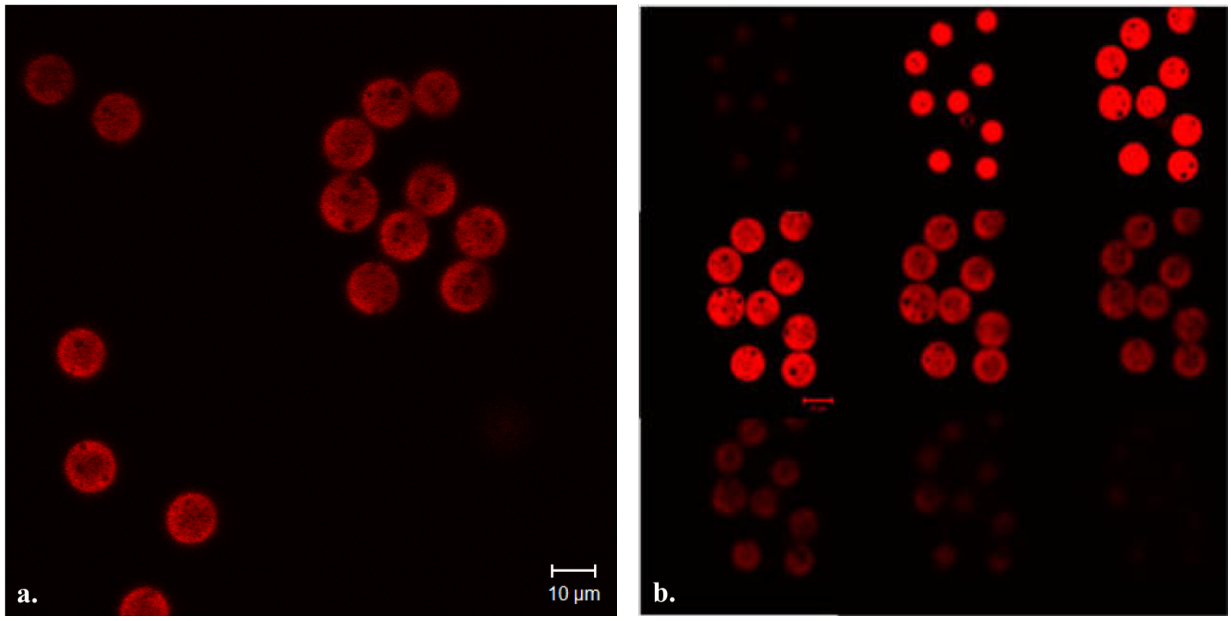

Figure 15. PC Ink; a. confocal image of microparticles floating in water (scale bar = 10 μm) and b. confocal z-stack images of microparticles floating in water (scale bar = 10 μm).

3.2.2 Poly(glycidol) microparticles

PG Ink 2 was utilized to fabricate poly(glycidol) microparticles. The target properties for these microparticles were medium to low network density, high hydrophilicity, and high to medium softness. Figure 16 shows a scheme that contains the chemical structures and the proposed structure for the crosslinked microparticles.

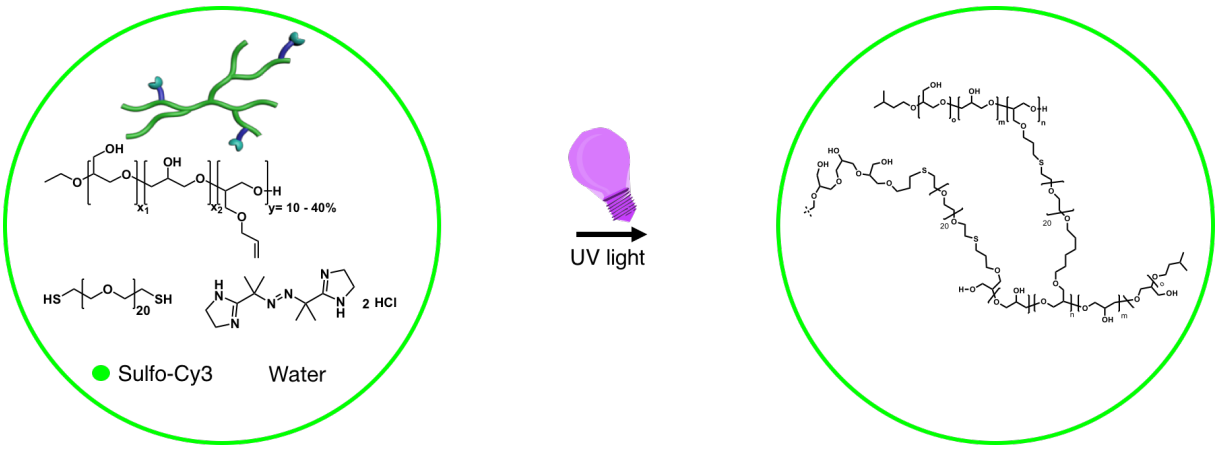

Figure 16. Chemical structures for the PG ink components and the crosslinked microparticle network.

The medium to low network density comes from the incorporation of 10 to 40% of reactive monomers in the copolymer and the incorporation of a crosslinker that has 20 repeat units, 10 times more repeat units than the poly(carbonate) ink crosslinker. The high hydrophilicity comes from the high number of hydrophilic end groups on the semibranched copolymer. The high to medium softness comes from the 10 to 40% of reactive monomer incorporation and the crosslinker that has 20 repeat units. The crosslinking for this ink also occurs through the thiolene "click" reaction. However, the solvent used in this ink is water. Additionally, the poly(glycidol) copolymer can be prepared through a green synthesis. Therefore, from copolymer preparation to the final formulation this ink has the ability to be completely green. This feature makes the ink attractive for the incorporation of biological therapeutics. However, due to the change in solvent, VA-044 and Sulfo-Cy3 are incorporated as the initiator and the fluorescent dye respectively.

As stated previously confocal imaging was utilized to investigate the distribution of the fluorescent molecule throughout the microparticle, as well as to investigate the shape and size precision of the fabricated microparticles. Figure 17a and 17b shows a still image and a z-stack of the microparticles floating in water respectively. Utilizing the software for the microscope, the microparticle size was determined as 2.4 ± 0.2 µm, resulting in a low CV of 8%.

Furthermore, as shown in Figure 17a and 17b the dye is homogenously distributed throughout the microparticles and the microparticles are spherical.

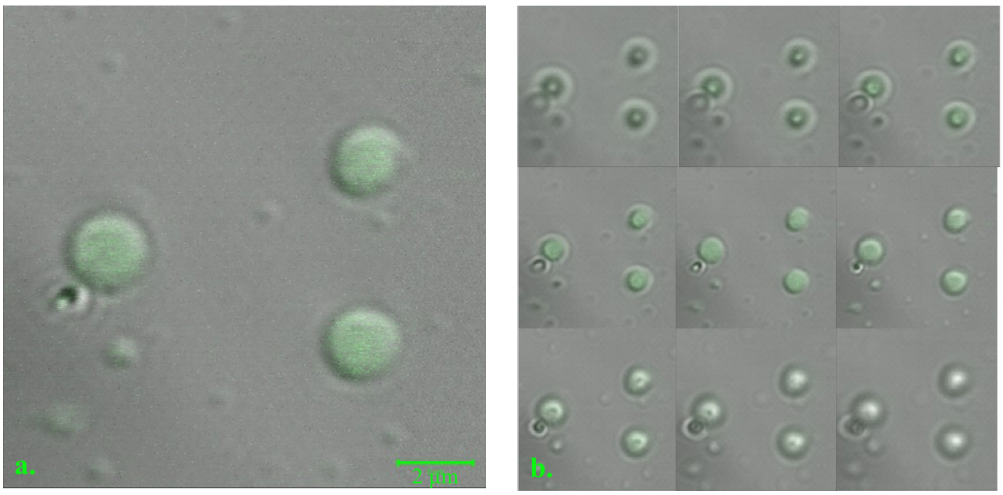

Figure 17. PG Ink; a. confocal image of microparticles floating in water (scale bar = 2 μm) and b. confocal z-stack images of microparticles flowing in water.

3.2.3 Poly(carbonate)-poly(glycidol) microparticles

PC:PG (70:30) Ink was utilized to fabricate poly(carbonate)-poly(glycidol) microparticles. The target properties for these microparticles were high to low network density, intermediate hydrophilicity, and high to low softness. Figure 18 shows a scheme that contains the chemical structures and the proposed crosslinked structure.

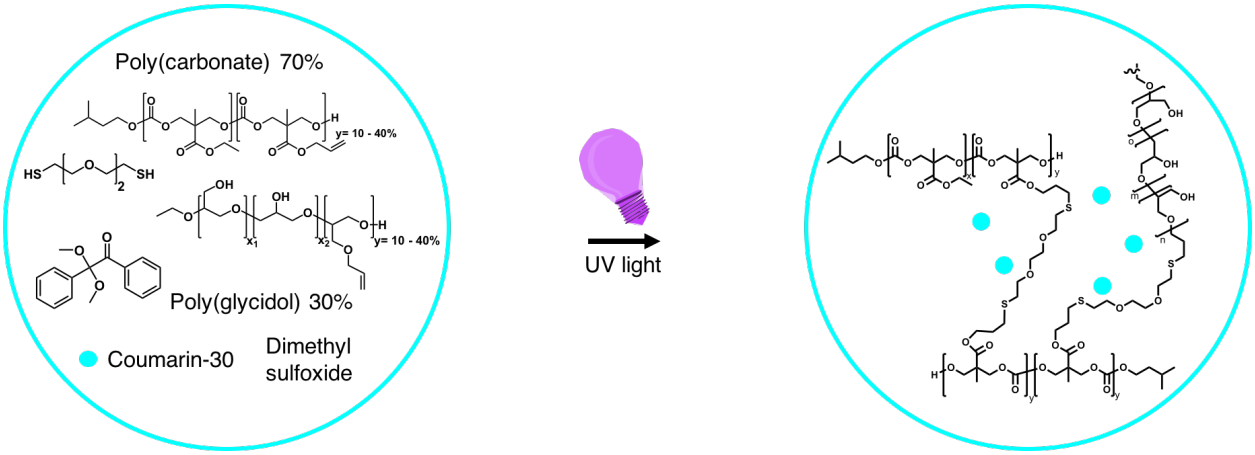

Figure 18. Chemical structures for the PC:PG (70:30) ink components and the crosslinked microparticle network.

The high to low network density comes from the incorporation of 10 to 40% of reactive monomers in the copolymer and the incorporation of a crosslinker that has 2 repeat units. However, a crosslinker of 20 repeat units could also be incorporated to expand the degree of tunability. The intermediate hydrophilicity comes from the incorporation of both hydrophilic and hydrophobic copolymers. The high to low softness comes from the 10 to 40% of reactive monomer incorporation and the utilization of a crosslinker that has 2 or 20 repeat units. The crosslinking for this ink also occurs through the thiolene "click" reaction. However, the solvent used in this ink is dimethyl sulfoxide. As stated previously dimethyl sulfoxide is important as the solvent for this ink because it can also dissolve diverse chemical species such as the incorporated hydrophilic and hydrophobic copolymers. Lastly, DMPA and coumarin-30 are incorporated as the initiator and dye respectively.

As stated previously confocal imaging was utilized to investigate the distribution of the fluorescent molecule throughout the microparticle, as well as to investigate the shape and size precision of the fabricated microparticles. Figure 19a and 19b shows a still image and a z-stack of microparticles floating in water respectively. Utilizing the software for the microscope, the microparticle size was determined as 13.3 ± 1.2 μm, resulting in a low CV of 9%. Furthermore, as shown in Figure 19a and 19b the dye is homogenously distributed throughout the microparticles and the microparticles are spherical.

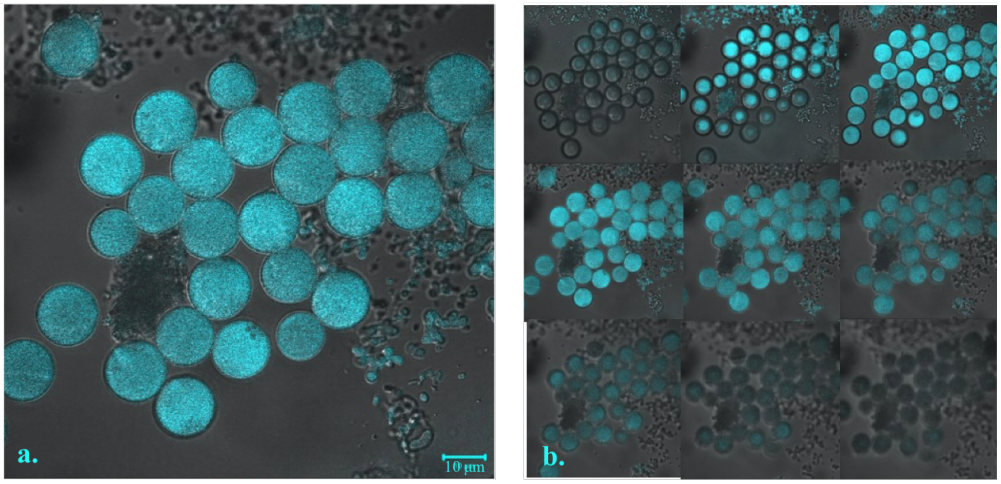

Figure 19. PC:PG (70:30) Ink; a. confocal image of microparticles floating in water (scale bar = 10 µm), and b. confocal z-stack images of microparticles floating in water.

3.2.4 Effect of copolymer molecular weight on gelation kinetics

The effect of copolymer molecular weight on the gelation kinetics was investigated. The gelation kinetics are important in printing applications to increase high-throughput production through increasing gelation kinetics. Figure 20 shows the poly(carbonate) copolymer molecular weight versus the gelling time for PC Ink formulations with three different molecular weight copolymers. The results show that as the copolymer molecular weight increases the PC Ink gelation time also increases. This trend was also observed for a glutaraldehyde crosslinked chitosan gelation studies performed by other researchers.[40]

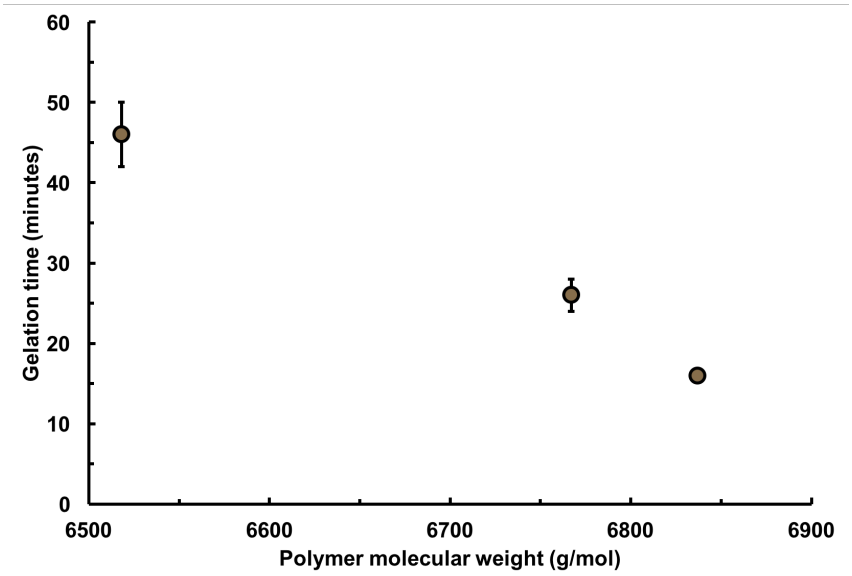

Figure 20. Effect of poly(carbonate) copolymer molecular weight on the PC Ink gelation kinetics; the molecular weight was varied and the copolymer concentration was kept constant. The poly(carbonate) copolymer contained 20% allyl incorporation.

3.2.5 Effect of copolymer concentration on gelation kinetics

The effect of copolymer concentration on the gelation kinetics was investigated. The copolymer concentration on the gelation kinetics is also important to ensure fast gelation kinetics to maximize the high-throughput production microparticles via piezoelectric ink jet printing. Figure 21 shows the effect of poly(carbonate) copolymer concentration on the PC Ink gelation time. As shown in Figure 21 the gelation kinetics have an exponential decay relationship with increasing copolymer concentration. Given this trend the optimal copolymer concentration to obtain fast gelation kinetics and use the least amount of material would be at approximately 18 wt% of copolymer.

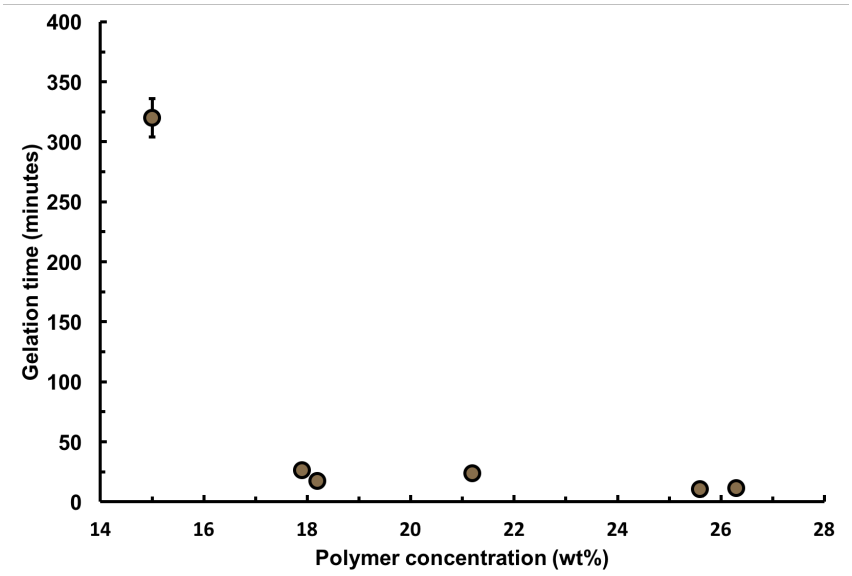

Figure 21. Effect of poly(carbonate) copolymer concentration on the PC Ink gelation kinetics; the concentration was varied and the copolymer molecular weight was kept constant. The poly(carbonate) copolymer contained 20% allyl incorporation.

3.2.6 Tuning microparticle size through the printing waveform and ink dilution

The volume of droplets ejected from a piezoelectric inkjet printing nozzle can be tuned by manipulating the nozzle size, temperature, and jetting waveform. Therefore, by tuning the droplet ejection volume, the final microparticle size can be tuned. Figure 22 shows an example of how the final microparticle size was tuned through the jetting waveform driving the droplet ejection. Figure 22a shows the two-step waveform recommended by the manufacturer (40 V max) which results in microparticles that are approximately 18 microns in size (Figure 22b). Whereas Figure 22c shows a push-pull waveform (12 V max) that results in microparticles that are approximately 16 microns in size as shown in Figure 22d.

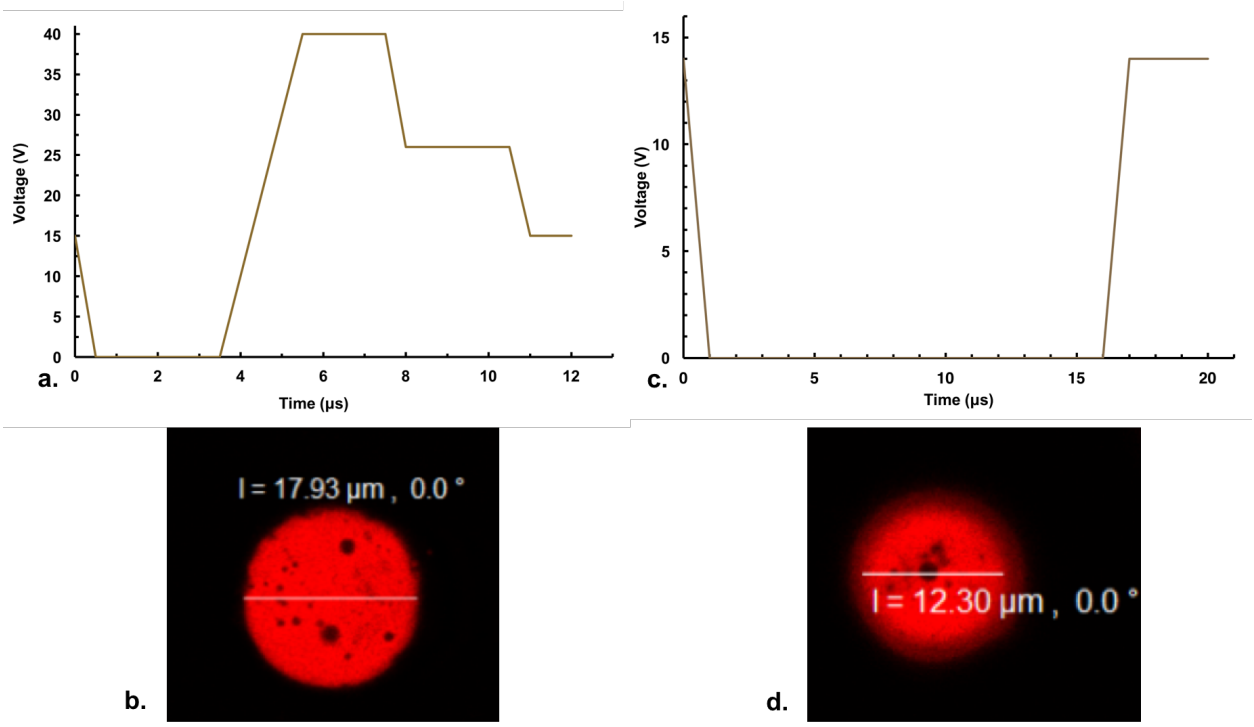

Figure 22. Microparticle size tuning by manipulating the jetting waveform; a. multipulse waveform (40 V max), b. 18 micron sized particle fabricated from the multipulse wavefrom (40 V max), c. push-pull waveform (12 V max), and d. 16 micron sized particle fabricated from the push-pull waveform.

We also discovered a way to tune the microparticle size through the ink copolymer concentration. We hypothesized that with a decrease in weight percent of copolymer solution, the solid amount in each ink droplet should decrease, which should then lead to a decrease in the size of the final crosslinked printed droplets. This hypothesis was investigated by decreasing the mass percent of the copolymer solution by 20% while keeping the volume constant. Figure 23 shows confocal microscope images of microparticles where a 20% reduction in copolymer concentration resulted in a 20% reduction in the microparticle size.

Figure 23. Microparticle size tuning through the ink copolymer concentration. A 20% reduction in copolymer concentration results in a 20% reduction in the microparticle size.

3.2.7 Mechanical Studies

Unconfined compression tests were utilized to verify the predicted structure-property relationships for the softness of bulk hydrogels prepared from the developed inks. The softness is important for modulating the circulation time of microparticles. As reported by Merkel et al. a 30x increase in microparticle softness results in an 8x increase in microparticle circulation time.[41] Figure 24 shows the stress versus strain curve for bulk hydrogels prepared from each copolymer ink. As predicted the hydrogels fabricated from the PG Ink (semibranched poly(glycidol), 20 R.U. cross-linker) were the softest, the PC Ink (linear poly(carbonate), 2 R.U. cross-linker) hydrogels were the least soft, and the hydrogels fabricated from PC:PG (70:30) Ink (linear poly(carbonate) and semibranched poly(glycidol), 2 R.U.) resulted in a hydrogel that had intermediate softness.

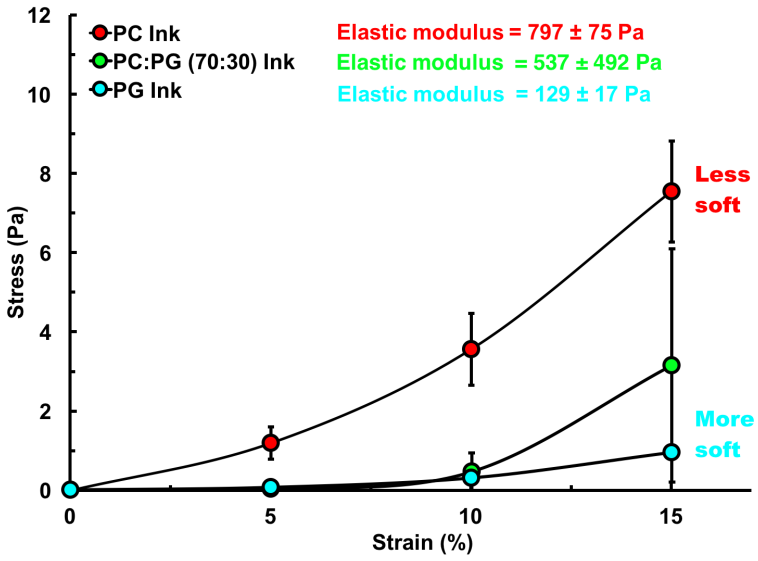

Figure 24. Stress versus strain curve as determined using unconfined compression tests on bulk hydrogels; PC Ink (red circles), PG Ink (green circles), and PC:PG (70:30) Ink (blue circles). All data represent the mean of triplicate samples ± 1 standard deviation.

3.2.8 Swelling Studies

Swelling studies were utilized to verify the predicted hydrophilicity for bulk gels fabricated from each copolymer ink. The swelling was quantified using the equilibrium swelling weight change which was determined as the point at which water stopped being absorbed and the weight stopped changing. The hydrophilicity is important for drug delivery applications because it directly effects the drug loading type and release profile. For example, hydrophobic microparticles are optimal for a high loading and extended release of hydrophobic drugs. Whereas hydrophilic microparticles are optimal for a high loading and extended release of hydrophilic drugs and biologicals. Figure 25 shows the equilibrium swelling weight change for gels prepared from each copolymer ink. The poly(carbonate) gels increased in weight by 1 ± 1% and as predicted were the most hydrophobic. The poly(glycidol) gels showed an increase in weight of 1112 ± 236% and were the most hydrophilic as predicted. The poly(carbonate):poly(glycidol) (70:30) gels as predicted

showed an intermediate weight change between the poly(carbonate) and the poly(glycidol), and had intermediate hydrophilicity between the poly(glycidol) and the poly(carbonate) gels.

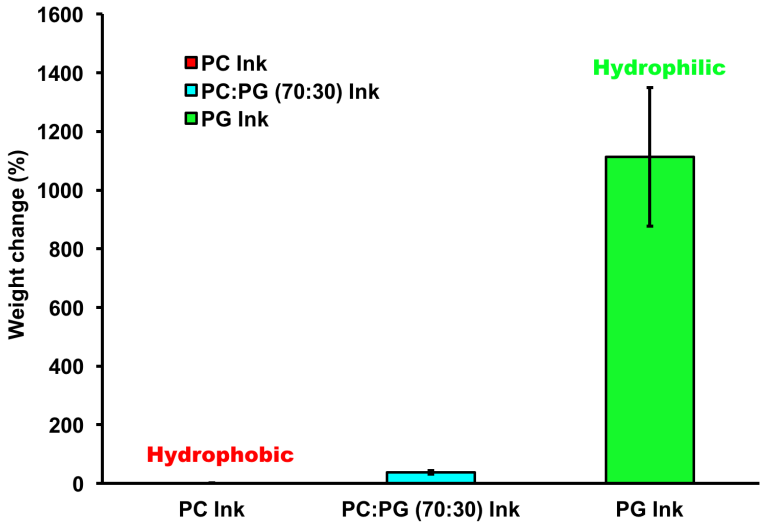

Figure 25. Swelling studies in deionized water at 37 ºC. Equilibrium weight change for bulk gels prepared from; PC Ink (red), PC:PG (70:30) Ink (blue), and PG Ink (green). All data represent the mean of triplicate samples ± 1 standard deviation.

3.3 Microparticle fabrication using photoreactive monomer inks and piezoelectric ink jet printing

The photoreactive copolymer inks allow for the fabrication of microparticles with a wide range of properties for a wide range of drug delivery applications, except for cases where an extreme extended release is needed. The goal for the development of this new extended release ink, was to prepare microparticles with the highest crosslinking density which should result in the longest extended release of all four inks. We sought to accomplish this goal by formulating this ink with 100% of photoreactive monomers as the precursory network components. In general, there are two significant differences with this monomer ink than the copolymer inks. First, the microparticle networks are prepared from readily available acrylate monomers, whereas for the copolymer inks, monomer and copolymer synthesis is required. This results in the new ink components being all commercially available and in a one-pot microparticle

fabrication method. Second, the light source was switched from a UV light to a low-cost visible light source, a simple desk lamp. Visible light is advantageous over UV light because it is not absorbed by biologicals and has an inherent lower energy.[42] Additionally, to increase the scalable potential of the process the substrate was switched from a lab-prepared sacrificial poly(glycidol) coated glass slide to a commercially purchased water soluble poly(vinyl alcohol) film. This substrate further increases the simplicity of the method and allows for applications in personalized medicine.

The target properties for these microparticles were high network density, low hydrophilicity, and low softness. Figure 26 shows the chemical structures and the proposed structure for the crosslinked microparticles.

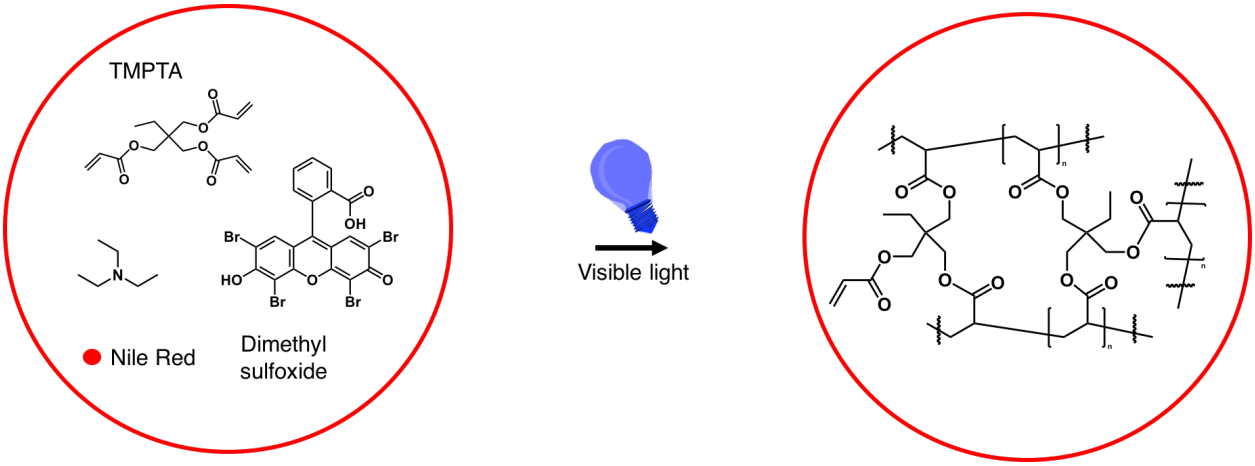

Figure 26. Chemical structures for the PA ink components and the crosslinked microparticle network.

The high network density and low softness was obtained from the 100% incorporation of photoreactive monomers, trimethylolpropane triacrylate (TMPTA). The monomer TMPTA is interesting because it has three vinyl groups that participate in the free radical polymerization.[43-44] The more reactive functional groups there are on the monomer, the higher the probability of the reaction, the faster the reaction kinetics. As mentioned previously the fast gelation kinetics

are important for high-throughput production of microparticles. The low hydrophilicity is obtained from the hydrophobic monomers which contain no hydrophilic functional groups. The incorporated initiator is Eosin y, which is activated by visible light. Due to the inherently lower energy of visible light, a co-initiator trimethylamine must be incorporated to lower the activation energy of initiation. However, a low-cost light source such as a simple desk lamp with a 2 W blue light bulb can be used. In a similar way as the PC Ink, the solvent dimethyl sulfoxide is utilized to allow for the dissolution of the ink's diverse chemical components such as the hydrophobic monomer trimethylolpropyl triacrylate and the hydrophilic initiator eosin y. Lastly, nile red was incorporated as a fluorescent dye.

3.3.1 Monomer ink optimization through gel yield studies

The monomer ink compositions were optimized through gel yield studies. Table 7 shows the compositions of each ink investigated. The first monomer ink denoted as PA Ink 1-AA was composed of eosin Y (initiator), ascorbic acid (co-initiator), trimethylolpropane triacrylate (monomer), dimethyl sulfoxide (solvent), and nile red (dye).

Table 7. Photoreactive monomer ink compositions investigated via gel yield studies.

Inks	Initiator (EQ)	Co-initiator (EQ)	Monomer (EQ)	Solvent (v%)	Dye
PA Ink 1-AA	EY (0.02)	AA (2.8)	TMPTA (99)	DMSO (33)	NR
PA Ink 1	EY (0.02)	EtO_3 (3.2)	TMPTA (99)	DMSO (33)	NR
PA Ink 2	EY (0.02)	EtO_3 (3.2)	TMPTA (99)	DMSO (70)	NR

[a.] Trimethylolpropane triacrylate (TMPTA), ascorbic acid (AA), nile red (NR), dimethyl sulfoxide (DMSO), eosin Y (EY), and trimethylamine (EtO_3).

The amount of DMSO added to PA Ink 1-AA was determined by finding the minimum amount needed to solubilize all components. This minimal amount of solvent maximizes the monomer concentration which should increase the rate of gelation. Ascorbic acid was initially chosen as the co-initiator since it was reported to help initiation under oxygen rich conditions.[45] However, as shown in Figure 27 the gel yield for PA Ink 1-AA was only 4 ± 1% after 5 minutes. Due to

this low yield we sought a more efficient co-initiator that could increase the equilibrium gel conversion. Previous studies have shown that the stronger reducing agent trimethylamine can efficiently co-initiate a visible light type-2 initiator such as Eosin Y.[46-47] Figure 27 shows that the gelation of PA Ink 1 co-initiated by trimethylamine resulted in a more significant gel yield of 52 ± 2% after 5 minutes. Next, we determined the most dilute ink that still resulted in a rapid 5 minute gelation. We determined this maximum dilution since in our previous paper we found that we could tune the microparticle size by reducing the concentration of the network precursors.[48] The most dilute ink that maintained gelation after 5 minutes is denoted as PA Ink 2 in Table 7. Figure 27 shows that PA Ink 2 resulted in approximately half the gel yield at equilibrium than PA Ink 1. This indicates that microparticles prepared from PA Ink 2 should be approximately half the size of particles prepared from PA Ink 1.

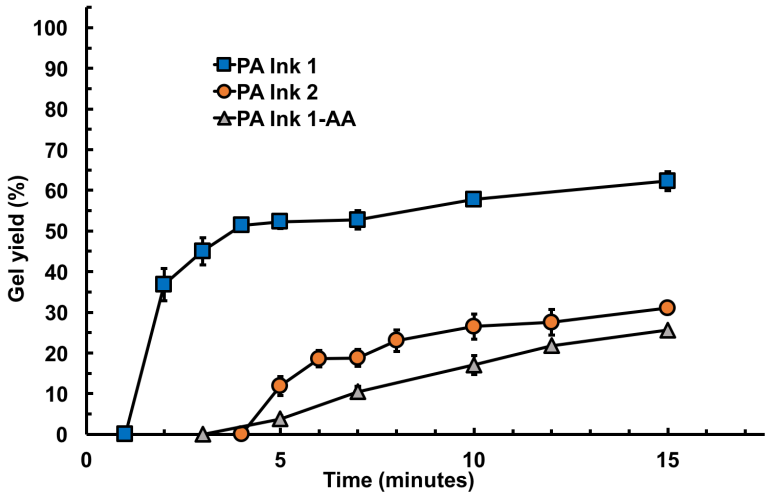

Figure 27. Gel yield over time for different ink compositions; PA Ink 1-AA (grey triangles), PA Ink 1 (blue squares), and PA Ink 2 (orange circles). All data represent the mean of triplicate samples ± 1 standard deviation.

3.3.2 Mechanical studies

The compressive modulus of bulk hydrogels fabricated used PA Ink 1 and 2 were determined utilizing unconfined compression testing. Mechanical properties are important for

modulating microparticle circulation time. As reported by Merkel et al. a 30x increase in microparticle softness results in an 8x increase in microparticle circulation time.[41] Figure 28a displays stress versus strain curves for bulk hydrogels prepared from PA Ink 1 and 2. The compressive modulus was determined utilizing the linear region of Figure 28a from 0 to 2% strain. Figure 28b shows that the compressive modulus for PA Ink 1 hydrogels was 113 ± 64 kPa, whereas the modulus for the PA Ink 2 hydrogels was 25 ± 9 kPa.

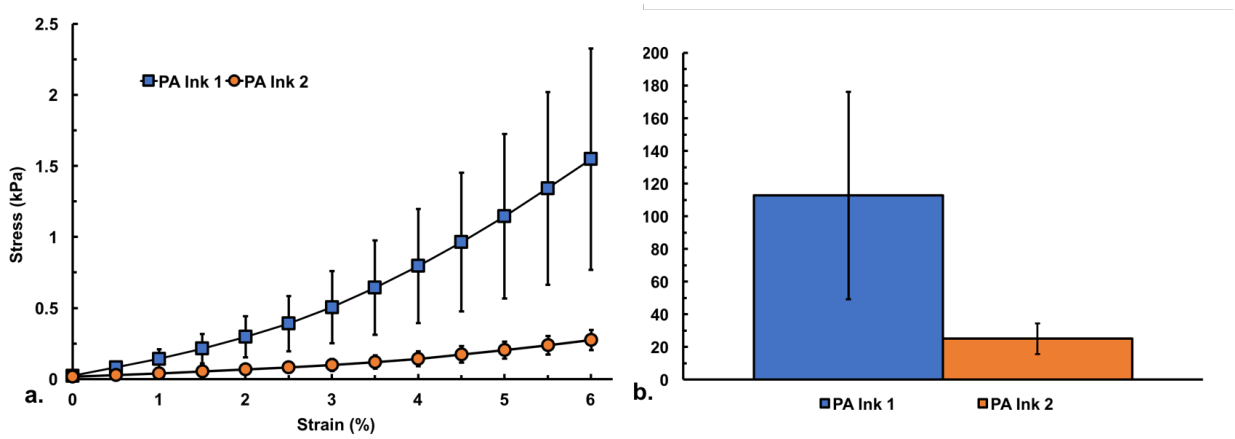

Figure 28. Mechanical compression data for bulk hydrogels; A) stress versus strain curves, PA Ink 1 hydrogels (blue squares) and PA Ink 2 hydrogels (orange circles), B) compressive modulus values, PA Ink 1 hydrogels (blue) and PA Ink 2 hydrogels (orange). All data represent the mean of quadruplicate samples ± 1 standard deviation.

Interestingly, the PA Ink 1 hydrogels were similar to that of white blood cells, and the PA Ink 2 hydrogels were similar to red bloods cells.[22] Microparticles with these mechanical properties have potential for unique biomedical applications, and would be optimal as vascular-targeted drug carriers.[22]

3.3.3 Swelling studies

The weight change of bulk freeze-dried gels in deionized water at 37 °C was investigated using swelling studies. The rate and capacity of gel weight increase (water uptake) is an indication of gel hydrophilicity which has a significant impact on the drug loading and release kinetics. Figure 29 shows the weight change of gels prepared from PA Ink 1 and 2. As shown in

Figure 29 the gel prepared from PA Ink 1 rapidly reached equilibrium within one minute and increased in weight by 7.8 ± 1.7%. Whereas the PA Ink 2 gel reached equilibrium within 15 minutes and increased in weight by 37.2 ± 1.2%. In general, the limited gel water uptake for both gels indicate that they are hydrophobic and would be optimal for hydrophobic drug loading. Additionally, PA Ink 2 gels should release drugs at a faster rate than PA Ink 1 gels.

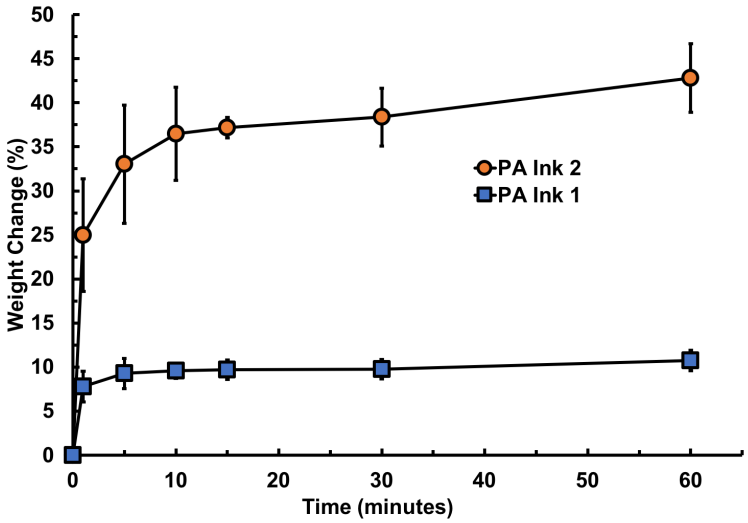

Figure 29. Weight change of bulk gels after soaking in deionized water at 37 °C; gels prepared from PA Ink 1 (blue squares) and PA Ink 2 (orange circles). All data represent the mean of triplicate ± 1 standard deviation.

3.3.4 Fabrication of one-pot crosslinked microparticles using inkjet printing

Figure 30 shows an overview of the printing process for microparticles fabricated using the monomer based inks. First, the network precursors are printed onto the poly(vinyl alcohol) (PVA) film using a 2831 Dimatix materials printer. After droplet ejection onto the substrates they are immediately illuminated with blue light to initiate network crosslinking.

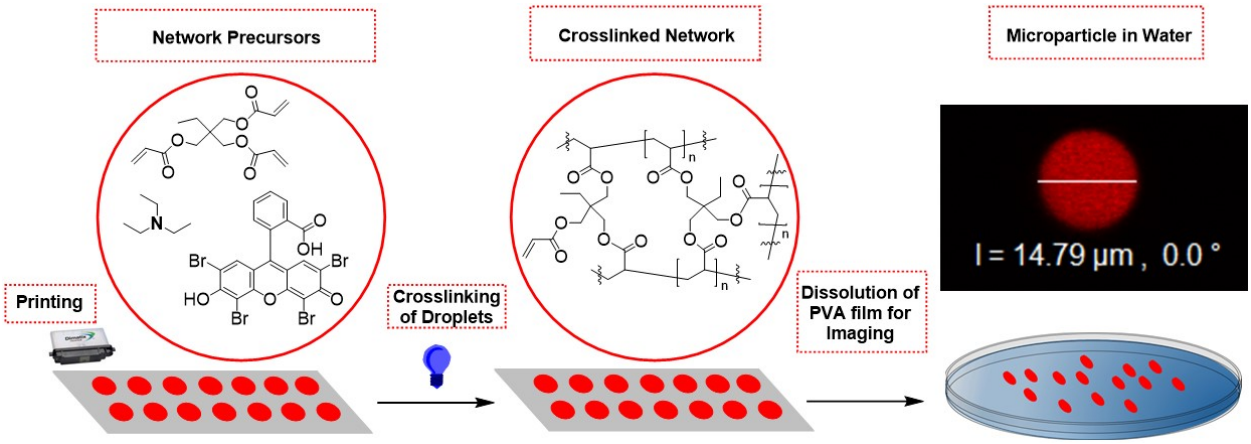

Figure 30. Illustration of the microparticle fabrication process. The chemical structures for the network precursors are eosin Y (initiator), trimethylamine (co-initiator), and trimethylolpropane triacrylate (monomer). The confocal image was taken of a microparticle fabricated using PA Ink 1 floating in water.

Shown in Figure 31a is a fluorescent microscope image of printed PA Ink 1 droplets on the PVA film. This image shows that the droplets were accurately and precisely ejected onto the substrate based on the programmed printing array. Next, the crosslinked microparticles were removed from the PVA substrate by dissolving the film in water. Confocal microscopy was then used to image the microparticles. Utilizing the software for the microscope, the PA Ink 1 microparticles were determined to be 14.4 ± 0.6 µm, resulting in a low CV of 4%. Furthermore, a z-stack confocal image of one microparticle, displayed in Figure 31B, indicates that the microparticle is spherical and the dye homogenously distributed throughout.

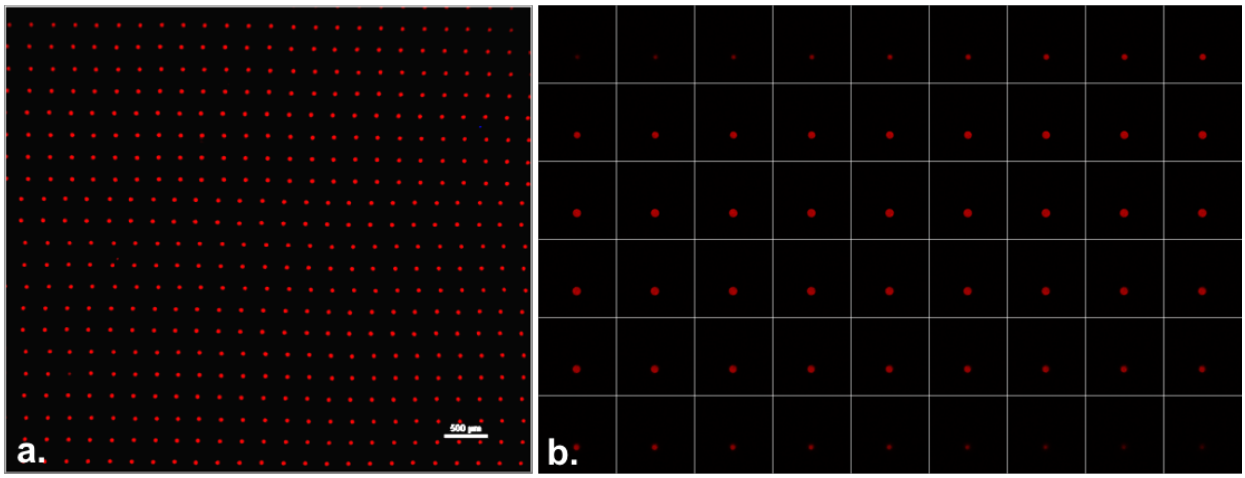

Figure 31. Confocal images of microparticles fabricated from PA Ink 1; a. wide field microscope image of microparticles on the water soluble poly(vinyl alcohol) film (scale bar = 500 μm) and b. confocal z-stack images of one microparticle suspended in water (scale bar = 20 μm).

We also demonstrated the technologies ability to tune the microparticle size through microparticle fabrication with the dilute PA Ink 2. Facile microparticle size tuning is important because it directly effects the type of administration that can be used for delivery and release kinetics. PA Ink 2 resulted in the fabrication of microparticles that were 7.1 ± 0.5 μm (CV=7%) in size as shown in Figure 32. An image of a microparticle fabricated from PA Ink 1 was included for comparison. By reducing the monomer concentration by 56%, the microparticle size was also reduced by 56%.

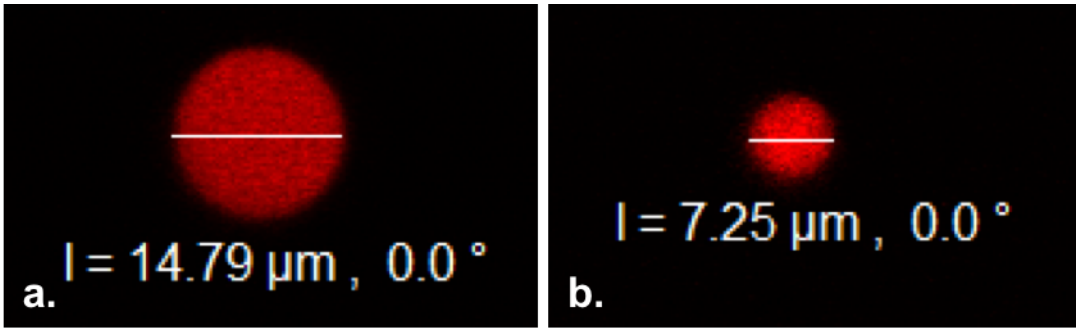

Figure 32. Confocal images of microparticles floating in water fabricated with; a. PA Ink 1 and b. PA Ink 2. The size of the microparticles were reduced by 56% by reducing the monomer concentration by 56%.

The microparticle sizes obtained for Ink 1 and 2 have shown promise for intracellular[49-50], injection[51], parenteral[52], oral[8], and inhalation[8-9, 53] for applications such as vaccinations, brucellosis, human papillomavirus, diabetes, inflammation, and asthma respectively.

3.3.5 Drug loading and encapsulation efficiency of a model hydrophobic drug

The drug loading and encapsulation efficiency of a model hydrophobic drug ivermectin (875.1 g/mol) was determined in bulk hydrogels fabricated from PA Inks 1 and 2. Here we determined that the order of component dissolution was important when preparing the ink. The drug was first dissolved in DMSO, eosin Y, and triethylamine by vortexing for a few minutes, then sonicating for 30 minutes at 37 °C. Once the drug was completely dissolved, trimethlyolpropane triacrylate was added and vortexed for a few minutes to obtain a homogenous solution. The drug loading was limited by its solubility in DMSO. After complete dissolution, the ink was gelled by illuminating the sample with blue light. Utilizing HPLC UV-VIS the drug loading and encapsulation efficiency was determined as 32.3 ± 2.0% and 98.1 ± 0.6% for PA Ink 1 and 29.7 ± 0.8 and 90.0 ± 2.5% for PA Ink 2 respectively.

3.4 One-pot microparticles for controlled pulmonary drug delivery to eliminate malaria

3.4.1 Ink formulation

The long-term goal of this project is to eliminate malaria. This work is focused on achieving a smaller goal towards this greater goal, the development of the optimal microparticles for malaria elimination. The goals to fabricate these microparticles were to 1) maximize network density, to minimize release rate and decrease doses needed, 2) maximize drug loading for a hydrophobic drug to decrease material needed for delivery, and 3) obtain an aerodynamic particle diameter of about 1 to 2 microns for efficient particle distribution in the deep lungs[4]. The strategy to accomplish goal 1) was to form the microparticle network from the monomer network

precursor, trimethylpropyl triacrylate. This should result in a very high network density microparticle which will minimize the release rate of drug. Additionally, to demonstrate the tunability of release the network density was tuned through the monomer concentration. From our previous work, we determined that a decrease in the monomer concentration resulted in decreased gel density, which should result in a faster release. The plan to achieve goal 2) was to use the hydrophobic network precursors trimethylolpropyl triacrylate to form the network, which should maximize hydrophobic drug loading. As previously mentioned we are able to incorporate up to 32 wt% in bulk gels. However, since the viscosity of the ink increases with increasing ivermectin concentration as shown in Figure 33, we were limited to a loading that results in a final dry weight of ivermectin in the microparticles of 13.1 wt%.

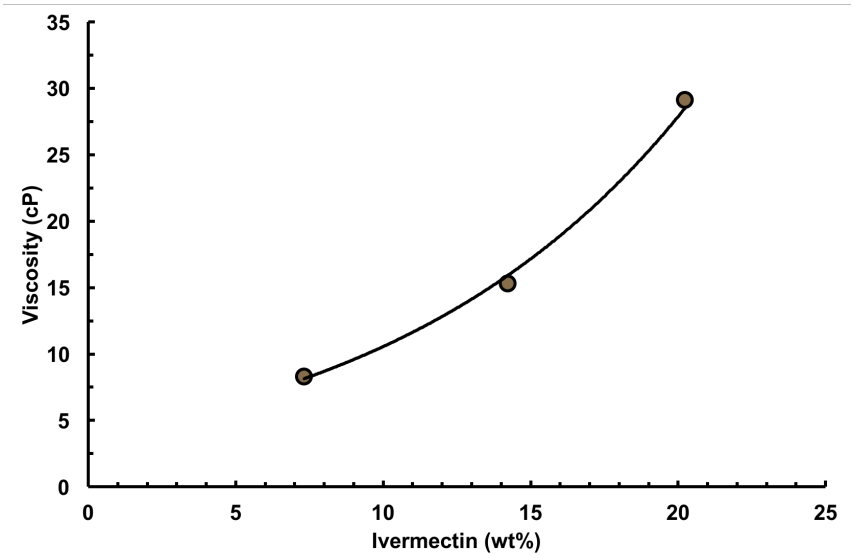

Figure 33. Viscosity of PA Ink 1 solutions containing different concentrations of ivermectin as determined using steady state flow rheometry measurements at 30 °C.

This ivermectin concentration results in an ink with a viscosity of 15 cP, the maximum reported viscosity that still obtains good printability as reported by the printer's manufacturer, Fujifilm Holdings America Corporation. Goal 3) was sought after by maximizing the ink viscosity to decrease the fluid volume ejected. In our previous work[48], we determined that 2 micron size

particles were the smallest that we could obtain. Therefore, in this work, the viscosity was increased as much as possible while still maintaining good printability (15 cP), to minimize the fluid volume ejected.

The ink formulation was completed by careful selection of a solvent and initiator. Eosin Y was selected as the initiator since it is initiated by blue light, an inherently low energy source. Furthermore, the light source used is cost-efficient, a simple desk lamp quipped with a 2 W blue light bulb. However, due to the inherently lower energy source used, a co-initiator triethylamine was incorporated to lower the activation energy of the eosin Y initiation. Lastly, the solvent selected was dimethyl sulfoxide (DMSO) which is advantageous for its ability to dissolve chemically diverse species such as the water-soluble eosin y and the hydrophobic drug ivermectin.

3.4.2 *In vitro* release of ivermectin from bulk gels

The *in vitro* ivermectin release kinetics was investigated using bulk gels fabricated from PA Ink 1-IV13wt% and PA Ink 2-IV13wt%. The studies were performed in perfect sink media at 37 °C to ensure the drug media concentration did not influence the release profile. Figure 34 shows that the release profile for the bulk gel prepared from Ink 1-IV13wt% had a small burst release of approximately 5% of ivermectin, after which there is a slow linear release for at least 21 days. On the other hand, the Ink 2-IV13wt% bulk gel profile had a larger burst release of approximately 10% of ivermectin, followed by a slower release rate that decreases nonlinearly over approximately two weeks. Given the release profiles shown in Figure 34 and the target extended release application, the PA Ink 1-IV13wt% formulation is optimal.

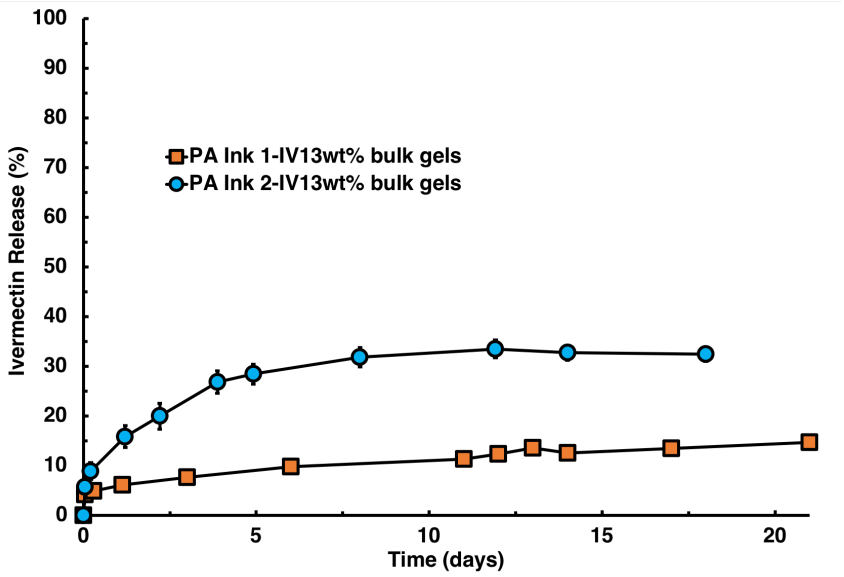

Figure 34. *In vitro* ivermectin release profiles from bulk gels; PA Ink 1-IV13wt% bulk gels (orange squares) and PA Ink 2-IV13wt% bulk gels (blue circles). All data represent the mean of triplicate ± 1 standard deviation.

3.4.3 *In vitro* degradation of bulk gels by reactive oxygen species

The *in vitro* degradation of bulk gels fabricated from PA Ink 1 and PA Ink 2 was investigated at conditions relevant in the lung alveoli. In this location within the lungs the likely mechanism for poly(acrylate) degradation is by reactive oxygen species. The hydrogen peroxide concentration found in this location is expected to be in the micromolar to tens of micromolar range.[31] Therefore, the degradation study was run at the higher end of the range, 100 micromolar. Additionally, cobalt chloride was added as a reducing agent to produce oxygen free radicals responsible for the oxidation of the poly(acrylate). Figure 35 shows that bulk gels fabricated from PA Ink 1 have a weight loss of 6% after 11 days. Whereas the bulk gels fabricated from PA Ink 2 have a much faster weight loss of 52% after 11 days. Therefore, there is a significant degree of degradation tunability obtained through changing the monomer concentration.

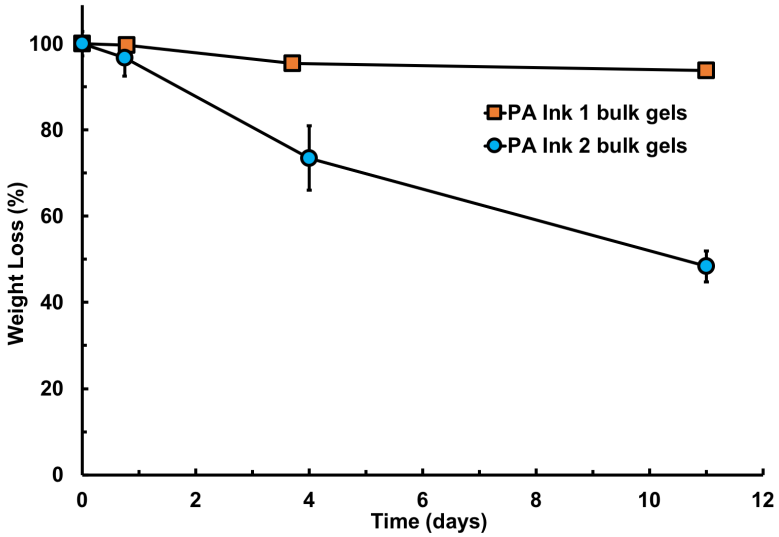

Figure 35. *In vitro* degradation of bulk gels fabricated using PA Ink 1 (orange squares) and PA Ink 2 (blue circles). The degradation media was composed of deionized water with 100 μM H_2O_2, 1.53 μM $CoCl_2$ at 37 °C. All data represent the mean of triplicate ± 1 standard deviation.

3.4.4 Ivermectin loaded microparticle fabrication

Ivermectin loaded microparticles were fabricated from PA Ink 1-IV13wt% and PA Ink 2-IV13wt%. Using the microparticle sizes as determined from SEM, the aerodynamic diameters were calculated using equation (9) as 1.6 ± 0.7 and 0.8 ± 0.2 microns for PA Ink 1-13wt% and PA Ink 2-IV13wt% respectively. The microparticles obtained from PA Ink 1-IV13wt% are almost exactly in the size range to obtain efficient distribution in the lung alveoli, 1-2 microns.[4] Additionally, the *in vitro* release profile for this ink also yielded the longest extended release of ivermectin, and is most desirable for the target application.

3.4.5 *In vitro* drug efficacy of ivermectin and ivermectin loaded microparticles

The *in vitro* drug efficacy of pure ivermectin and ivermectin loaded microparticles fabricated from PA Ink 1-IV13wt% was determined using three-day cell viability studies. The drug efficacy of pure ivermectin and PA Ink 1-IV13wt% microparticles was quantitated by determining the half maximal inhibitory concentration (IC_{50}), the concentration where only 50% of the cells remain alive after the time of the study. Regression analysis on the data showed that

pure ivermectin had an IC_{50} value of 33.2 ± 7.7 μg/mL whereas the PA Ink 1-IV13wt% microparticles had an IC_{50} value of 6.1 ± 0.9 μg/mL. The IC_{50} values indicate that the bioavailability of ivermectin is increased when releasing from the microparticles. This is likely due to the pure ivermectin samples degrading in solution before it is absorbed by the cells. Whereas for the PA Ink 1-IV13wt% microparticles, the ivermectin is protected within the microparticle until released, where the small released amount is immediately absorbed by the cells. The results indicate that less ivermectin will need to be delivered to achieve the same plasma concentrations as pure ivermectin delivery. In addition to drug efficacy, the effect of poly(acrylate) (PA) microparticles on cell viability was also determined to investigate poly(acrylate) cytocompatibility. As shown in Figure 36 the PA microparticles did not have a significant effect on the cell viability.

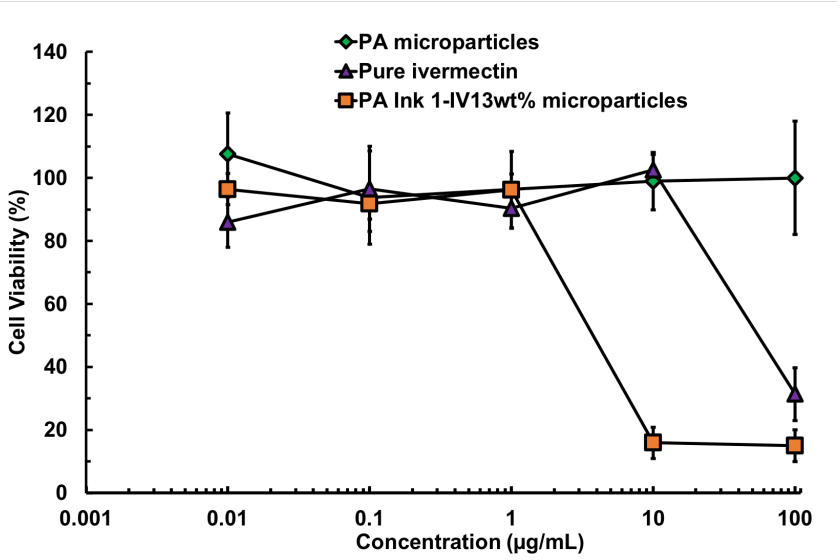

Figure 36. *In vitro* cell viability after 3 days of exposure to; pure ivermectin (purple triangles), PA Ink 1-IV13wt% microparticles (orange squares), and PA microparticles (green diamonds). All data represent the mean of triplicate ± 1 standard deviation.

3.4.6 *In vitro* transport of ivermectin from ivermectin loaded microparticles through a lung epithelial cell monolayer

An *in vitro* lung model illustrated in Figure 37 was utilized to investigate the *in vivo* ivermectin transport from the interior lung to the systematic circulation. This was done by determining the apparent permeability of ivermectin and utilization of an accurate *in vitro-in vivo* correlation[54] developed by Mathias et al. to predict the *in vivo* lung absorption profile. Mathias et al. quantitated the correlation accuracy by plotting predicted absorption values versus actual absorption values, which resulted in a linear plot with an R^2 value of 0.97.[54]

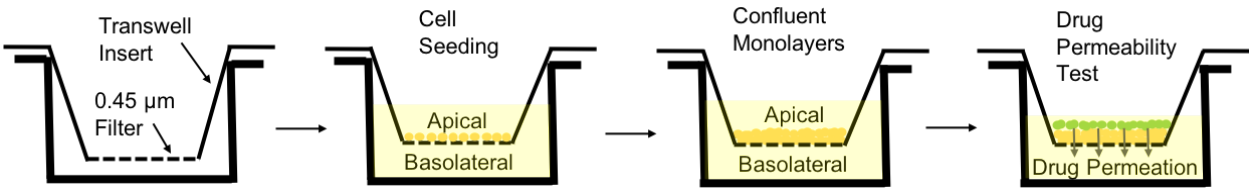

Figure 37. Illustration of the *in vitro* lung model utilized to investigate the *in vivo* ivermectin transport from the interior lung to the systematic circulation.

Figure 38 shows the ivermectin transport from the PA Ink 1-IV13wt% microparticles, the optimal microparticles for the target application. The apparent permeability coefficient for the ivermectin transport through the cell monolayer was determined as $1.3 \times 10^{-6} \pm 1.1 \times 10^{-7}$ cm/s using equation (13) and the initial steady state ivermectin transport.

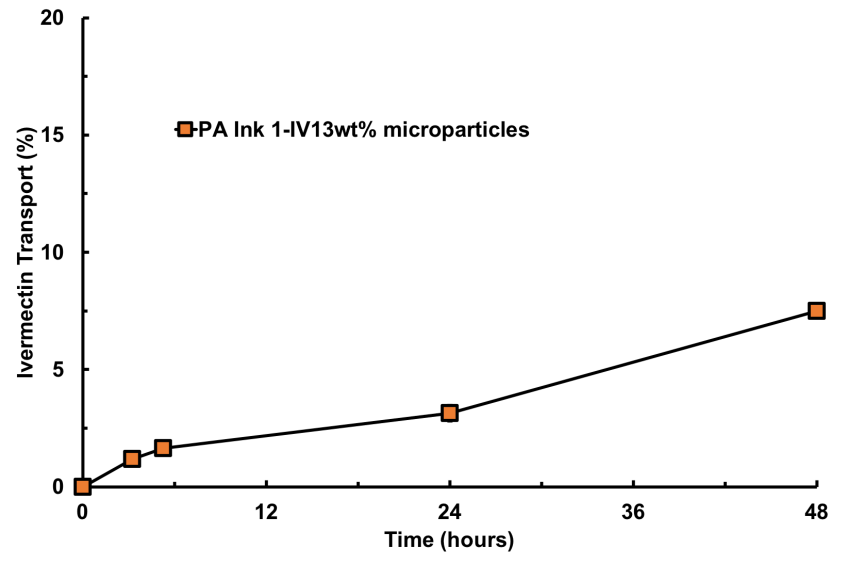

Figure 38. Ivermectin transport from PA Ink 1-IV13wt% microparticles through a rat lung epithelial cell monolayer. All data represent the mean of triplicate ± 1 standard deviation.

The predicted lung absorption was calculated by first determining the absorption constant using;

$$\log K_a = 0.811 \log(P_{APP}) - 1.99 \quad (22)$$

where K_a is the absorption constant and P_{APP} is the apparent permeability. The predicted absorption was then determined using;

$$\%\ \text{Absorbed} = A_{max}(1 - e^{-K_a t}) \quad (23)$$

where A_{max} is the maximum % absorbed and t is the time. Figure 38 shows the predicted ivermectin absorption over time *in vivo*. Ivermectin should have a linear absorption for up to about 10 days after which the release rate decreases nonlinearly. Given the achievement of the long 21 day extended release of ivermetin. Upon successful mass drug inhalation administration of PA Ink 1-IV13wt% microparticles, malaria would have a significantly higher chance of being eliminated over administration of conventional pure ivermectin tablets due to increased patient compliance.

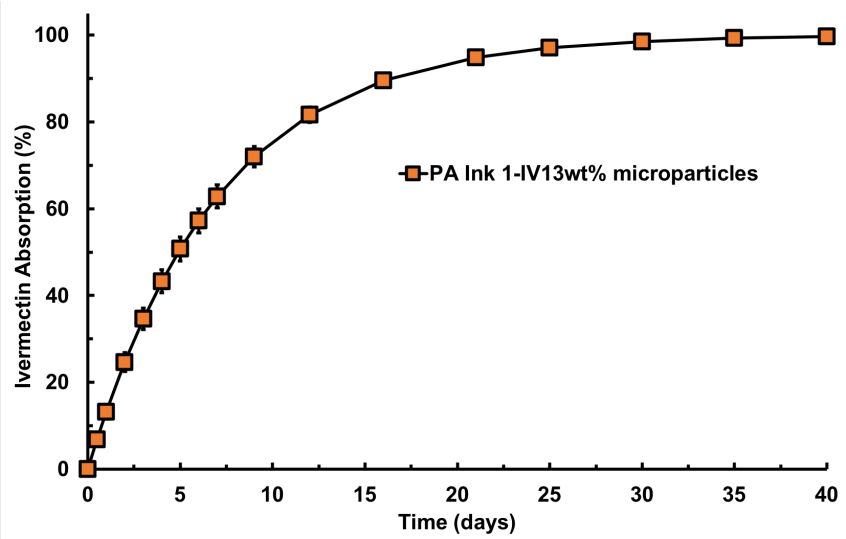

Figure 39. Predicted ivermectin absorption in rat lungs as determined using an *in vitro-in vivo* correlation.[54] The predicted profile was calculated using apparent permeability data determined in triplicate ± 1 standard deviation.

CHAPTER 4

4. CONCLUSIONS

In this work, we developed a comprehensive technology that can easily fabricate tunable microparticles at a high rate with low CV; and have the ability to encapsulate synthetic hydrophilic, synthetic hydrophobic, and/or biological drugs with high drug loading and encapsulation efficiency. This was accomplished by development of a small set of photoreactive copolymer and monomer inks that were utilized to fabricate microparticles with a wide range of softness, hydrophilicity, and network density. The two copolymer building blocks synthesized were a functionalized hydrophobic linear poly(carbonate) and hydrophilic semibranched poly(glycidol). Additionally, the semibranched poly(glycidol) was synthesized using a green synthesis. This resulted in the development of an ink that is completely green. The copolymers were functionalized with allyl groups that crosslink with dithiol crosslinkers through a thiolene "click" reaction after initiation by UV light. The monomer inks were formulated using a tri-functionalized monomer, trimethylolpropane triacrylate, that crosslinked via free radical polymerization after initiation by visible light. To ensure facile microparticle collection hydrophilic microparticles were fabricated using Teflon substrates whereas hydrophobic microparticles were fabricated using a water soluble poly(vinyl alcohol) film or sacrificial polymer coating. Fabricated dye loaded microparticles were then analyzed using confocal microscopy which confirmed the microparticle's spherical shape, uniformity of the dye distribution throughout the microparticles, and the high microparticle size precision. Additionally, we fabricated microparticles in a large size range from 1 to 18 microns at a high droplet production rate of 1 kHz. Furthermore, larger microparticle sizes would be easily obtainable with printer cartridges with larger nozzle diameters. The capability of the inks to

fabricate microparticles of a wide range of hydrophilicity and softness was verified using bulk swelling and unconfined compression tests respectively. The capability to tune the microparticle size traditionally through the jetting waveform was verified, and a new discovered method to tune the microparticle size through the network precursor concentration was presented. After property verification, the technology was utilized to engineer the optimal microparticles for a specific drug delivery application, malaria elimination. The prototype microparticles were then investigated using a series of *in vitro* tests to evaluate their success for malaria elimination via pulmonary drug delivery. The results from these experiments show promise that the microparticles should make a significant step towards malaria elimination, and also demonstrates the capability of the developed technology to fabricate the optimal microparticles for a target drug delivery application.

APPENDIX

Tables summarizing the publications reviewed for Sections 1.1 through 1.4

Table A1. Extracted data from 100+ publications mostly from 2010 to 2018 on microparticles prepared with single drug loading. Abbreviations; drug loading (DL), encapsulation efficiency (EE), average (A), standard deviation (SD), product yield (PY), reference (R), precipitation/physical entanglement (P), polymerization/covalent crosslinking (G), or ionic crosslinking (I).

Method	Matrix	Drug	Disease Treated	Route of Admin.	DL (%)	EE (%)	A ± SD (μm)	R
Emulsion-P	PLGA	Insulin	Diabetes	Inhalation	3±0.2	51±7	2.5±0.4	55
Emulsion-G	PMAA	Insulin (diffusion loading)	Diabetes	Oral		~85	1	56
Emulsion-G	poly(PEGDMA:MMA)	Insulin (diffusion loading)	Diabetes	Oral	1.87	82±6	25±3	57
Spray drying-P	Dextran-TMC	Insulin	Diabetes	Inhalation	9 to 9.7	90 to 97	10±4	9
Supercritical fluid-P	N-trimethyl chitosan microparticles	Insulin	Diabetes	Inhalation	48	97	2±2	10
Emulsion-P	PLGA-HPβCD/insulin	Insulin	Diabetes	Inhalation	1.4±0.4	59±16	26.2±1.2	58
Inkjet-P	PLGA	Paclitaxel	Cancer		10	100	NR	59
Inkjet-G	(poly(NIPAAm-co-MAA)) and HDDA	Fluorescein					23.42 ± 1.07	60
Emulsion-G	(P(NIPAM-co-AA))	Trypsin			49.3±2		7±~3	61
Emulsion-G	p-NIPAM	Horse radish peroxidase (diffusion loading)					1.762±.046	62
Emulsion-G	poly(acrylic acid-co-acrylamide)	Peptide (diffusion loading)					70 to 90 ± NR	63
Emulsion-G	oligoLA-PEO-PPO-PEO-oliogoLA	Bovine serum albumin, insulin, hemoglobin			9.7, 7, 8.7	NR	NR	64
Emulsion-P	PLGA	Bovine insulin	Diabetes			84±2	84±25 and 41±14	65
Emulsion-P	PLGA	Inactivated polio vaccination	Vaccine	Injection		~70±4	~8±3	51
Emulsion-G	PEGMA	Lysozyme (diffusion loading)			63	100	NR	66
Emulsion-P	polyester amide	Celecoxib	Knee osteoarthritis	Intra-articular	NR	NR	45±35	67
Emulsion-P	PEG-4-acr disulfydry peptide	Nanoparticles			85.9		1.9±2.7 to	68

	(enzymatically degrdable)						9.6±3.1 SW	
		AF 591 IgG			2			
Microfluidics	Phospholipid	Doxorubicin	Cancer		NR	94	50 - 200	69
Emulsion-I-P	PLLA-alginate	Metoclopramide	Heartburn		13.2±0.5	66.54 ±2.23	~200-300 (NR)	12
Emulsion-G	Peptide functionalized PEG	Dexamethasone	Inflammation	Inhalation	0.38	7.6	7.2±4.3	8
		Methylene blue			0.24	4.8	4.5±1.8	
		Horseradish peroxidase			1.87	37.4	7.5±3.9	
Spray drying-P	Mannitol-Lactose-Trehalose	siRNA loaded PLGA NP		Inhalation	0.0381±0.007			70
Spray drying-P	Maltose	Doxorubicin in nanoparticles	Cancer	Inhalation	3		3.45±1.99	71
Spray drying-P	PLGA-DPPC-PVA-Gelatin-cholesterol	Paclitaxel	Cancer	Inhalation	1.76	84.1		72
Spray drying-P	Mannitol, trehalose, dextran, L-leucine	Bacteriophage virus-like particle	Human papillomavirus	Oral and parenteral		64	4.6±1.7	52
Spray drying-P		Lysozyme				-25% activity		73
Spray drying-P	PLGA-DPPC-trimethylchitosan	Ropinirole hydrochloride	Parkinson's disease	Nasal	1.90±0.03	95.20 ±1.43	2.09±1.01	74
Film-G (prepared film and crushed and sieved)	poly(itaconic acid-co-N-vinyl-2-pyrrolione)	Salmon calcitonin		Oral	4.5±0.5	Diffusion loading	45-150	75
		Urokinase			1.9±0.1			
		Rituxan	B cell destruction		2.4±1.5			
Microfluidics-I	HE800 exopolysaccharide	Bovine serum albumin					102±5	76
Microfluidics-G	PEG-maleimide (protease degradable)	Peptide conjugated VEGF	Vascularization	Subcutaneous injection			50±5	77
Emulsion-G	Chitosan-Gelatin-thermoresponsive PEG	Folic acid			NR	NR	1±1	78
Microfluidics-G	PEG	Basic fibroblast growth factor			NR	80	42.4±8.6 to 142.1±25.6	79
		DNA nanoparticles						

Microfluidic-G	Hydrazide-aldehyde-functionalized carbohydrates	Bupivacaine	Anesthesia				49 to 92 ± 4	[80]
Emulsion-G	PMMA-EGDMA	Monosodium phosphate			3.1	95	95	[81]
Emulsion-P	acetylated dextran	HFG-f	Myocardial infarction	Intramyocardial	1.1±0.2	86±9	28.3±1.5	[82]
Emulsion-P	Polyketal-Drug conjugate	Estradiol	Inflammation		11.1±0.4	96.0	10.3±3.4	[83]
Emulsion-P	Vanillyl alcohol-containing copolyoxalate	Dexamethasone	Asthma	Inhalation	1	20	13±5	[53]
Cyclodextrin-CaO_3-P	Cyclodextrin-CaO_3	5-fluorouracil			NR		5±NR	[84]
		Na-L-thyroxine			NR		2±NR	
Emulsion-P	PEG-PBT	Anti-VEGF	Neovascular-AMD	IVT	22.1	90	64±32	[6]
Emulsion-G	PEG	Protein (post conjugation)	Targeting				31±7	[85]
Spray drying-P-I	Alginate	rhBMP-2	Bone regeneration	Scaffold	0.045 (NR)	45	5±5	[86]
Mineralization	$CaCO_3$/rGO-TEPA	Doxorubicin	Cancer		7.9	94.7	3±1	[87]
Spray drying-P	Chitosan	β-galactosidase	GI disorder	Oral			3.5±1.9	[88]
Emulsion-P	PLGA	L7/L12	Brucellosis	Intracellular	0.25	55.6	6±NR	[50]
Total Recirculation One Machine (Emulsion)-P	PLGA	GDNF	Parkinson's	Unilateral injection to brain	0.28 ± 0.05	70 ± 12	28 ± 8	[89]
Emulsion-I	Alginate	Hydrocortisone hemisuccinate	Colon-IBD	Oral	11.1	22	89.6 ± 1.0	[90]
Aerosolization-I	Alginate	Hydrocortisone hemisuccinate	Colon-IBD	Oral	8.8	22	51.8 ± 1.9	[90]
Microfluidics-P	PLLA	Paclitaxel	Cancer		4.6	97	31 ± 1	[21]
Emulsion-P	PLGA	Paclitaxel	Cancer		2.7	95	10 ± NR	[91]
Emulsion-P	PLGA	Paclitaxel	Cancer		4.7	85	16 ± NR	[92]
Emulsion-I	Alginate	Paclitaxel	Cancer		15.5	48	10 ± 3	[93]
Electrohydrodynamic atomization-P	PDLLA-PLLA	Paclitaxel	Cancer		1.6	45	14 ± 13	[94]
Supercritical fluid technology-P	PEG-PLLA	Paclitaxel	Cancer	IV	10.9±2.8	18.1	2.3	[95]

Supercritical fluid technology-P	PLLA	Paclitaxel	Cancer	IV	14.3	62.7	1.6±1.2	[19]
Microfluidics-P	PCL-PLA	None	N/A	N/A	N/A	N/A	26.5 ± 0.7	[96]
Microfluidics-P	PLGA-b-PEG	Paclitaxel	Cancer		9.25	92 ± 2	2.0 ± 0.3 to 4.5 ± 0.3	[97]
Spray drying-P	PLGA-L-leucine or L-aspartic acid	Rifampicin	Tuberculosis	Inhalation	19.2 ± 0.0 to 12.3 ± 0.0	96.2 ± 0.6 to 70.5 ± 0.1	5.9 ± 3.8 to 11.7 ± 6.8	[18]
Spray drying-P	Alginate	VEGF	N/A	N/A	4.9	49	3.9 ± NR	[98]
Spray drying-P	Hyaluronic acid	Budesonide	N/A	Inhalation	21.0 ± 0.3	91.5 ± 1.5	6.3 ± NR	[99]
Spray drying-P	PLGA	Methotrexate	Cancer/autoimmune disease	Inhalation	24.6 ± 0.4	91.3 ± 1.5	5.6 ± 0.7	[100]
Microfluidics-P	Phospholipids	Doxorubicin	Cancer	N/A	30	93 ± 2	100	[20]
Microfluidics-P	Polyacrylamide and polymethyl acrylate	Sodium fluorescein	Cancer	N/A	1	30	130 to 155 (<4.6% CV)	[14]
Spray drying - P	N-fumaroylated diketopiperazine	azithromycin	Pneumonia	Inhalation	23.9 ± 0.1, 48.2 ± 0.29	NR	NR	[17]

Table A2. Compilation of different drugs encapsulated in microparticles with their corresponding chemical structure and size as determined through a literature search of 100+ publications mostly from 2010 to 2018.

Drug	**Biological (Y/N)**	**Hydrophobic or Hydrophilic**	**Size (g/mol)**
Paclitaxel	N	Hydrophobic	854
Azithromycin	N	Hydrophobic	749
L7/L12	Y		
Hydrocortisone hemisuccinate	N	Hydrophilic	362
Glial cell line-derived neurotrophic factor	Y		
Insulin	Y	Hydrophilic	5,808
Doxorubicin	N	Hydrophobic	544
miR-34a	Y		
Recombinant L7/L12	Y		
β-galactosidase	Y		540,000
rhBMP-2	Y		26,000
Ovalbumin	Y		45,000
Bovine serum albumin	Y		69,000
Fluorescein	N	Hydrophilic	332
Trypsin	Y		23,300
Horse radish peroxidase	Y		44,000

Peptide	Y		
Hemoglobin	Y		16,000
Inactivated polio vaccination			
Lysozyme	Y		14,000
Celecoxib	N	Hydrophobic	381
AF 591 IgG	Y		150,000
Metoclopramide	N	Hydrophobic	300
Methylene blue	N	Hydrophilic	320
siRNA	Y		13,000
Bacteriophage virus-like particle			
Ropinirole hydrochloride	N	Hydrophilic	297
Salmon calcitonin	Y		3,454
Urokinase	Y		30,400
Rituxan	Y		35,000
Basic fibroblast growth factor	Y		18,000
Vascular endothelial growth factor	Y		38,000
Bupivacaine	N	Hydrophilic	288
Hepatocyte growth factor fragment	Y		
Estradiol	N	Hydrophilic	272
Dexamethasone	N	Hydrophobic	392
5-fluorouracil	N	Hydrophilic	130
Na-L-thyroxine	N	Hydrophilic	799
Anti-vascular endothelial growth factor	Y		150,000

Table A3. Extracted data from 100+ publications mostly from 2010 to 2018 on microparticles prepared with dual drug loading. Abbreviations; drug loading (DL), encapsulation efficiency (EE), average (A), standard deviation (S), reference (R).

Method	Matrix	Drug	Disease Treated	Route of Admin.	DL (%)	EE (%)	AV ± S (μm)	R
Emulsion-P-Por	PLGA	Doxorubicin	Cancer	Inhalation	0.773±0.03	77.2±0.9	46±21	[101]
		miR-34a			0.013±0.001	33.5±1.0		
Emulsion-P-Por	PLGA-PLLA	Paclitaxel	Cancer	Inhalation	0.9±0.06	90.1±6.3	35±9	[102]
		Doxorubicin			9.1±0.7	45.3±3.3		
Emulsion-P-Por	PLGA	Doxorubicin	Cancer	Inhalation	0.80±0.03	79.6±3.2	47±19	[103]
	PLGA	miR-519c			0.023±0.001	29.0±1.3		
Emulsion + Microfluidic-G	NiPAm	Nile red					140±10	[104]
		DAPI						
Microfluidic-P	Hypromellose acetate succinate	5FU	Cancer	Oral	0.0109 ± 0.00015		27 ± 0.8	[105]
		Curcumin	Cancer	Oral	0.009 ± 0.0013		27 ± 0.8	
Microfluidic-G	PEGDA	nanoparticles					2.8 ± 0.2 to	[106]
		Acryloyl-RhB					19.2 ± 0.9	

REFERENCES

1. Zhang, Y.; Chan, H. F.; Leong, K. W., Advanced materials and processing for drug delivery: the past and the future. *Adv. Drug Delivery Rev.* **2013,** *65* (1), 104-120.

2. Kohane, D. S.; Smith, S. E.; Louis, D. N.; Colombo, G.; Ghoroghchian, P.; Hunfeld, N. G.; Berde, C. B.; Langer, R., Prolonged duration local anesthesia from tetrodotoxin-enhanced local anesthetic microspheres. *Pain* **2003,** *104* (1-2), 415-421.

3. Kohane, D. S., Microparticles and nanoparticles for drug delivery. *Biotechnol. Bioeng.* **2007,** *96* (2), 203-209.

4. Patton, J. S.; Byron, P. R., Inhaling medicines: delivering drugs to the body through the lungs. *Nature Reviews Drug Discovery* **2007,** *6* (1), 67-74.

5. Oh, J. K.; Drumright, R.; Siegwart, D. J.; Matyjaszewski, K., The development of microgels/nanogels for drug delivery applications. *Prog. Polym. Sci.* **2008,** *33* (4), 448-477.

6. Adamson, P.; Wilde, T.; Dobrzynski, E.; Sychterz, C.; Polsky, R.; Kurali, E.; Haworth, R.; Tang, C.-M.; Korczynska, J.; Cook, F., Single ocular injection of a sustained-release anti-VEGF delivers 6months pharmacokinetics and efficacy in a primate laser CNV model. *J. Controlled Release* **2016,** *244* (Part A), 1-13.

7. Secret, E.; Crannell, K. E.; Kelly, S. J.; Villancio-Wolter, M.; Andrew, J. S., Matrix metalloproteinase-sensitive hydrogel microparticles for pulmonary drug delivery of small molecule drugs or proteins. *Journal of Materials Chemistry B* **2015,** *3* (27), 5629-5634.

8. Secret, E.; Crannell, K. E.; Kelly, S. J.; Villancio-Wolter, M.; Andrew, J. S., Matrix metalloproteinase-sensitive hydrogel microparticles for pulmonary drug delivery of small molecule drugs or proteins. *J. Mater. Chem. B* **2015,** *3* (27), 5629-5634.

9. Amidi, M.; Pellikaan, H. C.; de Boer, A. H.; Crommelin, D. J.; Hennink, W. E.; Jiskoot, W., Preparation and physicochemical characterization of supercritically dried insulin-loaded microparticles for pulmonary delivery. *Eur. J. Pharm. Biopharm.* **2008,** *68* (2), 191-200.

10. Shen, Y.-B.; Du, Z.; Tang, C.; Guan, Y.-X.; Yao, S.-J., Formulation of insulin-loaded N-trimethyl chitosan microparticles with improved efficacy for inhalation by supercritical fluid assisted atomization. *Int. J. Pharm.* **2016,** *505* (1), 223-233.

11. Chen, H.; Jia, F.; Zhu, C.; Xu, J.; Hua, X.; Xi, Z.; Shen, L.; Zhao, S.; Cen, L., Controllable preparation of SB-3CT loaded PLGA microcapsules for traumatic-brain-injury pharmaco-therapy. *Chem. Eng. J.* **2018,** (In Press.).

12. Lim, M. P. A.; Lee, W. L.; Widjaja, E.; Loo, S. C. J., One-step fabrication of core–shell structured alginate–PLGA/PLLA microparticles as a novel drug delivery system for water soluble drugs. *Biomaterials Science* **2013,** *1* (5), 486-493.

13. Gjoseva, S.; Geskovski, N.; Dimchevska, S.; Popeski-Dimovski, R.; Petruševski, G.; Mladenovska, K.; Goracinova, K., Design and biological response of doxycycline loaded chitosan microparticles for periodontal disease treatment. *Carbohydr. Polym.* **2018,** *186*, 260-272.

14. Khan, I. U.; Serra, C. A.; Anton, N.; Li, X.; Akasov, R.; Messaddeq, N.; Kraus, I.; Vandamme, T. F., Microfluidic conceived drug loaded Janus particles in side-by-side capillaries device. *Int. J. Pharm.* **2014,** *473* (1), 239-249.

15. Liu, M.; Yin, D.; Fu, H.; Deng, F.; Peng, G.; Shu, G.; Yuan, Z.; Shi, F.; Lin, J.; Zhao, L.; Yin, L.; Fan, G., Double-coated enrofloxacin microparticles with chitosan and alginate: Preparation, characterization and taste-masking effect study. *Carbohydr. Polym.* **2017,** *170*, 247-253.

16. Zhang, Z.; Wang, X.; Li, B.; Hou, Y.; Cai, Z.; Yang, J.; Li, Y., Paclitaxel-loaded PLGA microspheres with a novel morphology to facilitate drug delivery and antitumor efficiency. *RSC Advances* **2018,** *8* (6), 3274-3285.

17. Wang, Q.; Mi, G.; Hickey, D.; Li, Y.; Tu, J.; Webster, T. J.; Shen, Y., Azithromycin-loaded respirable microparticles for targeted pulmonary delivery for the treatment of pneumonia. *Biomaterials* **2018,** *160*, 107-123.

18. Takeuchi, I.; Taniguchi, Y.; Tamura, Y.; Ochiai, K.; Makino, K., Effects of l-leucine on PLGA microparticles for pulmonary administration prepared using spray drying: Fine particle fraction and phagocytotic ratio of alveolar macrophages. *Colloids and Surfaces A: Physicochemical and Engineering Aspects* **2018,** *537*, 411-417.

19. Kang, Y.; Wu, J.; Yin, G.; Huang, Z.; Liao, X.; Yao, Y.; Ouyang, P.; Wang, H.; Yang, Q., Characterization and biological evaluation of paclitaxel-loaded poly (L-lactic acid) microparticles prepared by supercritical CO2. *Langmuir* **2008,** *24* (14), 7432-7441.

20. Kong, F.; Zhang, X.; Zhang, H.; Qu, X.; Chen, D.; Servos, M.; Mäkilä, E.; Salonen, J.; Santos, H. A.; Hai, M., Inhibition of multidrug resistance of cancer cells by co-delivery of DNA nanostructures and drugs using porous silicon nanoparticles@giant liposomes. *Adv. Funct. Mater.* **2015,** *25* (22), 3330-3340.

21. He, T.; Liang, Q.; Zhang, K.; Mu, X.; Luo, T.; Wang, Y.; Luo, G., A modified microfluidic chip for fabrication of paclitaxel-loaded poly (l-lactic acid) microspheres. *Microfluidics and Nanofluidics* **2011,** *10* (6), 1289-1298.

22. Fish, M. B.; Fromen, C. A.; Lopez-Cazares, G.; Golinski, A. W.; Scott, T. F.; Adili, R.; Holinstat, M.; Eniola-Adefeso, O., Exploring deformable particles in vascular-targeted drug delivery: Softer is only sometimes better. *Biomaterials* **2017,** *124*, 169-179.

23. CDC's Malaria Program. https://www.cdc.gov/malaria/resources/pdf/fsp/cdc_malaria_program_508.pdf.

24. *World Malaria report 2014*. World Health Organization: Geneva, 2014.

25. Singh, B. N.; Kim, K. H., Floating drug delivery systems: an approach to oral controlled drug delivery via gastric retention. *J. Controlled Release* **2000,** *63* (3), 235-259.

26. Bellinger, A. M.; Jafari, M.; Grant, T. M.; Zhang, S.; Slater, H. C.; Wenger, E. A.; Mo, S.; Lee, Y.-A. L.; Mazdiyasni, H.; Kogan, L., Oral, ultra–long-lasting drug delivery: Application toward malaria elimination goals. *Sci. Transl. Med.* **2016,** *8* (365), 365ra157-365ra157.

27. TABLETS STROMECTOL (IVERMECTIN). https://www.merck.com/product/usa/pi_circulars/s/stromectol/stromectol_pi.pdf (accessed December 21).

28. Fukushima, K.; Pratt, R. C.; Nederberg, F.; Tan, J. P.; Yang, Y. Y.; Waymouth, R. M.; Hedrick, J. L., Organocatalytic approach to amphiphilic comb-block copolymers capable of stereocomplexation and self-assembly. *Biomacromolecules* **2008,** *9* (11), 3051-3056.

29. Hu, X.; Chen, X.; Xie, Z.; Liu, S.; Jing, X., Synthesis and characterization of amphiphilic block copolymers with allyl side-groups. *J. Polym. Sci., Part A: Polym. Chem.* **2007,** *45* (23), 5518-5528.

30. Spears, B. R.; Waksal, J.; McQuade, C.; Lanier, L.; Harth, E., Controlled branching of polyglycidol and formation of protein–glycidol bioconjugates via a graft-from approach with "PEG-like" arms. *Chem. Commun.* **2013,** *49* (24), 2394-2396.

31. Shlyonsky, V.; Boom, A.; Mies, F., Hydrogen peroxide and sodium transport in the lung and kidney. *BioMed Research International* **2016,** *2016*, 7.

32. Molinari, G.; Soloneski, S.; Reigosa, M. A.; Larramendy, M. L., In vitro genotoxic and cytotoxic effects of ivermectin and its formulation ivomec® on Chinese hamster ovary (CHOK1) cells. *J. Hazard. Mater.* **2009,** *165* (1–3), 1074-1082.

33. Hutter, V.; Hilgendorf, C.; Cooper, A.; Zann, V.; Pritchard, D. I.; Bosquillon, C., Evaluation of layers of the rat airway epithelial cell line RL-65 for permeability screening of inhaled drug candidates. *Eur. J. Pharm. Sci.* **2012,** *47* (2), 481-489.

34. Lang, S.; Langguth, P.; Oschmann, R.; Traving, B.; Merkle, H. P., Transport and metabolic pathway of thymocartin (TP4) in excised bovine nasal mucosa. *J. Pharm. Pharmacol.* **1996,** *48* (11), 1190-1196.

35. Stevens, D. M.; Watson, H. A.; LeBlanc, M.-A.; Wang, R. Y.; Chou, J.; Bauer, W. S.; Harth, E., Practical polymerization of functionalized lactones and carbonates with Sn(OTf)2 in metal catalysed ring-opening polymerization methods. *Polymer Chemistry* **2013,** *4* (8), 2470-2474.

36. Siebert, M.; Keul, H.; Möller, M., Synthesis of well-defined polystyrene-block-polyglycidol (PS-b-PG) block co-polymers by anionic polymerization. *Designed Monomers and Polymers* **2010,** *13* (6), 547-563.

37. Kainthan, R. K.; Janzen, J.; Levin, E.; Devine, D. V.; Brooks, D. E., Biocompatibility Testing of Branched and Linear Polyglycidol. *Biomacromolecules* **2006,** *7* (3), 703-709.

38. Song, G. Y.; Wang, J.; Shin, J. Y.; Song, S. I.; Kim, I., Dendritic hyperbranched polyglycidol/folic acid conjugate for targeting drug delivery system. *J. Controlled Release* **2013,** *172* (1), e31.

39. Hoyle, C. E.; Bowman, C. N., Thiol–Ene click chemistry. *Angew. Chem. Int. Ed.* **2010,** *49* (9), 1540-1573.

40. Mi, F.-L.; Kuan, C.-Y.; Shyu, S.-S.; Lee, S.-T.; Chang, S.-F., The study of gelation kinetics and chain-relaxation properties of glutaraldehyde-cross-linked chitosan gel and their effects on microspheres preparation and drug release. *Carbohydr. Polym.* **2000,** *41* (4), 389-396.

41. Merkel, T. J.; Jones, S. W.; Herlihy, K. P.; Kersey, F. R.; Shields, A. R.; Napier, M.; Luft, J. C.; Wu, H.; Zamboni, W. C.; Wang, A. Z.; Bear, J. E.; DeSimone, J. M., Using mechanobiological mimicry of red blood cells to extend circulation times of hydrogel microparticles. *Proceedings of the National Academy of Sciences* **2011,** *108* (2), 586-591.

42. Jung, K.; Xu, J.; Zetterlund, P. B.; Boyer, C., Visible-light-regulated controlled/living radical polymerization in miniemulsion. *ACS Macro Lett.* **2015,** *4* (10), 1139-1143.

43. Magdassi, S., *The chemistry of inkjet inks*. World scientific Singapore: 2010.

44. Khudyakov, I. V.; Legg, J. C.; Purvis, M. B.; Overton, B. J., Kinetics of photopolymerization of acrylates with functionality of 1−6. *Ind. Eng. Chem. Res.* **1999,** *38* (9), 3353-3359.

45. Nakayama, Y.; Matsuda, T., Photocurable surgical tissue adhesive glues composed of photoreactive gelatin and poly (ethylene glycol) diacrylate. *J. Biomed. Mater. Res.* **1999,** *48* (4), 511-521.

46. Hao, Y.; Shih, H.; Muňoz, Z.; Kemp, A.; Lin, C.-C., Visible light cured thiol-vinyl hydrogels with tunable degradation for 3D cell culture. *Acta Biomater.* **2014,** *10* (1), 104-114.

47. Nakayama, Y.; Kameo, T.; Ohtaka, A.; Hirano, Y., Enhancement of visible light-induced gelation of photocurable gelatin by addition of polymeric amine. *Journal of Photochemistry and Photobiology A: Chemistry* **2006,** *177* (2–3), 205-211.

48. Spears, B. R.; Marin, M. A.; Chaker, A. N.; Lampley, M. W.; Harth, E., Precise microscale polymeric networks through piezoelectronic inkjet printing. *ACS Biomater. Sci. Eng.* **2016,** *2* (8), 1265-1272.

49. De Koker, S.; Fierens, K.; Dierendonck, M.; De Rycke, R.; Lambrecht, B. N.; Grooten, J.; Remon, J. P.; De Geest, B. G., Nanoporous polyelectrolyte vaccine microcarriers. A formulation platform for enhancing humoral and cellular immune responses. *J. Controlled Release* **2014,** *195*, 99-109.

50. Singh, D.; Goel, D.; Bhatnagar, R., Recombinant L7/L12 protein entrapping PLGA (poly lactide-co-glycolide) micro particles protect BALB/c mice against the virulent B. abortus 544 infection. *Vaccine* **2015,** *33* (24), 2786-2792.

51. Tzeng, S. Y.; Guarecuco, R.; McHugh, K. J.; Rose, S.; Rosenberg, E. M.; Zeng, Y.; Langer, R.; Jaklenec, A., Thermostabilization of inactivated polio vaccine in PLGA-based microspheres for pulsatile release. *J. Controlled Release* **2016,** *233*, 101-113.

52. Saboo, S.; Tumban, E.; Peabody, J.; Wafula, D.; Peabody, D. S.; Chackerian, B.; Muttil, P., Optimized formulation of a thermostable spray-dried virus-like particle vaccine against human papillomavirus. *Mol. Pharm.* **2016,** *13* (5), 1646-1655.

53. Jeong, D.; Kang, C.; Jung, E.; Yoo, D.; Wu, D.; Lee, D., Porous antioxidant polymer microparticles as therapeutic systems for the airway inflammatory diseases. *J. Controlled Release* **2016,** *233*, 72-80.

54. Mathias, N. R.; Timoszyk, J.; Stetsko, P. I.; Megill, J. R.; Smith, R. L.; Wall, D. A., Permeability characteristics of calu-3 human bronchial epithelial cells: in vitro-in vivo correlation to predict lung absorption in rats. *J. Drug Target.* **2002,** *10* (1), 31-40.

55. Emami, J.; Hamishehkar, H.; Najafabadi, A. R.; Gilani, K.; Minaiyan, M.; Mahdavi, H.; Nokhodchi, A., A novel approach to prepare insulin-loaded poly (lactic-co-glycolic acid) microcapsules and the protein stability study. *J. Pharm. Sci.* **2009,** *98* (5), 1712-1731.

56. Sajeesh, S.; Bouchemal, K.; Marsaud, V.; Vauthier, C.; Sharma, C. P., Cyclodextrin complexed insulin encapsulated hydrogel microparticles: An oral delivery system for insulin. *Journal of Controlled Release* **2010,** *147* (3), 377-384.

57. Kumar, A.; Lahiri, S. S.; Singh, H., Development of PEGDMA: MAA based hydrogel microparticles for oral insulin delivery. *Int. J. Pharm.* **2006,** *323* (1–2), 117-124.

58. Ungaro, F.; d'Emmanuele di Villa Bianca, R.; Giovino, C.; Miro, A.; Sorrentino, R.; Quaglia, F.; La Rotonda, M. I., Insulin-loaded PLGA/cyclodextrin large porous particles with improved aerosolization properties: In vivo deposition and hypoglycaemic activity after delivery to rat lungs. *J. Controlled Release* **2009,** *135* (1), 25-34.

59. Lee, B. K.; Yun, Y. H.; Choi, J. S.; Choi, Y. C.; Kim, J. D.; Cho, Y. W., Fabrication of drug-loaded polymer microparticles with arbitrary geometries using a piezoelectric inkjet printing system. *Int. J. Pharm.* **2012,** *427* (2), 305-310.

60. Yang, J.; Katagiri, D.; Mao, S.; Zeng, H.; Nakajima, H.; Kato, S.; Uchiyama, K., Inkjet printing based assembly of thermoresponsive core–shell polymer microcapsules for controlled drug release. *Journal of Materials Chemistry B* **2016,** *4* (23), 4156-4163.

61. Lai, E.; Wang, Y.; Wei, Y.; Li, G.; Ma, G., Covalent immobilization of trypsin onto thermo-sensitive poly (N-isopropylacrylamide-co-acrylic acid) microspheres with high activity and stability. *J. Appl. Polym. Sci.* **2016,** *133* (21).

62. Gawlitza, K.; Georgieva, R.; Tavraz, N.; Keller, J.; von Klitzing, R., Immobilization of water-soluble HRP within poly-N-isopropylacrylamide microgel particles for use in organic media. *Langmuir* **2013,** *29* (51), 16002-16009.

63. Månsson, R.; Frenning, G. r.; Malmsten, M., Factors affecting enzymatic degradation of microgel-bound peptides. *Biomacromolecules* **2013,** *14* (7), 2317-2325.

64. Zhang, Y.; Zhu, W.; Wang, B.; Ding, J., A novel microgel and associated post-fabrication encapsulation technique of proteins. *J. Controlled Release* **2005,** *105* (3), 260-268.

65. Kharel, S.; Lee, W. L.; Lee, X. Y.; Loo, S. C. J., Osmogen-Mediated One-Step Technique of Fabricating Hollow Microparticles for Encapsulation and Delivery of Bioactive Molecules. *Macromol. Biosci.* **2016,** *17* (4), in press.

66. Rios, J. L.; Lu, G.; Seo, N. E.; Lambert, T.; Putnam, D., Prolonged release of bioactive model proteins from anionic microgels fabricated with a new microemulsion approach. *Pharm. Res.* **2016,** *33* (4), 879-892.

67. Janssen, M.; Timur, U. T.; Woike, N.; Welting, T. J.; Draaisma, G.; Gijbels, M.; van Rhijn, L.; Mihov, G.; Thies, J.; Emans, P., Celecoxib-loaded PEA microspheres as an auto regulatory drug-delivery system after intra-articular injection. *J. Controlled Release* **2016,** *244* (Part A), 30-40.

68. Wanakule, P.; Liu, G. W.; Fleury, A. T.; Roy, K., Nano-inside-micro: Disease-responsive microgels with encapsulated nanoparticles for intracellular drug delivery to the deep lung. *J. Controlled Release* **2012,** *162* (2), 429-437.

69. Kong, F.; Zhang, X.; Hai, M., Microfluidics fabrication of monodisperse biocompatible phospholipid vesicles for encapsulation and delivery of hydrophilic drug or active compound. *Langmuir* **2014,** *30* (13), 3905-3912.

70. Jensen, D. M. K.; Cun, D.; Maltesen, M. J.; Frokjaer, S.; Nielsen, H. M.; Foged, C., Spray drying of siRNA-containing PLGA nanoparticles intended for inhalation. *J. Controlled Release* **2010,** *142* (1), 138-145.

71. Roa, W. H.; Azarmi, S.; Al-Hallak, M. H. D. K.; Finlay, W. H.; Magliocco, A. M.; Löbenberg, R., Inhalable nanoparticles, a non-invasive approach to treat lung cancer in a mouse model. *J. Controlled Release* **2011,** *150* (1), 49-55.

72. Mu, L.; Feng, S. S., Fabrication, characterization and in vitro release of paclitaxel (Taxol®) loaded poly (lactic-co-glycolic acid) microspheres prepared by spray drying technique with lipid/cholesterol emulsifiers. *J. Controlled Release* **2001,** *76* (3), 239-254.

73. Ji, S.; Thulstrup, P. W.; Mu, H.; Hansen, S. H.; van de Weert, M.; Rantanen, J.; Yang, M., Effect of ethanol as a co-solvent on the aerosol performance and stability of spray-dried lysozyme. *Int. J. Pharm.* **2016,** *513* (1–2), 175-182.

74. Karavasili, C.; Bouropoulos, N.; Sygellou, L.; Amanatiadou, E. P.; Vizirianakis, I. S.; Fatouros, D. G., PLGA/DPPC/trimethylchitosan spray-dried microparticles for the nasal delivery of ropinirole hydrochloride: in vitro, ex vivo and cytocompatibility assessment. *Materials Science and Engineering: C* **2016,** *59*, 1053-1062.

75. Koetting, M. C.; Guido, J. F.; Gupta, M.; Zhang, A.; Peppas, N. A., pH-responsive and enzymatically-responsive hydrogel microparticles for the oral delivery of therapeutic proteins: Effects of protein size, crosslinking density, and hydrogel degradation on protein delivery. *J. Controlled Release* **2016,** *221*, 18-25.

76. Zykwinska, A.; Marquis, M.; Sinquin, C.; Cuenot, S.; Colliec-Jouault, S., Assembly of HE800 exopolysaccharide produced by a deep-sea hydrothermal bacterium into microgels for protein delivery applications. *Carbohydr. Polym.* **2016,** *142*, 213-221.

77. Foster, G. A.; Headen, D. M.; González-García, C.; Salmerón-Sánchez, M.; Shirwan, H.; García, A. J., Protease-degradable microgels for protein delivery for vascularization. *Biomaterials* **2017,** *113*, 170-175.

78. Wang, K.; Lin, S.; Nune, K.; Misra, R., Chitosan-gelatin-based microgel for sustained drug delivery. *J. Biomater. Sci. Polym. Ed.* **2016,** *27* (5), 441-453.

79. Deveza, L.; Ashoken, J.; Castaneda, G.; Tong, X.; Keeney, M.; Han, L.-H.; Yang, F., Microfluidic synthesis of biodegradable polyethylene-glycol microspheres for controlled

delivery of proteins and DNA nanoparticles. *ACS Biomater. Sci. Eng.* **2015,** *1* (3), 157-165.

80. Kesselman, L. R.; Shinwary, S.; Selvaganapathy, P. R.; Hoare, T., Synthesis of monodisperse, covalently cross-linked, degradable "smart" microgels using microfluidics. *Small* **2012,** *8* (7), 1092-1098.

81. Kim, J.-W.; Ko, J.-Y.; Jun, J.-B.; Chang, I.-S.; Kang, H.-H.; Suh, K.-D., Multihollow polymer microcapsules by water-in-oil-in-water emulsion polymerization: morphological study and entrapment characteristics. *Colloid. Polym. Sci.* **2003,** *281* (2), 157-163.

82. Suarez, S. L.; Muñoz, A.; Mitchell, A. C.; Braden, R. L.; Luo, C.; Cochran, J. R.; Almutairi, A.; Christman, K. L., Degradable acetalated dextran microparticles for tunable release of an engineered hepatocyte growth factor fragment. *ACS Biomater. Sci. Eng.* **2016,** *2* (2), 197-204.

83. Guo, S.; Nakagawa, Y.; Barhoumi, A.; Wang, W.; Zhan, C.; Tong, R.; Santamaria, C.; Kohane, D. S., Extended release of native drug conjugated in polyketal microparticles. *JACS* **2016**.

84. Lakkakula, J. R.; Kurapati, R.; Tynga, I.; Abrahamse, H.; Raichur, A. M.; Krause, R. W. M., Cyclodextrin grafted calcium carbonate vaterite particles: efficient system for tailored release of hydrophobic anticancer or hormone drugs. *RSC Advances* **2016,** *6* (106), 104537-104548.

85. Jivan, F.; Yegappan, R.; Pearce, H.; Carrow, J. K.; McShane, M.; Gaharwar, A. K.; Alge, D. L., Sequential thiol–ene and tetrazine click reactions for the polymerization and functionalization of hydrogel microparticles. *Biomacromolecules* **2016,** *17* (11), 3516-3523.

86. Quinlan, E.; López-Noriega, A.; Thompson, E.; Kelly, H. M.; Cryan, S. A.; O'Brien, F. J., Development of collagen–hydroxyapatite scaffolds incorporating PLGA and alginate microparticles for the controlled delivery of rhBMP-2 for bone tissue engineering. *J. Controlled Release* **2015,** *198*, 71-79.

87. Li, J.; Jiang, H.; Ouyang, X.; Han, S.; Wang, J.; Xie, R.; Zhu, W.; Ma, N.; Wei, H.; Jiang, Z., CaCO3/Tetraethylenepentamine-graphene hollow microspheres as biocompatible bone drug carriers for controlled release. *ACS Appl. Mater. Interfaces* **2016**.

88. Estevinho, B. N.; Ramos, I.; Rocha, F., Effect of the pH in the formation of β-galactosidase microparticles produced by a spray-drying process. *Int. J. Biol. Macromol.* **2015,** *78*, 238-242.

89. Garbayo, E.; Ansorena, E.; Lana, H.; Carmona-Abellan, M. d. M.; Marcilla, I.; Lanciego, J. L.; Luquin, M. R.; Blanco-Prieto, M. J., Brain delivery of microencapsulated GDNF induces functional and structural recovery in parkinsonian monkeys. *Biomaterials* **2016,** *110*, 11-23.

90. Samak, Y. O.; El Massik, M.; Coombes, A. G., A Comparison of aerosolization and homogenization techniques for production of alginate microparticles for delivery of corticosteroids to the colon. *J. Pharm. Sci.* **2016,** *106* (1), 208-216.

91. Chakravarthi, S. S.; De, S.; Miller, D. W.; Robinson, D. H., Comparison of anti-tumor efficacy of paclitaxel delivered in nano- and microparticles. *Int. J. Pharm.* **2010,** *383* (1–2), 37-44.

92. Tsai, M.; Lu, Z.; Wientjes, M. G.; Au, J. L.-S., Paclitaxel-loaded polymeric microparticles: quantitative relationships between in vitro drug release rate and in vivo pharmacodynamics. *Journal of Controlled Release* **2013,** *172* (3), 737-744.

93. Alipour, S.; Montaseri, H.; Tafaghodi, M., Preparation and characterization of biodegradable paclitaxel loaded alginate microparticles for pulmonary delivery. *Colloids and Surfaces B: Biointerfaces* **2010,** *81* (2), 521-529.

94. Davoodi, P.; Ng, W. C.; Yan, W. C.; Srinivasan, M. P.; Wang, C.-H., Double-walled microparticles-embedded self-cross-linked, injectable, and antibacterial hydrogel for controlled and sustained release of chemotherapeutic agents. *ACS Appl. Mater. Interfaces* **2016,** *8* (35), 22785-22800.

95. Huang, X.; Zhang, Y.; Yin, G.; Pu, X.; Liao, X.; Huang, Z.; Chen, X.; Yao, Y., Tumor-targeted paclitaxel-loaded folate conjugated poly (ethylene glycol)-poly (l-lactide) microparticles produced by supercritical fluid technology. *J. Mater. Sci. Mater. Med.* **2015,** *26* (2), 1-14.

96. Vladisavljević, G. T.; Ekanem, E. E.; Zhang, Z.; Khalid, N.; Kobayashi, I.; Nakajima, M., Long-term stability of droplet production by microchannel (step) emulsification in microfluidic silicon chips with large number of terraced microchannels. *Chem. Eng. J.* **2018,** *333*, 380-391.

97. Hussain, M.; Xie, J.; Hou, Z.; Shezad, K.; Xu, J.; Wang, K.; Gao, Y.; Shen, L.; Zhu, J., Regulation of drug release by tuning surface textures of biodegradable polymer microparticles. *ACS Appl. Mater. Interfaces* **2017,** *9* (16), 14391-14400.

98. Quinlan, E.; López-Noriega, A.; Thompson, E. M.; Hibbitts, A.; Cryan, S. A.; O'Brien, F. J., Controlled release of vascular endothelial growth factor from spray-dried alginate microparticles in collagen–hydroxyapatite scaffolds for promoting vascularization and bone repair. *J. Tissue Eng. Regen. Med.* **2017,** *11* (4), 1097-1109.

99. Liu, T.; Han, M.; Tian, F.; Cun, D.; Rantanen, J.; Yang, M., Budesonide nanocrystal-loaded hyaluronic acid microparticles for inhalation: in vitro and in vivo evaluation. *Carbohydr. Polym.* **2018,** *181*, 1143-1152.

100. de Oliveira, A. R.; Mesquita, P. C.; Machado, P. R. L.; Farias, K. J. S.; de Almeida, Y. M. B.; Fernandes-Pedrosa, M. F.; Cornélio, A. M.; do Egito, E. S. T.; da Silva-Júnior, A. A., Monitoring structural features, biocompatibility and biological efficacy of gamma-irradiated methotrexate-loaded spray-dried microparticles. *Materials Science and Engineering: C* **2017,** *80*, 438-448.

101. Wang, C.; Wu, D.; Yang, J.; Han, H.; Xing, Z.; Zhang, Y.; Yang, Y.; Li, Q., Porous PLGA microparticles to encapsulate doxorubicin and polyethylenimine/miR-34a for inhibiting the proliferation and migration of lung cancer. *RSC Adv.* **2015,** *5* (99), 81445-81448.

102. Lee, W. L.; Guo, W. M.; Ho, V. H. B.; Saha, A.; Chong, H. C.; Tan, N. S.; Tan, E. Y.; Loo, S. C. J., Delivery of doxorubicin and paclitaxel from double-layered microparticles: The effects of layer thickness and dual-drug vs. single-drug loading. *Acta Biomater.* **2015,** *27*, 53-65.

103. Wu, D.; Wang, C.; Yang, J.; Wang, H.; Han, H.; Zhang, A.; Yang, Y.; Li, Q., Improving the intracellular drug concentration in lung cancer treatment through the codelivery of doxorubicin and miR-519c mediated by porous PLGA microparticle. *Mol. Pharm.* **2016,** *13* (11), 3925-3933.

104. Jagadeesan, D.; Nasimova, I.; Gourevich, I.; Starodubtsev, S.; Kumacheva, E., Microgels for the encapsulation and simulus-responsive release of molecules with distinct polarities. *Macromol. Biosci.* **2011,** *11* (7), 889-896.

105. Maher, S.; Santos, A.; Kumeria, T.; Kaur, G.; Lambert, M.; Forward, P.; Evdokiou, A.; Losic, D., Multifunctional micro-spherical magnetic and pH responsive carriers for combination

anticancer therapy engineered by droplet-based microfluidics. *Journal of Materials Chemistry B* **2017,** *5* (22), 4097-4109.

106. Yang, Y.-J.; Tang, B.; Zhang, L.; Wang, C.; Ma, H.-T.; Pang, D.-W.; Zhang, Z.-L., On-demand one-step synthesis of small-sized fluorescent-magnetic-bifunctional microparticles on a droplet-splitting chip. *Journal of Materials Chemistry B* **2018,** (6), 961-965.